

---

Doctoral

Engineering

---

2016

## Fatigue Properties Of Magnetorheological Elastomers And The Design Of Interfacial Layers To Improve Fatigue Life.

Yanfen Zhou

Technological University Dublin, yanfen.zhou@mydit.ie

Follow this and additional works at: <https://arrow.tudublin.ie/engdoc>



Part of the [Engineering Mechanics Commons](#), and the [Materials Science and Engineering Commons](#)

---

### Recommended Citation

Zhou, Y. (2016) *Fatigue properties of magnetorheological elastomers and the design of interfacial layers to improve fatigue life*. Doctoral Thesis, Technological University Dublin. doi:10.21427/D75315

This Theses, Ph.D is brought to you for free and open access by the Engineering at ARROW@TU Dublin. It has been accepted for inclusion in Doctoral by an authorized administrator of ARROW@TU Dublin. For more information, please contact [arrow.admin@tudublin.ie](mailto:arrow.admin@tudublin.ie), [aisling.coyne@tudublin.ie](mailto:aisling.coyne@tudublin.ie), [vera.kilshaw@tudublin.ie](mailto:vera.kilshaw@tudublin.ie).

**Fatigue properties of magnetorheological  
elastomers and the design of interfacial layers  
to improve fatigue life**

**Yanfen Zhou**



**Doctor of Philosophy (PhD)**

**School of Mechanical and Design Engineering**

**Dublin Institute of Technology**

**Supervisors: Prof. Stephen Jerrams, Dr. Anthony Betts, Prof. Gerry Farrell,**

**Dr. Lin Chen**

**May 2016**

## Abstract

The primary aim of this PhD programme was to understand the fatigue behaviour of magnetorheological elastomers (MREs) and provide a reliable fatigue life predictor for this class of materials. To realise this aim required the study of the dynamic behaviour of MREs using the equi-biaxial bubble inflation test method. Isotropic and anisotropic MREs were fabricated from silicone rubber (SR) filled with soft carbonyl iron (CI) particles. The equi-biaxial fatigue behaviour of these samples was determined using a bubble inflation method. Wöhler (S-N) curves for both isotropic and anisotropic MREs were produced by subjecting the compounds to cycling over a range of stress amplitudes ( $\sigma_a$ ). Changes in physical properties, including variation in stress-stretch ratio relations, complex modulus ( $E^*$ ), dynamic stored energy ( $W_D$ ) and damping loss factor ( $\eta$ ) during the fatigue process, were analysed. In cyclic testing, a limiting value of  $E^*$  was reached at which fatigue failure occurred in SR based MREs and this supports previous findings for non-strain crystallising rubbers (ethylene propylene diene monomer (EPDM) and styrene-butadiene rubber (SBR)) subjected to uniaxial and equi-biaxial loading. It was also substantiated that the dynamic stored energy criterion can be used as a predictor in determining the fatigue life of MREs irrespective of loading levels, the carbonyl iron content, the directionality of the particles and whether or not an external magnetic field was applied.

Interfacial layers play an important role in improving the fatigue resistance of MRE compounds by offering a sensible transition in physical properties between the matrix elastomer and the ferromagnetic particles. An initial attempt to modify the surface of carbonyl iron particles by using a sol-gel method was introduced in this research. Characterisation of MREs with coated particles suggested that the

dispersion of particles in silicone rubber was greatly improved after polysiloxane encapsulation.

Consequently, the next phase of the research programme will focus on the design of interfacial layers using the sol-gel method. The coated particles will be used in the fabrication of MREs and the equi-biaxial fatigue behaviour of these samples will be studied to determine the effect of variations in interfacial layers on the fatigue resistance of the composites.

## **Declaration**

I certify that this thesis which I now submit for examination for the award of Doctor of Philosophy (PhD), is entirely my own work and has not been taken from the work of others, save to the extent that such work has been cited and acknowledged within the text of my own work.

This thesis was prepared according to the regulations for postgraduate study by research of the Dublin Institute of Technology (DIT) and has not been submitted in whole or in part for another award by any other third level institution.

The work reported on in this thesis conforms to the principles and requirements of the DIT's guidelines for ethics in research.

DIT has permission to keep, lend or copy this thesis in whole or in part, on the condition that any such use of the material of the thesis be duly acknowledged.

Signature\_\_\_\_\_ Date\_\_\_\_\_

Candidate

## **Acknowledgments**

Undertaking PhD research in DIT has been a valuable and impressive experience for me. It would not have been possible without the support and assistance of many people.

First and foremost, I would like to thank my supervisors Prof. Stephen Jerrams, Dr. Anthony Betts, Prof. Gerry Farrell and Dr. Lin Chen. Their extensive knowledge and experience has been of great importance to me in this research. In particular, Prof. Stephen Jerrams reached retirement from DIT in the third year of my PhD study, but continued to provide guidance, tremendous support and knowledgeable contributions to the research. I feel grateful to Dr. Anthony Betts for his constructive suggestions in respect of the chemical work and the insightful routine discussions of this research. Thanks are due to Dr. Lin Chen for supporting me so much in setting up the experiments and carrying out the fatigue testing.

The research work would not have been possible without the support of the Irish Research Council for Science, Engineering and Technology (IRCSET) and DIT's Fiosraigh Scholarship Programme, so I offer thanks to IRC and DIT for their financial support.

I wish to thank the entire Centre for Elastomer Research (CER) team and the Focas Research Institute in DIT, particularly Dr. Niall Murphy and Mark Johnson for the mechanical testing of MREs. I must also thank Anne Shanahan for her support in SEM work.

Many thanks are due to Sean Keane and Neil Branigan for their kind help in the material fabrication process.

I would like to extend my thanks to the Centre for Microscopy Analysis (CMA) in Trinity College Dublin (TCD) where a lot of SEM and EDS work was undertaken.

I greatly appreciate the help received from Lin Chen and his wife Jiemei Zhan during the first two years of my study. They were always so considerate and provided me with much assistance in my daily life in Dublin.

I gave birth to my lovely son Lewis in the final year of PhD study. Thanks for all the understanding and every care my supervisors, my friends and my family have given to me during this particular time. Special thanks go to my beloved husband Liang Jiang who gave me so much care throughout this crucial time in my life. Thanks also to my son Lewis for being such a good boy and bringing so much happiness and joy to me and Liang. Finally, thanks for all the continuous support and encouragement that my parents and brothers have given me throughout my education and pursuit of a PhD degree abroad.

## Nomenclature

$E^*$	complex modulus	MPa
$N$	number of cycles	dimensionless
$N_f$	number of cycles at failure	dimensionless
$P$	pressure	bar
$T$	temperature	°C
$t$	specimen thickness	mm
$W_S$	stored energy	N/mm <sup>2</sup>
$W_D$	dynamic stored energy	N/mm <sup>2</sup>
$\Delta W$	dissipated energy	N/mm <sup>2</sup>
$X$	displacement	mm
$\lambda$	stretch ratio	dimensionless
$\rho$	density	g/cm <sup>3</sup>
$\sigma$	stress	MPa
$\sigma_a$	stress amplitude	MPa
$\sigma_{Eng}$	engineering stress	MPa
$\eta$	damping loss factor	dimensionless
$G'$	storage shear modulus	MPa
$G''$	loss shear modulus	MPa

## Abbreviations

MR	Magnetorheological
MREs	Magnetorheological Elastomers
MRFs	Magnetorheological Fluids
CI	Carbonyl Iron
SR	Silicone Rubber
SEM	Scanning Electron Microscopy
EDS	Energy-Dispersive X-ray Spectrometers
FTIR	Fourier Transform Infrared Spectroscopy
TGA	Thermal Gravimetric Analyzer
AA	Acrylic Acid
TEOS	Tetraethyl Orthosilicate

# Table of Contents

<b>Chapter 1</b>	<b>Introduction</b>	<b>1</b>
1.1	The motivation for the research programme	1
1.2	Aims and objectives	2
1.3	Research methodology	3
1.4	Contributions to knowledge	4
1.5	Structure of the thesis	5
<b>Chapter 2</b>	<b>Literature review</b>	<b>7</b>
2.1	Evolution of MREs	7
2.2	Composition of MREs	8
2.2.1	Elastomeric matrix	8
2.2.2	Magnetisable particles	11
2.3	Microstructure of MREs	12
2.4	Properties of MREs	14
2.5	Factors that influence the properties of MREs	18
2.5.1	Magnetic field strength	18
2.5.2	Magnetic particles	19
2.5.3	Additives	20
2.5.4	Interfacial adhesion	22
2.5.5	Frequency	24
2.5.6	Strain amplitude	25
2.6	Applications of MREs	26
2.7	Elastomer behaviour	27
2.7.1	Nonlinear elasticity	28

2.7.2	Viscoelasticity .....	29
2.7.3	Mullins effect .....	31
2.7.4	Payne effect.....	33
<b>2.8</b>	<b>Fatigue of Elastomers.....</b>	<b>35</b>
<b>2.9</b>	<b>Summary .....</b>	<b>39</b>
<b>Chapter 3</b>	<b>Materials and methods .....</b>	<b>42</b>
<b>3.1</b>	<b>Materials.....</b>	<b>42</b>
<b>3.2</b>	<b>Fabrication of MREs.....</b>	<b>43</b>
<b>3.3</b>	<b>Equi-biaxial testing.....</b>	<b>43</b>
3.3.1	Theory .....	44
3.3.2	Testing methods .....	46
3.3.3	Fatigue data analysis .....	47
<b>3.4</b>	<b>Spectroscopy and microscopy observation .....</b>	<b>50</b>
<b>Chapter 4</b>	<b>Equi-biaxial fatigue behaviour of MREs with different microstructures .....</b>	<b>51</b>
<b>4.1</b>	<b>Introduction .....</b>	<b>51</b>
<b>4.2</b>	<b>Quasi-static test.....</b>	<b>52</b>
<b>4.3</b>	<b>Fatigue life.....</b>	<b>53</b>
<b>4.4</b>	<b>Stress-strain behaviour .....</b>	<b>55</b>
<b>4.5</b>	<b>Complex modulus .....</b>	<b>57</b>
<b>4.6</b>	<b>Dynamic stored energy .....</b>	<b>58</b>
<b>4.7</b>	<b>Damping loss factor .....</b>	<b>61</b>
<b>4.8</b>	<b>Fracture surface analysis.....</b>	<b>63</b>
<b>4.9</b>	<b>Summary .....</b>	<b>67</b>

<b>Chapter 5</b>	<b>Equi-biaxial fatigue behaviour of isotropic MREs with a range of magnetic particle contents.....</b>	<b>69</b>
5.1	Introduction .....	69
5.2	Quasi-static test.....	70
5.3	Fatigue life.....	72
5.4	Complex modulus .....	76
5.5	Dynamic stored energy .....	81
5.6	Damping loss factor .....	85
5.7	Summary .....	88
<b>Chapter 6</b>	<b>Equi-biaxial fatigue behaviour of MREs subjected to magnetic fields during cyclic testing .....</b>	<b>91</b>
6.1	Introduction .....	91
6.2	Effect of magnetic fields on fatigue life of MREs .....	92
6.3	Stress-strain behaviour .....	96
6.4	Complex modulus .....	97
6.5	Dynamic stored energy .....	99
6.6	Damping loss factor .....	102
6.7	Summary .....	104
<b>Chapter 7</b>	<b>Preliminary research into interfacial layer design in MREs ..</b>	<b>106</b>
7.1	Introduction .....	106
7.2	Coating process.....	106
7.3	Chemical structure .....	107
7.4	Surface morphology .....	107
7.5	Thermal stability .....	109
7.6	Effect of coating on surface morphology of MREs .....	110

7.7	Summary .....	111
Chapter 8	Conclusions and proposed future work .....	113
8.1	Conclusions .....	113
8.2	Proposed future work .....	116
References	.....	120
Appendix A	ESSIL 291 resin and catalyst.....	133
Appendix B	Halbach Array .....	137
List of publications	.....	140

## List of Figures

Figure 2-1 Schematic of (a) isotropic and (b) anisotropic MREs .....	13
Figure 2-2 An elastomer chain segment: (a) relaxed, with a random coil conformation; (b) extended, due to an external stress.....	28
Figure 2-3 Stress-strain responses of a 50 phr carbon-black filled SBR subjected to a simple uniaxial tension (- - -) and to a cyclic uniaxial tension (—) with increasing maximum stretch every 5 cycles [154].....	32
Figure 2-4 Variation of complex Young's modulus with the dynamic strain amplitude for natural rubber vulcanisates containing various proportions of carbon black [157] .....	34
Figure 2-5 Variation of $\tan\delta$ with strain amplitude for natural rubber vulcanisates containing various proportions of carbon black [157] .....	34
Figure 3-1 Surface morphologies of carbonyl iron particles .....	42
Figure 3-2 The equal-biaxial bubble inflation test system.....	44
Figure 3-3 Membrane stress at the bubble pole [202].....	45
Figure 3-4 (a) A disc test specimen; (b) An inflated disc test specimen .....	46
Figure 3-5 Diagrammatic calculation of $E^*$ from stress-strain curves .....	48
Figure 3-6 Diagrammatic representation of stored energy from stress-strain curves .....	49
Figure 3-7 Diagrammatic representation of dynamic stored energy for different test procedures [200].....	50
Figure 4-1 SEM images of (a and a') isotropic and (b and b') anisotropic MREs	51
Figure 4-2 Engineering stress-stretch ratio curves for isotropic and anisotropic MREs from quasi-static testing.....	52

Figure 4-3 Plot of stress amplitudes versus fatigue life for isotropic and anisotropic MREs.....	53
Figure 4-4 Plot of maximum strain versus fatigue life for isotropic and anisotropic MREs .....	54
Figure 4-5 Stress-stretch ratio curves of isotropic MREs and anisotropic MREs for an engineering stress control fatigue test for selected cycles, $\sigma_a = 0.75$ MPa.....	56
Figure 4-6 Stress-stretch ratio curves for isotropic and anisotropic MREs at $\sigma_a = 0.9$ MPa.....	57
Figure 4-7 $E^*$ versus cycles for different stress amplitudes for isotropic and anisotropic MREs.....	58
Figure 4-8 Dynamic stored energy versus cycles for isotropic MREs and anisotropic MREs.....	59
Figure 4-9 Dynamic stored energy at failure versus cycles at failure for isotropic and anisotropic MREs .....	60
Figure 4-10 Damping loss factor versus cycles for isotropic MREs and anisotropic MREs .....	62
Figure 4-11 Damping loss factor for isotropic and anisotropic MREs at $\sigma_a = 0.9$ MPa.....	63
Figure 4-12 Typical failure modes for isotropic and anisotropic MREs: (a) and (b) isotropic MREs, quasi-static tests and fatigue tests at $\sigma_a = 1.4$ MPa, (c) isotropic MREs, fatigue tests at $\sigma_a < 1.4$ MPa and (d) anisotropic MREs, quasi-static tests and fatigue tests at all $\sigma_a$ .....	64
Figure 4-13 Surface morphology of a crack tip in a fatigue failed anisotropic MRE .....	65

Figure 4-14 SEM images of fracture surface for isotropic MREs at different $\sigma_a$ : (a) 1.4 MPa, (b) 1.05 MPa, (c) 0.9 MPa and (d) 0.75 MPa.....	65
Figure 4-15 SEM images of fracture surface for anisotropic MREs at different $\sigma_a$ : (a) 1.4 MPa, (b) 1.05 MPa, (c) 0.9 MPa and (d) 0.75 MPa.....	66
Figure 5-1 Surface morphologies of isotropic MREs containing different volume fractions of CI .....	70
Figure 5-2 Equi-biaxial quasi-static stress-stretch ratio curves of MREs with various CI contents. Samples were tested in the absence of a magnetic field .....	71
Figure 5-3 Equi-biaxial quasi-static stress-stretch ratio curves of MREs at stretch ratio below 1.1.....	72
Figure 5-4 Wöhler curves for SR and SR based MREs with different CI contents. Samples were tested in the absence of a magnetic field .....	73
Figure 5-5 Plot showing dependence of fatigue life on maximum strain for isotropic MREs with different CI contents. Samples were tested in the absence of a magnetic field.....	76
Figure 5-6 Changes in $E^*$ during the fatigue process for isotropic MREs containing different volume fractions of CI. Samples were tested in the absence of a magnetic field.....	77
Figure 5-7 Stress-strain curves for the first cycle induced by different stress amplitudes (CI = 15%).....	78
Figure 5-8 Stress-stretch ratio curves for SR based MREs with 20% and 30% CI during a fatigue test at $\sigma_a = 0.75$ MPa: (a) 20% CI, sample failed at 1430 cycles and (b) 30% CI, sample failed at 1314 cycles.....	79

Figure 5-9 Evolution of dynamic stored energy against cycles for isotropic MREs with different CI contents. Samples were tested in the absence of a magnetic field .....	82
Figure 5-10 Plots of stored energy density at failure versus cycles at failure for isotropic SR based MREs with different CI contents. Samples were tested in the absence of a magnetic field .....	83
Figure 5-11 Damping loss factor versus cycles for isotropic MREs with different CI contents. Samples were tested in the absence of a magnetic field .....	86
Figure 5-12 Plots of dissipated energy density versus cycles for isotropic MREs with different CI contents. Samples were tested in the absence of a magnetic field .....	87
Figure 6-1 Equi-biaxial fatigue test setup for fatigue testing in the presence of an external magnetic field provided by Halbach Array .....	91
Figure 6-2 Wöhler curves of MREs with various CI contents tested without and with a magnet .....	92
Figure 6-3 Plot showing dependence of fatigue life on maximum strain for isotropic MREs with different CI content. Samples were tested in the presence of a magnetic field .....	95
Figure 6-4 Stress-stretch ratio curves for MREs with 20% CI during a fatigue test at $\sigma_a = 0.75$ MPa, (a) with and (b) without magnetic fields applied .....	96
Figure 6-5 Evolution of $E^*$ during testing for MREs with various CI contents. Samples were tested in the presence of a magnetic field .....	98
Figure 6-6 Evolution of stored energy density versus cycles for isotropic MREs with different CI contents. Samples were tested in the presence of a magnetic field .....	100

Figure 6-7 Stored energy density at failure versus cycles at failure for isotropic MREs with different CI contents. Samples were tested in the presence of a magnetic field.....	100
Figure 6-8 Damping loss factor versus cycles for isotropic MREs with different CI contents. Samples were physically tested in magnetic fields.....	102
Figure 6-9 Plots of dissipated energy density versus cycles for isotropic MREs with different CI contents. Samples were physically tested in magnetic fields..	103
Figure 7-1 FTIR of CI and coated CI.....	107
Figure 7-2 Photo micrographs showing the surface morphologies of (a) uncoated and (b) coated CI particles .....	108
Figure 7-3 EDS analysis of uncoated and TEOS coated CI particles .....	109
Figure 7-4 TGA curves of pure and TEOS coated CI particles .....	110
Figure 7-5 Surface morphologies of MREs fabricated using (a) pure CI particles and (b) TEOS coated CI particles .....	111
Figure 8-1 The inflation of an anisotropic MRE showing inflation ellipses and failure direction diagrammatically .....	118
Figure A-1 Physical properties of ESSIL 291 resin.....	133
Figure A-2 Mechanical properties of ESSIL 291 resin.....	134
Figure A-3 Physical properties of ESSIL 291 catalyst .....	135
Figure A-4 Mechanical properties of ESSIL 291 catalyst .....	136
Figure B-1 A diagrammatic view of the Halbach Cylinder (Array) (dimensions in inches [*] and mm).....	137
Figure B-2 Variation in magnetic flux density in the plane of maximum flux density .....	138
Figure B-3 Variation of flux density in the vertical plane at the array centre ....	138

Figure B-4 Schematics of (a) an MRE curing mould, (b) the MRE curing mould fastened in a frame and (c) the frame together with the mould placed inside the Halbach Array ..... 139

## List of Tables

Table 2-1 Parameters of several different grades of CI used for MREs from BASF .....	11
Table 4-1 Quasi-static test results for isotropic and anisotropic MREs.....	52
Table 5-1 $UTS$ and $\lambda_{max}$ for MREs with various CI contents .....	71
Table 5-2 The gradient of S-N curves of each sample.....	73
Table 5-3 Values for $A_1$ and $A_2$ for a series of MREs with different CI contents .	74
Table 5-4 $\sigma_{FCon}$ for MREs with various CI contents .....	74
Table 5-5 $E^*$ just prior to failure of isotropic MREs with different CI contents (without magnetic fields) .....	81
Table 5-6 Values for $B_1$ and $B_2$ for a series of MREs with different CI contents .	84
Table 5-7 Values for $W_{DCon}$ for MREs with various CI contents.....	84
Table 5-8 Values of $\eta$ at failure for MREs with different CI contents (without magnetic fields).....	87
Table 6-1 Fatigue life of MREs tested with and without magnetic fields .....	93
Table 6-2 Values for $A_1$ and $A_2$ for MREs tested in magnetic fields.....	94
Table 6-3 Values of $\sigma_{FCon}$ for MREs in the presence of magnetic fields .....	94
Table 6-4 $E^*$ at failure for MREs tested with magnetic fields applied.....	99
Table 6-5 Values for $B_1$ and $B_2$ for MREs tested with magnetic fields applied..	101
Table 6-6 Values for $W_{DCon}$ for MREs with various CI contents subjected to magnetic fields .....	101
Table 6-7 Values of $\eta$ at failure for MREs with different CI contents (with magnetic fields applied) .....	104

# Chapter 1 Introduction

Research investigating the equi-biaxial fatigue behaviour of silicone based MREs is described in this thesis. In this chapter, initially the motivation for the research programme is introduced and the central research question is posed. The primary research aim derived from this question and the resulting specific objectives are outlined. The methodologies employed in achieving the proposed objectives are specified. The contribution of the thesis to the relevant research field is then outlined and finally the structure of the thesis, introducing briefly the content of each chapter, is described.

## 1.1 The motivation for the research programme

Magnetorheological (MR) materials belong to a category of smart materials that are developed to meet the increasing demands of modern society. Magnetorheological elastomers (MREs) are a variant of MR materials with mechanical properties that are reversibly and instantaneously controlled by an external magnetic field. The field dependence of the mechanical properties of MREs enables the design and manufacture of controllable elastomeric components, such as engine mounts and vibration control systems, that have the potential to enhance performance and handling in automotive applications. The mechanical properties of MREs have a very large bearing on whether components manufactured from them will find wide practical applications. Current physical characterisation of mechanical properties of MREs only focuses on uniaxial testing which involves static and dynamic tensile testing, compression testing and shear testing. However, the functionality required of most rubber components

means that they are subjected to repeated complex loading and high deformations in service. Uniaxial testing is consequently unrepresentative of actual component behaviour. In order to obtain more precise and accurate service life predictions, multi-axial testing methods are necessary.

In addition, for engineering applications, the dynamic mechanical properties of MREs, resulting from repeated complex loading, high speeds and temperature variation, necessitates fatigue life prediction and understanding fatigue properties of MREs to ensure that the materials will meet the heightened demands placed on them.

Previous research into non strain-crystallising rubbers (EPDM, SBR) found that when subjected to uniaxial and equi-biaxial loading, these materials displayed a limiting value of complex modulus ( $E^*$ ) at failure and conform to a dynamic stored energy criterion for predicting fatigue life.

Based on these considerations, the question posed by this research programme can be stated simply as:

How can fatigue resistance in an MRE subjected to equi-biaxial dynamic loading be characterised?

## **1.2 Aims and objectives**

The primary aim of this research is to investigate the dynamic equi-biaxial fatigue behaviour of MREs under cyclic loading. Consequently, the specific objectives to assist the achievement of the research aim of the project are to:

- 1) Evaluate the fatigue resistance of isotropic and anisotropic MREs under equi-biaxial cyclic loading.

- 2) Study stress-strain relations during cycling to provide an understanding of equi-biaxial fatigue in the material.
- 3) Investigate the influence of microstructure, the magnetic particle content and the presence of an external magnetic field on the equi-biaxial fatigue behaviour of silicone based MREs.
- 4) Determine if there is a limiting complex modulus ( $E^*$ ) for isotropic and anisotropic MREs at equi-biaxial fatigue failure.
- 5) Determine if a dynamic stored energy criterion can be used for predicting fatigue lives of MREs.

### **1.3 Research methodology**

The research methodology consists of the following aspects:

- 1) A review of current available literature including MREs, elastomeric material behaviour and fatigue of elastomers.
- 2) Fabrication of a series of MREs with different microstructures (isotropic and anisotropic) and a range of magnetic particle contents; fabricated in the absence of and in the presence of an external magnetic field.
- 3) Fatigue testing of fabricated MREs by subjecting the specimens to equi-biaxial cyclic loading induced by hydraulic inflation and deflation in the bubble inflation test system.
- 4) Production of Wöhler (S-N) curves from the test data by relating fatigue life to stress amplitude.
- 5) Analysis of the stress-strain behaviour of MREs during the fatigue process.

- 6) Calculation of variation in complex modulus ( $E^*$ ), dynamic stored energy ( $W_D$ ) and damping loss factor ( $\eta$ ) from the stress-stretch ratio curves obtained.
- 7) Derivation of general equations relating fatigue life to stress amplitude and dynamic stored energy.

## **1.4 Contributions to knowledge**

Research into MREs has been focused on the field-induced changes in their viscoelastic properties. There is a dearth of information about the fatigue properties of MREs although fatigue strength is arguably the most important characteristic required from modern materials, especially when their potential engineering applications are considered. This research provides the first insight into the fatigue behaviour of MREs under equi-biaxial cyclic loading. The first Wöhler curves for isotropic and anisotropic silicone based MREs were produced. This allows fatigue life prediction of MREs under various loading conditions.

Fatigue testing of MREs with a range of magnetic particle contents in the absence and in the presence of external magnetic fields provides a useful insight into the equi-biaxial fatigue behaviour of MREs in the situation where magnetic fields are switched on and off and also provides a reliable reference for the design of MREs with suitable particle contents to fulfil practical applications for the material.

Observation of changes in complex modulus with accumulation of cycles provided understanding of the mechanical deterioration that takes place during the fatigue process in MREs. The determination of a limiting value of complex modulus at failure can be used as an indicator of the timely replacement of MRE based components before failure occurs.

The dynamic stored energy criterion, as a fatigue life predictor for MREs, strengthens previous conclusions deduced for conventional elastomers and is also a novel contribution to the fatigue life prediction of smart materials.

## **1.5 Structure of the thesis**

A review of the published literature on MREs, elastomeric behaviour and fatigue of elastomers is summarised in Chapter 2. This chapter begins with a short description of the evolution of MREs followed by a detailed introduction to the composition, microstructure, properties (including factors influencing the properties) and potential applications of MREs. Basic insights into elastomeric behaviour and fatigue life prediction in elastomers are given at the end of Chapter 2.

Chapter 3 consists of a description of materials and methods employed in this research. An introduction to the fabrication process of isotropic and anisotropic MREs is described. The theory and procedure for the dynamic equi-biaxial fatigue testing of the materials are introduced. The analyses of fatigue testing data which include the production of Wöhler curves, the calculation of complex modulus, dynamic stored energy and damping loss factor are then described.

In Chapter 4, the equi-biaxial fatigue behaviour of MREs with different microstructures is introduced. Equi-biaxial fatigue behaviour of isotropic MREs with a range of magnetic particle contents in the absence and in the presence of external magnetic fields are described in Chapter 5 and Chapter 6 respectively. In each chapter, the results determined from experimentation and the corresponding discussions on the findings are given. The results mainly include characterisation of the microstructure of fabricated MREs, Wöhler curves for isotropic and

anisotropic MREs and changes in physical properties, such as stress-strain behaviour, complex modulus, dynamic stored energy and damping loss factor during the fatigue process. Preliminary research into interfacial layer designs with the aim of improving the fatigue resistance of MREs is briefly introduced in Chapter 7. The main conclusions drawn from the experimental results are summarised in Chapter 8. Recommendations for future work are also presented in this chapter.

# Chapter 2 Literature review

## 2.1 Evolution of MREs

Magnetorheological (MR) materials belong to a category of so-called smart materials whose rheological properties can be controlled rapidly and reversibly by the application of an external magnetic field [1]. Magnetorheological materials consist of micron sized magnetically permeable particles suspended in a non-magnetic medium. Upon application of a magnetic field, the rheological properties of these materials are rapidly and reversibly altered [2]. The mechanism responsible for this bulk effect is the induced magnetic interaction of particles within the matrix.

The history of magnetorheological materials can be traced to the early 20<sup>th</sup> century when Winslow discovered the electrorheological effect and patented a device to induce this effect in 1947 [3]. Later, Rabinow [4] discovered magnetorheological fluids (MRFs) at the US National Bureau of Standards in 1948.

Magnetorheological fluids are colloidal suspensions which can have their phase changed between liquid and solid under the control of a magnetic field. The quick response, rapid reversibility and controllable performance of MRFs make them excellent candidates in applications where controlled energy dissipation is required. Such applications include controllable dampers for use in vehicle suspensions [5-7], brakes and clutches for exercise equipment [8-10].

It has been reported that the Audi motor company has successfully resolved the long-standing conflict between cabin comfort and driving dynamics by replacing a conventional shock absorber fluid with a magnetorheological fluid system whose physical properties can be controlled by means of an electromagnetic field. This

highly innovative technology has already made its mark in the Audi R8 high-performance sports car, the TT and the Audi A1 Sportback concept car [11].

However, despite their good performance and few successful commercial applications, MR fluids exhibit distinct shortcomings, such as deposition, sedimentation, environmental contamination and sealing problems. These shortcomings hinder their wider application [12]. Magnetorheological elastomers (MREs) offer a feasible solution to overcome the disadvantages of MR fluids.

Magnetorheological elastomers are solid analogues of magnetorheological fluids. Compared with MRFs, the obvious advantage of MREs is that the particles do not undergo sedimentation with time and consequently exhibit stable MR performance. The thermal stability of MREs is also greater than that of MRFs and their resistance to degradation is higher. The response time of an MRE to the application of a magnetic field is less than milliseconds [13] and so is even superior to the rapid responses achieved using MRFs. MREs have a controllable field-dependent modulus while MR fluids have a field-dependent yield stress. MRFs are normally used in viscosity controllable devices whereas MREs are solid and could be used for stiffness controllable devices.

## **2.2 Composition of MREs**

### **2.2.1 Elastomeric matrix**

Various elastomers can be used as matrices to fabricate MREs with different properties. The polymer matrix plays an important role in the mechanical performance of MREs and the selection of a suitable matrix material is of significant importance when considering the possible applications and long-term stability of the composite. Up to now, silicone rubber has generally been chosen

as the matrix material in most MREs [14-22] due to its specific features that allow for the improvement of the magnetorheological effect [23]. It possesses a higher relative magnetorheological effect for a low zero-field modulus than alternative elastomers. Furthermore, it can be simply processed from liquid precursors and thus allows the magnetisable particles to be easily suspended and homogeneously dispersed in its structure. In addition, due to the low viscosity of silicone precursors, the particles can move in the matrix to readily form a columnar structure upon application of an external magnetic field during the curing process. However, the mechanical properties of silicone rubber cannot satisfy some application requirements [24]. For example, silicone based MREs are inappropriate for products where abrasion resistance or high tensile strength and stiffness are required.

In order to provide an MRE with heightened physical properties, natural rubber, which has a higher tensile strength, has been selected as a matrix material [21, 25, 26]. Chen et al. [25] produced natural rubber based MREs and found that unsurprisingly the mechanical properties in terms of tensile/tear strength, resilience factor and hardness for this compound are generally better than those of silicone rubber based MREs. For example, both the tensile strength and the tear strength of natural rubber based MREs were almost 10 times those of silicone rubber based MREs for the same content of iron particles and plasticiser. It was also found that for natural rubber based MREs, when the iron particle content was 80 wt% and the external magnetic flux density was 1 T, the field-induced increase in shear modulus reached 3.6 MPa which corresponded to a relative MR effect (see Section 2.4) of 133%. Ginder et al. [26] developed a family of MREs comprising micrometer-sized carbonyl iron particles (see Section 2.2.2) embedded

in natural rubber using conventional rubber mixing techniques. The field-dependence of mechanical properties of the resulting composites enabled the construction of controllable elastomeric components, such as suspension bushing, that are likely to prove advantageous in certain automotive applications. Despite the good physical properties of natural rubber, its high viscosity during processing makes it difficult for the magnetic particles to form chain-like structures when fabricated under a magnetic field [27].

Polyurethane (PU) is regarded as a promising matrix material for MREs in practical applications due to its uncomplicated processability and easily varied properties [27-31]. Polyurethane gels have low hardness (less than 10 Shore A) and low stiffness (Young's modulus can be as low as 0.1 MPa), which lead to relatively high property changes when an external magnetic field is applied to MREs fabricated from these polymers. Urethane elastomers have better thermal degradation stability than natural rubber and higher mechanical stability than silicone rubber. Typical PU elastomers are (AB)<sub>n</sub>-type multiblock copolymers comprised of alternating soft polyether or polyester polyol segments and hard segments based on isocyanates and chain extenders. The properties of PU elastomers, such as tensile strength, stiffness, friction coefficient and chemical resistance, can be easily adjusted by changing the types of soft and hard segments and the content of the hard segments [32].

In order to obtain MREs with a comprehensive range of properties, polymer blends [32-37] and block copolymers [38] were used as matrix materials. It was found [32] that under the same testing conditions, these MREs based on silicone rubber/PU had superior MR effects to those of MREs based on pure silicone rubber or polyurethane. When the weight ratio of PU/silicone rubber was set at 1

to 1 for these composites, a maximum modulus increase of 0.5 MPa could be achieved in a magnetic field of 0.2 T.

### 2.2.2 Magnetisable particles

Carbonyl iron (CI) is the most widely used magnetisable particle because of its excellent soft magnetic property (the term ‘soft’ relates to that class of metals or alloys which can be easily magnetized and demagnetized as opposed to ‘hard’ magnetic materials used for permanent magnets), high saturation magnetisation and spherical shape. Hence CI is appropriate for numerous MR applications [19, 39-41]. Carbonyl iron is a highly pure iron, prepared by the chemical decomposition of purified iron pentacarbonyl. It usually has the appearance of grey powder composed of spherical microparticles. Most of the impurities in the carbonyl iron are carbon, oxygen and nitrogen. BASF invented carbonyl iron powder in 1925 and claim to be the world’s leading producer. The parameters of several commonly used carbonyl iron powders supplied by BASF are listed in Table 2-1.

**Table 2-1 Parameters of several different grades of CI used for MREs from BASF**

<b>Grade</b>	<b>Fe min. (%)</b>	<b>C max. (%)</b>	<b>N max. (%)</b>	<b>O max. (%)</b>	<b>d50<sup>1</sup> value(microns)</b>
CC	99.5	0.05	0.01	0.18–0.35	3.8–5.3
CM	99.5	0.03	0.01	0.1–0.25	7.0–9.5
CS	99.5	0.03	0.01	0.12–0.30	6.0–7.0
CN	99.5	0.03	0.01	0.10–0.25	6.5–8.0

Besides carbonyl iron, other magnetic particles such as iron sand [42], metallic iron [43], Fe<sub>3</sub>O<sub>4</sub> [39, 44], Fe nanowires [45] and nickel [46, 47] have also been

---

<sup>1</sup> d50 is also known as the median diameter or the medium value of the particle size distribution, it is the value of the particle diameter at 50% in the cumulative distribution.

used in MREs. There are some MREs with hard magnetic particles like those that include  $\text{BaFe}_{12}\text{O}_{19}$  or  $\text{SrFe}_{12}\text{O}_{19}$  [48] and NdFeB particles [49]. However, these materials remain magnetised after the external magnetic field is turned off [50]. It is apparent from the available literature [17, 51] that the particle concentration should be limited to a certain range (normally 10 vol%–50 vol%) dependent on the matrix material used. High magnetic particle concentration influences the long-term stability of MREs, which may be attributed to a large amount of oxygen on the surface of the particles [52].

### **2.3 Microstructure of MREs**

MREs can be fabricated either in the absence of, or in the presence of a magnetic field during the curing process. The former technique results in isotropic or homogenous MREs [32, 35, 53-57] while the latter results in anisotropic or structured MREs [17, 58-64] as shown schematically in Figure 2-1. When an external magnetic field is applied, the filler particles are magnetised and magnetic dipoles are formed. While the elastomer still has a low viscosity, the dipoles can turn and move slightly along the magnetic field lines, forming chain-like structure in the composite. The distribution of magnetic particles in MREs is influenced by many factors, such as the magnetic interaction forces between particles, orientation and magnetic field strength, the volume fraction of particles and temperature. It was found that the particles can form separate chains, three-dimensional network structures or even more complicated structures where the particles have multiple interaction points [65, 66]. These aligned composites are strongly anisotropic in their mechanical, electrical, magnetic and thermal behaviour [67].

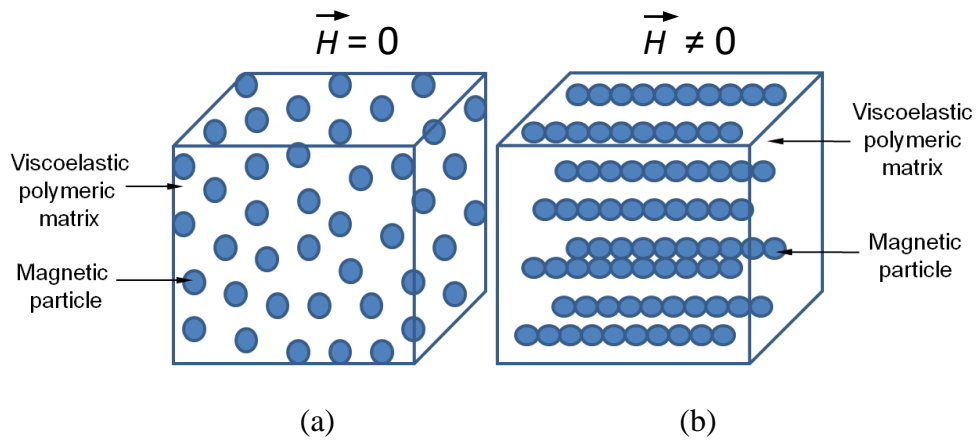


**Figure 2-1 Schematic of (a) isotropic and (b) anisotropic MREs**

Davis [65] stated that the alignment of the particles does not affect the zero-field shear modulus of an MRE composite. Davis concluded from his finite element analysis that the zero-field shear modulus perpendicular to the particle chain of aligned composites was no larger than the modulus measured for the same material with a homogeneous distribution of particles.

Boczkowska and Awietjan [68] found that different iron particle volumes led to different formations of the microstructure and the resultant microstructure had a significant influence on the elastic properties of the composite material. Also, the orientation of the iron particles into aligned chains was possible for lower volume contents (11.5 vol% or less) of ferromagnetic fillers. A high carbonyl iron volume content (33 vol%) in the matrix led to the formation of more complex microstructures similar to three-dimensional lattices. They [62] also found that the field strength used during curing had a significant effect on the microstructure of the MREs and, in consequence, on their properties. Experimental results have shown that the application of higher magnetic fields ( $\geq 300$  mT) during curing lead to higher values of the anisotropy coefficient and to the formation of wider

particle chains consisting of a larger number of particles. At the same time, the spaces between the chains appeared to be greater.

Choi [69] investigated the effect of curing time on the microstructure and properties of anisotropic MREs. Microscopy observation showed that the alignment of the magnetic particles occurred mainly in the early stages of the curing process and once the particles were aligned, their position did not change with increases in curing time. However, samples cured for periods shorter than the solidification time of the matrix elastomer exhibited lower shear moduli.

Although anisotropic MREs can be produced with particles aligned into columnar chains in the matrix, the conventional methods of fabricating MREs under an external magnetic field have many shortcomings which greatly limit their industrial application. Firstly, conventional rubber compounding and mixing equipment must be modified to include a magnetic field during crosslinking. Secondly, thick section MREs cannot be practically fabricated because the magnetic flux density decreases sharply as the thickness of the MRE increases. Thirdly, the chain direction of anisotropic MREs must be carefully considered when the material is to be used in a particular device [53].

## **2.4 Properties of MREs**

MREs are viscoelastic materials. MRE properties are generally characterised and described by equations typical for viscoelastic materials, with additional parameters describing the influence of external magnetic fields on the rheological properties. The change in viscoelastic properties of an MR material when subjected to a magnetic field is defined as the MR effect, which is one of the most important and most extensively studied properties of MR materials. It was found

[70] that the MR effect is related to the magnetic particles tendency to change their position under the influence of an applied magnetic field. The magnetic field induces dipole movements in the ferromagnetic particles, which tend to obtain positions at a minimum energy state. The movement of the particles introduces deformations in the elastomer matrix, which results in increases of shear modulus and stiffness in the MREs. In addition, the interactions between particles in a magnetic field cause their attraction to each other, which also introduces a deformation in the elastomeric matrix and consequently increases the stiffness of the material and its shear modulus.

The MR effect can be described by both absolute and relative MR effects. Absolute MR effect ( $\Delta G$ ) is the difference between the maximum shear modulus ( $G_{max}$ ) achieved in the presence of a magnetic field and the shear modulus obtained without a magnetic field ( $G_0$ , also termed the zero field modulus). The absolute MR effect can be described by the equation:

$$\Delta G = G_{max} - G_0 \quad (2.1)$$

The relative MR effect ( $\Delta G_r$ ) is the ratio of the absolute effect to the zero field modulus ( $G_0$ ) and is given by:

$$\Delta G_r = \frac{\Delta G}{G_0} \cdot 100\% \quad (2.2)$$

It is known from the available literature that the maximum increase in the shear modulus due to the MR effect is about 50–60% of the zero-field modulus, depending on the matrix elastomer [67]. For harder elastomers like natural rubber, the relative increase has typically been 30–40% [71]. The maximum increase in the shear modulus is obtained at magnetic saturation when the filler particles are fully magnetised. According to current research, anisotropic MREs produce much

larger MR effects than those of isotropic MREs [26, 72]. In addition to the material's microstructure, the MR effect also depends on many other factors such as the content of magnetic particles, the magnetic field strength, the frequency of oscillations and the amplitude of the applied strain and so on.

In the past decade, most of the research into MREs has focused on the field-induced shear property [33, 73-75] of the material. Changes in the rheological properties are usually described by the shear modulus: storage modulus ( $G'$ ) and loss modulus ( $G''$ ) [76-78].  $G'$  is defined by the ratio of the elastic stress to strain and it describes the amount of strain energy that is temporarily stored during deformation and can be later recovered.  $G''$  is expressed by the ratio of viscoelastic stress to strain and it represents the energy dissipated in the form of heat. Moduli  $G'$  and  $G''$  are dependent on the frequency of oscillation, stress ratio and temperature. The higher the frequency of oscillation, the higher are the values of  $G'$  and  $G''$ . A rise in temperature generally leads to a decrease in  $G'$  and an increase in  $G''$  [79].

The ratio of  $G''$  to  $G'$  is called the loss angle ( $\tan\delta$ ) which determines the damping properties of viscoelastic materials. In MREs, the energy dissipation mainly comes from the matrix and the interfaces between the matrix and the particles [40]. Yang et al [80] developed a theoretical model to analyse the damping behaviour of MREs and found that the intrinsic damping plays a dominant role when the CI content and strain amplitude are low. However, the interface damping is predominant at higher strain amplitudes or higher CI contents. MRE performance for various devices is highly dependent on the damping properties of the MRE materials used. It is known [81] that for MRE based vibration isolators, when the excitation signal is in the resonance frequency band of the system, more vibration

energy can be dissipated by increasing the loss factor of the MRE, which is good for suppressing increases in amplitude. In the vibration isolation frequency band of the system, a low loss factor can lead to better vibration isolation effectiveness. The study of Sun et al [82] unsurprisingly indicated that the vibration reduction effect clearly increased when the damping ratio reduced from 0.05 to 0.005. Hoang et al [83] also observed this increased tendency of vibration reduction effect as the damping ratio reduced from 0.35 to 0.05. Although in some studies it is stated that MR effect also includes a magnetically induced change in damping properties [84], most research has shown that the magnetic field does not have a significant influence on the damping properties of MREs [54, 63, 81, 85].

As elastomer based composites bear high compressive loads and so changes in the mechanical properties of MREs under compression have also been investigated [17, 20, 55, 67, 86, 87]. The magnetically induced reversible change in the composite stiffness under compression has also been included in defining the MR effect. Quasi-static compression tests [17, 86] showed that the static stiffness of various MREs increased in a magnetic field and the field-induced change in the modulus is dependent on the field strength. The dynamic compressive behaviour of MREs has not yet been studied extensively. Kallio and co-workers [67] found that the stiffness of aligned MREs under dynamic compression loading increased with increasing testing frequency but decreased with increasing strain amplitude. Koo et al [88] investigated the dynamic compression properties of MREs under cyclic loading and proposed a phenomenological model to explain the experimental results.

The mechanical properties of MREs were also determined under tension deformation. Schubert and Harrison [19] compared the behaviour of silicone

based MREs containing carbonyl iron subjected to compression, tension and pure shear deformation at large strains. They found that the highest MR effect was achieved under uniaxial tension, where the anisotropic MREs with 30% volume fractions of iron exhibited a 284% relative increase in moduli, hence almost three times stiffer than in the no-field state. Sun et al [72] conducted both dynamic (low strain) and quasi-static tensile tests (high strain) on isotropic and structured *cis*-polybutadiene rubber based MREs with various iron particle contents. It was shown that the outcomes of static testing differed from dynamic tension measurements due to a different mechanism of energy loss. Zhou and Li [89] studied the dynamic behaviour of an MRE under uniaxial deformation and revealed that the mechanical behaviour was nonlinear and the field-dependent behaviour of the MRE was associated with the applied frequency. The static and dynamic tensile testing of MREs with particles oriented in the form of chains have shown the composites to exhibit much higher Young's moduli by comparison with MREs having isotropically distributed particles [84].

## **2.5 Factors that influence the properties of MREs**

### **2.5.1 Magnetic field strength**

It is well known that the presence of external magnetic fields can remarkably increase the shear strength of both isotropic and anisotropic MREs. It has been reported [63] that a maximum increase in shear modulus is obtained at magnetic saturation when the filler particles are fully magnetised. The saturation of MRE composites starts at a magnetic flux density of about 0.8 T and increasing the flux density over 1 T does not increase the shear modulus further [71]. At low or moderate magnetic flux densities, the increase in the modulus is shown to be

proportional to the field strength [88, 90, 91]. Gordaninejad et al [86] studied the behaviour of thick (6.35–25.4 mm) MREs under quasi-static compression and shear deformation. It was observed that with the increase in the applied magnetic field, the field induced changes in modulus varied from exhibiting a linear behaviour at lower applied magnetic fields to having a nonlinear response at higher magnetic fields.

### **2.5.2 Magnetic particles**

As an important component in the fabrication of MREs, both the type of magnetisable particles and their size and shape have an influence on the properties of the material. Demchuk and Kuz'min [76] studied the effect of magnetic particle size on the shear storage and loss modulus of isotropic and aligned MREs. It was found that, in the absence of a magnetic field, the modulus of MREs with larger particles (13  $\mu\text{m}$ ) was less than that with smaller particles (3.5  $\mu\text{m}$ ). Under a magnetic field, the situation was reversed, because the magnetic field induced modulus increased in the MREs with larger particles and significantly exceeded that of the MREs with smaller particles. Alternatively, the loss factor decreased as a result of either the stronger magnetic field or increased particle size. Boczkowska et al [92] used three types of ferromagnetic particles with average particle sizes ranging from 1 to 70  $\mu\text{m}$  to fabricate MREs and found that the highest MR effect was achieved for samples with 6–9  $\mu\text{m}$  carbonyl iron powder when the volume fraction of particles was maintained at 11.5%. Lokander et al [54, 75] studied isotropic MREs prepared by using large irregular shaped iron particles and fabricated in the absence of magnetic fields. They found that the absolute MR effect of this kind of MRE increased exponentially with increasing

iron concentration up to a critical particle volume concentration (approximately 38 vol%), independent of the matrix material. The modulus of these MRE composites increased as much as 0.4 MPa for a magnetic field of 0.24 T. The composition of carbonyl iron particles also had an influence on the mechanical properties of MREs [93]. The samples with low carbon contents showed higher magneto-induced storage shear moduli than those of samples with high carbon contents.

In addition, the concentration of magnetic particles significantly influences the properties of MREs. Generally, the content of magnetisable particles should be higher than 50 wt% (about 12.3 vol%) in order to obtain a significant MR effect. But deterioration of the mechanical properties is a key issue that affects the practical application of MR elastomers. Generally, the MR effect on shear modulus was found to increase with increasing volume percentage of iron. From the available literature [65] it appeared that the maximum MR effect on composite stiffness was obtained when the filler content was nearly 30 vol%. However, high iron concentration deteriorates the mechanical properties and influences the long-term stability of MREs [75].

### **2.5.3 Additives**

To some extent, additives can also influence the properties of MREs. It was found that additives such as paraffin oil [54] can reduce the stiffness of a matrix and thus produce a stronger MR effect. Gong et al [53] found that when silicone oil was added to the composite, the magnetic particles formed a kind of self-assembled microstructure which was composed of additives and particles dispersed in the matrix. When this kind of MRE was exposed to a magnetic field, the particles in

the microstructure were magnetised and moved slightly by the lubrication of the additive to form a regular configuration, which resulted in a high MR effect. In addition, the presence of silicone oil could improve the wetting of iron particles, increase the adhesion between them and the elastomer and also prevent the particles from aggregating into larger clusters [35].

In order to develop new MREs with high MR effects, good tensile strengths and relatively low damping ratios, Chen [94] selected carbon black as an additive to modify and improve the mechanical properties of natural rubber based MREs. Carbon black was chosen because of its importance as a reinforcing filler in polymer engineering, especially for rubber compounds. The experimental results demonstrated that the addition of carbon black into the matrix led to a well-bound microstructure and resulted in a high MR effect, low damping ratio and improved tensile strength. These results can hopefully be applied to solve the shortcomings existing in conventional MREs.

The MR effect of MREs can be substantially improved by incorporating certain kinds of plasticisers. In particular, the research of Lokander [54] has shown that the relative MR effect of isotropic MREs can be increased by the addition of plasticiser. Wu [95] showed that diisooctyl phthalate (DOP) plasticisation can enhance both the absolute and relative MR effect of PU based MREs simultaneously. With 70 wt% carbonyl iron and 15 wt% DOP, the absolute and relative MR effects on anisotropic PU MREs were 3.5 and 58 times respectively that of the PU MRE without the plasticiser at the same iron content.

Gong et al [81] selected polycaprolactone (PCL) as a temperature controllable component in the *cis*-polybutadiene rubber based MREs. As the PCL is a phase change material, it can transfer from a semi-crystalline solid to a liquated soft

material when the surrounding temperature is increased above the PCL melting point and consequently the damping properties of MREs can be controlled by varying the temperature.

#### **2.5.4 Interfacial adhesion**

The conventional procedure for fabricating MREs has been to directly mix the magnetisable particles into the elastomer matrices prior to vulcanisation, in the same way as manufacturing carbon black-filled rubber. The problem with this is the unsatisfactory dispersion of magnetisable particles in the rubber matrix [96]. It is generally conceded that, when mixing an inorganic substance with an elastomeric matrix, incompatibility between the materials may lead to poor stability and diminished mechanical properties of the composite. This situation is analogous to polymer blends and, in most cases, the two components phase separate into discrete domains. In order to produce adhesion and promote the formation of finely divided inorganic domains into polymer matrices, it is common to introduce adhesion promoters which are capable of reacting with both the inorganic filler and the polymer matrix, thus creating chemical or physical bonds between the two components and improved homogeneity of the blends is achieved. Various coating methods including in-situ polymerisation, solvent evaporation and the sol-gel method have been used to modify the surface of magnetic particles and consequently improve their dispersion in polymer matrices. Li et al [97] introduced an emulsion polymerisation in modifying the surface of carbonyl iron particles by using methyl methacrylate (MMA). It was shown that the formation of poly (methyl methacrylate) (PMMA), deriving from the emulsion of its monomer MMA, between magnetic particles and an elastomer matrix can

effectively increase the interfacial adhesion between them and promotes particle dispersion. Consequently, the MRE samples with PMMA coated particles showed larger storage moduli, smaller loss factors and smaller Payne effects. Fuchs et al [98] introduced the atom transfer radical polymerisation (ATRP) technique for surface polymerisation of iron particles with fluorinated styrene as a monomer. It was shown that silicone based MREs with surface coated iron particles have a higher oxidation stability than MREs with untreated iron particles. Fan et al [85] selected maleic anhydride (MA) as the compatibiliser to modify the interface of MREs with improved damping properties. The compatibility between the magnetic particles and rubber matrix can be enhanced with an increase of MA content. The enhancement of the bond between the two phases resulted in a change of mechanical properties: an increase in shear storage modulus, a reduction of loss factor, a more stable loss factor, enhancement of tensile strength and a reduction of the MR effect.

Among various modification approaches, the bifunctional coupling agent treatment using organosilanes based coupling agents is the most successful and cost effective way to treat the inorganic fillers and provide superior bonding at the polymer/filler interface. The molecules of the organosilanes carry two different reactive groups on their silicon atom. The hydrolysable groups (such as methoxy, ethoxy or acetoxy) can interact with inorganic materials and the organofunctional groups (such as amino, vinyl or sulphide) also allow them to react with the rubber matrix. Therefore, they can act as a 'bridge' between the inorganic and organic materials to provide better bonding at interfaces, improve filler dispersibility in the polymer matrix and enhance the properties of the composite [99].

Some research has been carried out on modification of carbonyl iron particles using silane coupling agents and the surface modified particles were used as fillers in silicone rubber [57, 100] and polyurethane rubber [96] based MREs. The results showed that the silane coupling agents improved the dispersion of iron particles and the interfacial interaction between particles and the matrix. The mechanical and damping performance of MREs increased to some extent due to increased dispersion and interaction. However, the coupling agents were disadvantageous in terms of improving the MR effect. This is because the uniform dispersion of iron particles decreased the size of iron agglomerates, which was considered to decrease the MR effect.

### **2.5.5 Frequency**

MREs have mostly been tested at relatively low frequencies ranging between 1 Hz and 50 Hz to measure the changes in dynamic shear modulus induced by external magnetic fields [54, 71, 75]. Ginder et al [101] used a tuned vibration absorber to measure the dynamic shear modulus of MR elastomers containing 27% volume fractions of iron particles in a frequency range over 1 kHz and found that the MR effect was also substantial at higher frequencies.

Zhou and Li [89] found that the field-dependent behaviour of anisotropic silicone based MRE was associated with the applied frequency. In the low frequency range (10 Hz, 50 Hz and 80 Hz), the mechanical properties of the MRE changed only slightly with the applied magnetic field; in the moderate frequency range (100 Hz and 110 Hz), the field-dependent properties were more evident and they were highly nonlinear; in the high frequency range (120 Hz and 125 Hz), the field-dependent properties deviated from those of the moderate frequency range, which

caused the area enclosed by the hysteresis loops in the two measured acceleration domains, to decrease in size with the applied magnetic field.

### **2.5.6 Strain amplitude**

The field induced mechanical changes of MREs also depend on the strain amplitude applied. This is attributed to the dependence of the magnetic forces on the distance between the dipoles. In general, the shear modulus of aligned MREs decreases with increasing strain [37, 54, 101]. The decrease of storage shear modulus with the strain amplitude was attributed to the molecules of the rubber matrix beginning to slide when the shear strain increased. Due to the increase of the distance between the ends of two molecule chains, the chains were more easily separated when the shear stress was applied [37]. The strain-dependent behaviour of shear modulus was also related to the opening of the network structure of aggregates when the strain increased, which is common to particle-reinforced vulcanised rubbers and is known as the Payne effect [102].

The maximum MR effect based on shear modulus can be obtained at relatively small strain amplitudes of 1–2%. In this strain range, the distance between the particles in a chain is minimised and the magnetic interaction is at its strongest. When the external mechanical stress exceeds the magnetic stress holding the particle chain together, the particle chain starts to yield and the MR effect diminishes. Shiga et al [103] found that the shear storage modulus starts to decrease gradually with increasing strain when the strain amplitude is increased over 1%. Jolly et al [71] noticed a pronounced drop in the MR effect and a corresponding increase in field dependent energy dissipation ( $\tan\delta$ ) at strain levels above 1–2%. Lokander et al [54, 75] studied the dynamic shear modulus for

isotropic MR elastomers with different filler particles and matrix materials. The modulus was measured with strain amplitudes of up to 11%, at frequencies of 2, 10 and 50 Hz, both with and without an external magnetic field applied. They found that the MR effect of the isotropic MREs decreased rapidly with increasing applied strain within the measured strain range, independent of the testing frequency.

## **2.6 Applications of MREs**

The field dependent rheological response of MREs offers numerous potential engineering applications such as adaptive tuned vibration absorbers [83, 104-110], vibration isolators [111-120], dampers [121] and stiffness tuneable mounts [67]. For example, Fuchs et al [105] invented a tuneable vibration isolation device comprising a magnetorheological elastomer. The vibration isolator can be constructed to provide shock absorption in one, two or three directions. Coupling the tuneable device to a sensor feedback and a control system provides fast and accurate vibration isolation and energy dissipation for shock events in a variety of applications. Deng and co-workers [11, 63] developed an adaptive tuned vibration absorber (ATVA) based on the unique characteristics of MREs and the modulus of the absorber was controlled by an applied magnetic field. Compared with the traditional tuned vibration absorber, the absorption capacity of the newly developed ATVA was enhanced and could achieve reductions as high as 25 dB. Hoang et al [83] prepared a conceptual ATVA with soft MREs for vibration reduction of vehicle power train systems. As the elastic moduli of these soft MREs increased significantly due to the MR effect, the ATVA alternative worked effectively over a wide frequency range instead of a narrow bandwidth as is the

case for a conventional dynamic absorber. Opie and Yim [111] proposed a variable stiffness vibration isolator (VSVI) and experimental results showed that the MRE isolator reduced the resonances and payload velocity by 16–30%.

The Ford Motor Company has patented an automotive bushing employing a magnetorheological elastomer [122, 123]. The stiffness of the bushing is adjusted based on the state of the automobile's power train to reduce suspension deflection and improve passenger comfort. In 1999, they also patented an elastomer control module which includes a magnetorheological elastomer [124].

MREs have also been used as basic materials to develop adaptive seismic isolators for civil engineering applications [125-128]. The results showed that the proposed system has the potential to outperform the conventional system in reducing the responses of the structures during seismic excitations [127].

## **2.7 Elastomer behaviour**

An elastomer is defined as a crosslinked amorphous polymer above its glass transition temperature [129]. Elastomers are polymers which have the property of hyperelasticity. They are made of long chains of atoms, mainly carbon, hydrogen and oxygen, which have a degree of crosslinking with their neighbouring chains. It is these crosslinking bonds that pull the elastomer back into shape when the deforming force is removed [130]. Under normal conditions, the long chain molecules making up an elastomeric material irregularly coiled. With the application of force, however, the molecules tend to straighten out in the direction in which they are being pulled. Upon release, the molecules spontaneously return to their normal compact, random arrangement [131].

### 2.7.1 Nonlinear elasticity

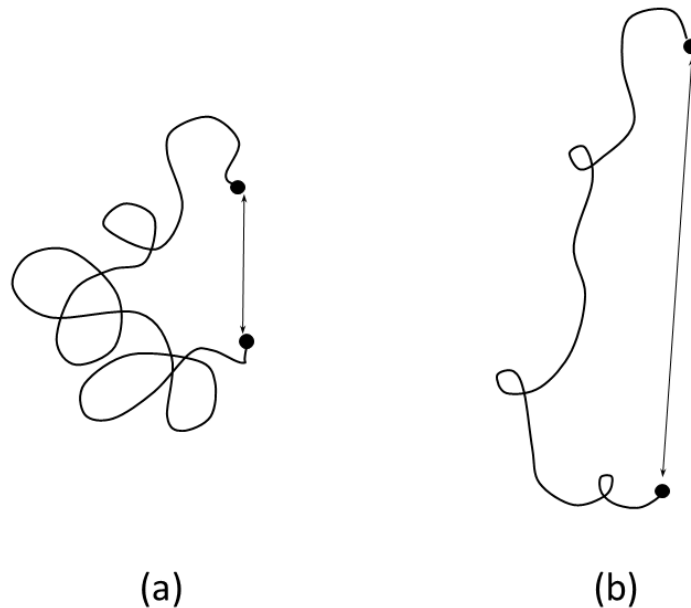


**Figure 2-2 An elastomer chain segment: (a) relaxed, with a random coil conformation; (b) extended, due to an external stress**

One of the most important properties of elastomers is their ability to undergo high levels of elastic deformation, which means they can undergo pronounced and reversible stretch [132]. In the relaxed state the polymer chains of an elastomer form random coils with an average end-to-end distance  $r_0$ , as shown in Figure 2-2 (a). Under external loading, the chains are stretched out and oriented to a more linear form which has an average end-to-end distance  $r$ , as shown in Figure 2-2 (b). The distance between the ends of chain segments can be increased corresponding to strains of a few hundred percent. This explains the ability of elastomers to achieve very high strains. With unloading, the stretched chains return to the coil like state and this behaviour can be explained by the law of thermodynamics, in that the retractive stress of an elastomer arises through the reduction of entropy rather than through changes in enthalpy. It is this reduced entropy that makes

rubber bands ‘snap back’ when released (returning them to their position of maximum entropy) [133].

Unlike metals, elastomers generally exhibit non-linear stress-strain behaviour. The stiffness changes during extension and so does not comply with Hooke’s Law as for metals that are strained within their elastic limit. There are two main approaches that can be used to describe the hyperelastic behaviour of elastomers. These are the molecular or statistical theory and one of numerous phenomenological approaches. The development of statistical theory was advanced markedly by Treloar [134]. This theory is also known as the kinetic theory since deformation is related to thermal motions of molecules and analogous to kinetic theories of gases. Since rubber is assumed to possess maximum entropy (maximum randomness) in the unstrained state, the work required to deform a rubber elastically is considered to be related to the decrease in entropy when the molecules are forced to take up less probable configurations [135]. However, the phenomenological approaches are not reliant on the arrangement of the molecular structure but are based on mathematical descriptions of the stress-strain behaviour. These theories attempt to represent the large strain behaviour of unfilled elastomers while endeavouring to extend the concepts to describe the behaviour of filled elastomers. Major contributions to phenomenological approaches were made by Gent [136], Mooney [137], Rivlin [138] and Ogden [139, 140].

### **2.7.2 Viscoelasticity**

An elastomer simultaneously exhibits a combination of instantaneous elastic deformation and time dependent viscous behaviour [141]. Generally, viscoelasticity refers to both time and temperature dependent mechanical

behaviour. In service, elastomers can experience some or all of the following effects: stress relaxation, creep, set, hysteresis (energy loss during cyclic deformation) and heat generation, which are manifestations of the viscous properties of elastomers [142].

Stress relaxation is defined as the decline in stress over time at a constant deformation. Conversely, when a rubber sample is subjected to a constant load, an increase in the deformation takes place over time and this behaviour is called creep. Both responses can be explained by migration of entanglements and thermally induced chain vibration [143].

Set is the residual deformation of an elastomeric sample after it has been deformed and the deformation force or displacement is removed [144]. The magnitude of set depends on the amount of filler, the maximum elongation of the specimen prior to loading and duration of the deformation. For unfilled elastomers, the magnitude of the residual strain is negligible. However, set is significant in filled compounds and is an important parameter in maintaining component functions, for instance when elastomers are used in efficient seals. Set is normally expressed as a percentage of the applied deformation for a particular recovery time.

Particle-reinforced elastomers exhibit a marked hysteretic response in the loading-unloading process in uniaxial tension, compression or shear. The difference in the stresses observed in a cycle corresponding to the same strain level when loading and unloading depends primarily on the amount of filler in the compound [145]. The difference is negligible for unfilled rubbers but becomes significant for elastomers with high filler content. The stress difference is greatest during the first

loading-unloading cycle and approaches a constant value after a number of cycles. The strain energy enclosed in the hysteresis loop is dissipated as heat.

### **2.7.3 Mullins effect**

Filled elastomers present a loss of stiffness leading to cyclic stress softening and stress hysteresis. This phenomenon is named after the researcher who conducted an extensive study into carbon black filled rubber vulcanisates and hence is termed the Mullins effect [146]. The most important assumption of Mullins's model is that the reloading path is the same as the unloading path provided the maximum strain of the first loading is not exceeded, as shown in Figure 2-3. In tests with constant displacement amplitude, the stress reduction between successive loading cycles is especially significant during the first and second cycles and becomes negligible after about 5 to 10 cycles (and sometimes more cycles depending on the type and content of fillers) for many rubbers, depending on the amount of filler and maximum extension [147].

Different physical interpretations have been provided in order to explain the softening phenomenon. The stiffness reduction observed was initially attributed solely to the rupture of filler clusters and to the separation of weak polymer chains from the fine particle fillers [148]. However, the concept of rubber-filler interaction is not on its own sufficient to explain this phenomenon since the effect is present in unfilled as well as reinforced elastomers. Other micro-mechanical interpretations have been advanced such as chain slipping [149], bond rupture [150, 151], disentanglement [152] and more complex composite structure formation [153].

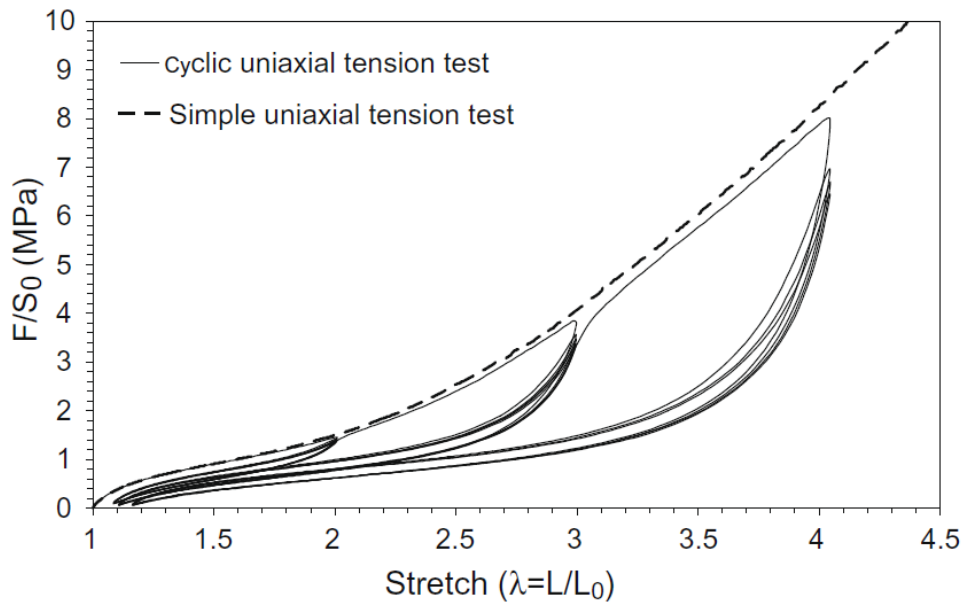


**Figure 2-3 Stress-strain responses of a 50 phr carbon-black filled SBR subjected to a simple uniaxial tension ( - - - ) and to a cyclic uniaxial tension ( — ) with increasing maximum stretch every 5 cycles [154]**

Healing from the Mullins effect has been observed through the recovery of permanent set or a return to the initial values of the stress at fixed strains or of the complete stress-strain response [154]. Mullin [146] studied the recovery effect in a filled natural rubber which was stretched up to 420%. By measuring the stress at elongation of 200% and comparing to that measured on the material stretched to the same elongation for the first time after various recovery periods, he found that the recovery showed a dependence on temperature. At room temperature, less than 20% recovery was observed while an 80% recovery was reached at 100 °C after two days. Laraba-Abbes et al [155] showed a complete recovery of the softening (stress-strain response similar to the virgin material) of a carbon-black filled natural rubber exposed to 95 °C *in vacuo* during 48 hours. At high temperatures, Harwood and Payne [39] studied the stress-recovery in unfilled vulcanised natural rubber with different types of crosslinking. After a first cyclic load, the materials

were heated *in vacuo* at 100 °C for 24 hours. When the samples were stretched for a second time and the stress-strain responses compared with the initial one, it was found that the recovery was almost complete for monosulfide crosslinked and carbon to carbon crosslinked vulcanisates.

#### **2.7.4 Payne effect**

The modulus of filled rubbers decreases with increasing applied dynamic strain up to intermediate amplitudes (as shown in Figure 2-4). Systematic investigations into this behaviour were carried out by Fletcher and Gent in the early 1950's [156]. Later, more comprehensive works were published by Payne [157-160]. Consequently, this phenomenon has been customarily referred to as the Payne effect. The Payne effect is of great importance to the tyre industry, because the non-linearity it describes is in the range of strain most frequently encountered in tyre operations. The Payne effect depends on the filler content of the material and vanishes for unfilled elastomers.

Differing from the Mullins effect which occurs under large deformation, the Payne effect is observed under cyclic loading conditions with small strain amplitudes at frequency of 0.1 Hz and above [157, 161, 162]. Above approximately 0.1% strain amplitude, the storage modulus decreases rapidly with increasing amplitude. At sufficiently large strain amplitudes, the storage modulus approaches a lower bound which is close to that of unfilled rubber. In the region where the storage modulus decreases, the loss modulus shows a maximum, so a maximum  $\tan\delta$  value is observed at a strain corresponding to the inflexion point on the Young's modulus curve, as shown in Figure 2-5.

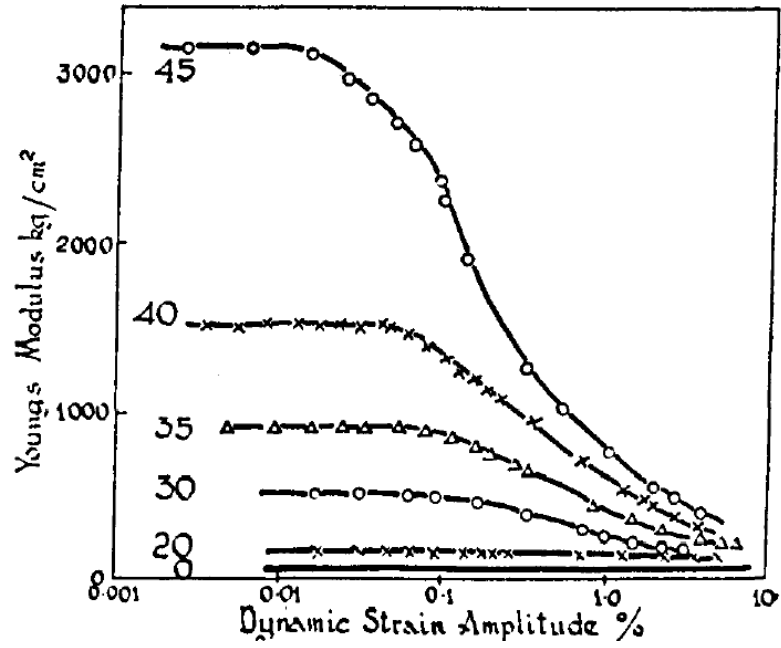


Figure 2-4 Variation of complex Young's modulus with the dynamic strain amplitude for natural rubber vulcanisates containing various proportions of carbon black [157]

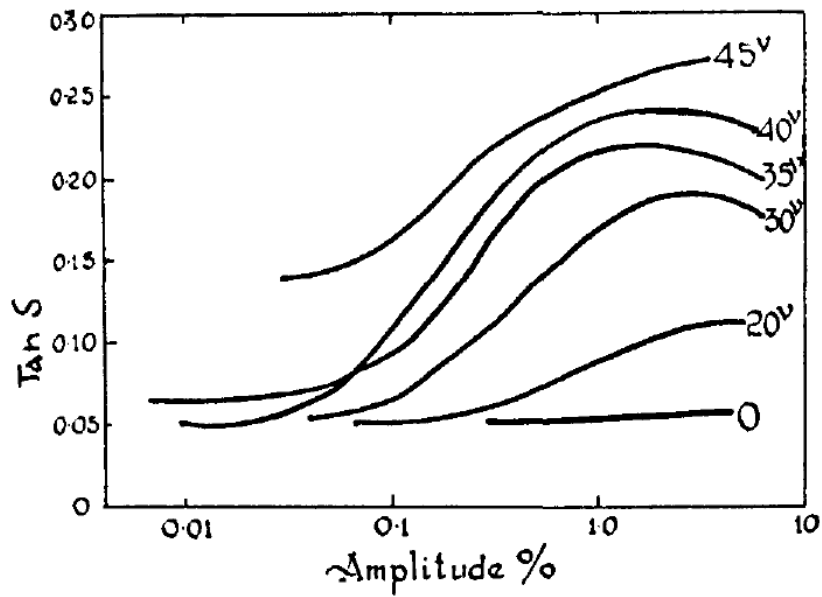


Figure 2-5 Variation of  $\tan \delta$  with strain amplitude for natural rubber vulcanisates containing various proportions of carbon black [157]

However, there is still controversy on the question of what mechanisms are really responsible for this effect. Payne concluded that the nonlinear behaviour of filled vulcanisates is due to the breakdown of the carbon black network structure. It was also proposed that the energy involved in this breakdown is from the Van der Waals attractive forces between the carbon black particles [163]. Funt [164] proposed a bound-rubber/entanglement model to explain the Payne effect. In his model, the breaking and reforming of the number of entanglements causes the changes in dynamic modulus with strain amplitude. The bound rubber is defined as the remaining rubber attached to the filler surface after a thorough solvent extraction process on an uncured rubber sample to remove all free unbound rubber. Without special chemical treatment, the bound rubber is usually formed by physical adsorption of rubber molecular chains on the filler surfaces after mechanical mixing [165]. It is often assumed that the higher the bound rubber for a given carbon black surface area, the stronger the filler-rubber interaction. Sternstein and Zhu [166] developed a filler-matrix interaction model to account for the Payne effect. They proposed that temporary bonding of chains to the filler surface resulted in trapped entanglements. Applied strain (or stress) aided the release of the trapped entanglements and thereby led to the reduction in dynamic modulus.

## **2.8 Fatigue of Elastomers**

Mechanical fatigue of elastomers is manifested in a progressive reduction of the physical properties as a result of crack propagation during continuous dynamic excitation. Models for predicting the fatigue life of elastomers follows two approaches. One approach is based on crack nucleation which considers that a

material has an intrinsic life determined by the history of stress or strain. The fatigue crack nucleation life can be deduced from a consideration of the occurrence of a crack of a certain size. The earliest known study of this approach was by Wöhler [167] whose work on fatigue of railroad axles marked the first systematic investigation of stress versus cycles to failure (S-N) curves which were also known as Wöhler curves. Later on, a similar approach was applied to characterise the fatigue behaviour of rubber [168] and it remains in use today due to its convenience as it is formulated in terms of stress and strain at each material point of a test sample or component.

Widely used fatigue life parameters for crack nucleation prediction in elastomers are maximum principal stress [169, 170], maximum principal strain [168, 171-173] and strain energy density [170, 173-175]. Nevertheless, Mars and Fatemi indicated that none of these is applicable to multi-axial loading conditions [176]. As most rubber fatigue experiments are conducted by applying a certain displacement to specimens, it is quite common to relate fatigue life to strain values. Previous studies [168, 177] showed that for elastomers that strain crystallise, increasing minimum strain can significantly enhance fatigue life. Roberts and Benzies [171] and Roach [172] investigated fatigue life under conditions of simple and equi-biaxial tension and found that when plotted against maximum stretch ratio, fatigue life was higher in simple tension than in equi-biaxial tension. They found the difference was pronounced in NR and much less pronounced in SBR. Several years later, Ro [173] reanalysed these data and concluded that it was not possible to unify simple and equi-biaxial tension data.

Under uniaxial tension-tension cyclic loading, when fatigue life of natural rubber was plotted as a function of stress amplitude and mean stress, it was observed that

for a given stress amplitude, fatigue life increased with mean stress [169]. The physical origin of this phenomenon is not well-known but it is often attributed to strain-induced crystallisation. Abraham et al [178] showed that for a constant stress amplitude, fatigue life of carbon black filled EPDM increased by a factor greater than 10 despite the concurrent increase in maximum stress. As EPDM is not a strain crystallising material, they ascribed this phenomenon of increased fatigue life with increased maximum stress to the properties of the rubber-filler system. Their research on an SBR tyre tread elastomer showed a similar effect [179].

After the development of a fracture mechanism for rubber in the 1960s, strain energy density came into use as a parameter to predict fatigue crack nucleation [180]. Under simple loading conditions, the energy release rate is proportional to the product of strain energy density and crack size [174]. Therefore, strain energy density may be considered as a measure of the energy release rate of naturally occurring flaws in relation to the phenomenon observed during the propagation of microscopic defects. Roberts and Benzies [171] and Roach [172] found that when compared on the basis of equal strain energy density, the fatigue life of natural rubber under equi-biaxial tension was longer than that under simple tension by a factor of approximately four. For SBR, equi-biaxial tension fatigue life was longer than simple tension fatigue life by a factor of about 16, when compared on the basis of equal strain energy density. This is an opposite outcome to that shown by the results based on maximum principal strain. Roach proposed that for simple tension, the strain energy density is available for flaw growth, while for equi-biaxial tension, only one half of the strain energy density is available for flaw growth. This hypothesis gave the best correlation between simple and equi-biaxial

tension fatigue data. Despite these observations, Ro [173] and Abraham et al [170] concluded that strain energy density is a more reliable fatigue life predictor than strain or stress based predictors, especially for non-relaxing testing conditions. The crack nucleation approach offers simplicity and familiarity as it is based on quantities that are defined at each material point by the principles expressed in continuum mechanics [181].

Another available approach is the crack growth method which considers pre-existing cracks or flaws. This approach, originally applied to glass specimens, was introduced by Griffith [182] and further developed for elastomers by Rivlin and Thomas [183], Greensmith [184], Lindley [185] and Young [186] who related the tearing energy (energy release rate) to the strain energy density for classic fracture mechanics of rubber tests specimens such as the single edge specimen or the trouser specimen. Tearing energy ( $T$ ) was defined as the change of stored mechanical energy ( $\partial U$ ) caused by the crack growth per unit area ( $\partial A$ ) as given in Eqn. 2.3.

$$T = \frac{\partial U}{\partial A} \quad (2.3)$$

However, a major practical challenge in using the crack growth approach in rubber is that it requires knowing the initial location and state of the crack that causes the final failure and this is especially problematical when the geometry and loading are complicated [187].

Most recently, a critical plane approach [181, 188-196] has been developed for predicting the fatigue life of various elastomers. The critical plane can be defined as the plane in which a crack will initiate and propagate and can be determined by maximizing a fatigue indicator expressed in terms of energy [189, 194], stress

[190, 195, 196] or strain. For example, Mars [189] proposed an energy based critical plane predictor—using crack energy density by assuming that only a certain part of the strain energy density is available for crack growth. The stress based critical plane criterion was proposed by Saintier et al [190] for rubbers that exhibit strain induced crystallinity (e.g. natural rubber). In their formulation, two mechanisms have to be considered: (i) the induced damage by cyclic loading and (ii) the reinforcement due to the induced crystallinity. Verron and Andriyana [191] proposed a conceptually interesting criterion based on the configurational mechanics framework which assumes the existence of intrinsic defects in rubbers. The critical plane predictor proposed by Verron and Andriyana was employed later by others [197] to investigate the fatigue behaviour of rubbers under multi-axial loading. However, researchers have shown that failure often emanates from large flaws of 200  $\mu\text{m}$  that are not in the vicinity of an assumed critical plane [198, 199], and this necessitated the use of alternative methods to characterise fatigue in this research. In this light, the approach advocated by Abraham et al [170, 178, 179] to determine fatigue life was adopted using Wöhler curves based on alternating stress and dynamic stored energy criteria. Similarly, the concept of an MRE exhibiting a limiting complex modulus at failure was explored.

## **2.9 Summary**

In this chapter, some basic insights into MRE structure and properties, elastomer behaviour and rubber fatigue have been given. The following conclusions from this chapter require emphasis:

- 1) Various elastomers including silicone rubber, natural rubber, polyurethane and hybrid polymers based on a mixture of two or more of these

elastomers can be used to fabricate MREs with different properties. Carbonyl iron is the most widely used magnetic particle because of its excellent soft magnetic property, high saturation magnetisation and spherical shape.

- 2) Microstructures of MREs can be controlled by fabricating the composite either with or without an external magnetic field. Anisotropic MREs with particles aligned in columnar chains in the direction of the magnetic field have more functionality than isotropic MREs, but conventional methods of fabricating MREs under an external magnetic field have many shortcomings which greatly limit their industrial application.
- 3) Mechanical properties of MREs, including modulus and damping capability, show a dependence on the matrix materials, the type of magnetic particles as well as their size and volume fraction, external magnetic field, additives, interfacial layers between the matrix and the magnetic particles, the testing frequency and the strain amplitude applied. Test methods to determine the mechanical properties of MREs have predominantly involved static and dynamic uniaxial tensile testing, compression testing and shear testing.
- 4) Due to the field dependent rheological response of MREs, they have many interesting engineering applications.
- 5) Elastomers exhibit specific viscoelastic behaviour when undergoing deformation. Fatigue properties of elastomers have been studied experimentally and theoretically for decades. Fatigue life predictors for elastomers have been proposed and more sophisticated approaches are

under development to provide better understanding of the complicated behaviour of elastomers subjected to various loading conditions.

In conclusion, many of the findings reviewed have contributed significantly to the research field of MRE fabrication and characterisation, but a great deal of research still needs to be done and further studies are necessary to more accurately understand and improve this smart material and develop potential applications. With regard to the physical characterisation of the mechanical properties of MREs, only uniaxial testing results are available from the current literature. However, the service requirements of most rubber components results in them being subjected to complex dynamic loading and high deformations. Uniaxial testing is consequently unrepresentative of the actual behaviour of MRE components in service. Furthermore, fatigue resistance, one of the most critical physical properties required in a rubber is virtually unresearched for MREs. In particular, the high dynamic loading experienced by machine parts necessitates understanding fatigue properties in MREs. However, as stated, from the available literature the fatigue resistance of MREs has yet to be studied in any depth. In order to carry out representative fatigue testing and obtain realistic life prediction, multi-axial testing methods are essential. Abraham's theories [200] related to a limiting complex modulus and dynamic stored energy predictor lend themselves to a comprehensive study of MRE fatigue life using equi-biaxial dynamic bubble inflation.

# Chapter 3 Materials and methods

## 3.1 Materials

A two component, room temperature vulcanised (RTV) silicone rubber, procured from Axson Technology, UK, was used as the matrix material to fabricate MREs. The physical and mechanical properties of two components are shown in Appendix A. This material was chosen because the modulus of silicone allows mobility of the ferromagnetic particles so that an MRE material capable of demonstrating a pronounced MR effect can be easily processed.

Soft carbonyl iron (CI, CS grade,  $d_{50} = 6.0\text{--}7.0\ \mu\text{m}$ ,  $\rho = 7.86\ \text{g/cm}^3$ , supplied by BASF, Germany) was selected as the magnetic particle because it possesses excellent soft magnetic properties and high saturation magnetisation. The surface morphology of the selected particles at different magnifications is shown in Figure 3-1.

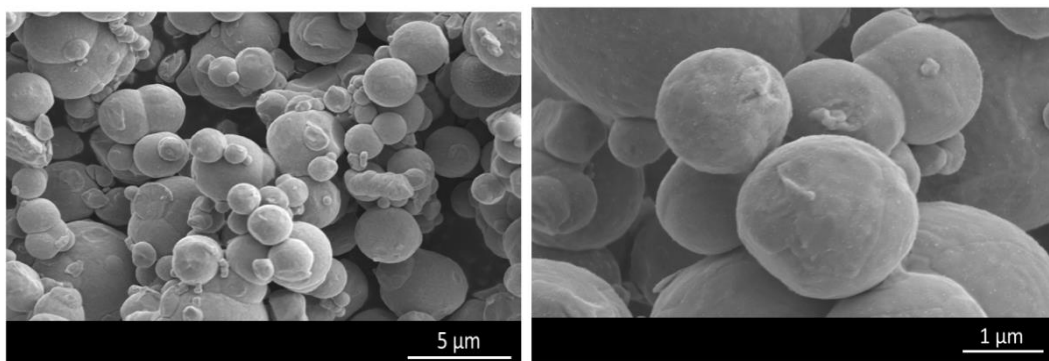


Figure 3-1 Surface morphologies of carbonyl iron particles

### **3.2 Fabrication of MREs**

Firstly, silicone rubber was mixed with a catalyst at a 10:1 ratio, before carbonyl iron particles were incorporated into the mixture and mechanically stirred to distribute the particles evenly in the elastomer matrix. The whole mixture was degassed in a vacuum to remove entrapped air bubbles and then poured into a mould. After further degassing in the mould, the compound was kept at room temperature for 48 hours to allow solidification. For anisotropic MREs, the compound was cured in the presence of a magnetic field using a Halbach Array (a permanent magnet array) which can provide a mean magnetic flux density of 400 mT after degassing. The magnetic flux density applied during fabrication had a significant influence on the configuration of the particles. With the increase of magnetic flux density, the thickness of the columns and the space between them increased [90]. From the available literature [22, 58, 61, 81], a magnetic flux density of 400 mT was at a reasonable level to produce MREs with directionalised particles and to induce a noticeable MR effect during the testing process. The thickness of the MRE samples fabricated was 1 mm. A schematic diagram of the Halbach Array and the distribution of the magnetic flux density in two mutually perpendicular planes can be found in Appendix B.

### **3.3 Equi-biaxial testing**

Equi-biaxial fatigue behaviour of both the isotropic and anisotropic MREs was determined by using the dynamic bubble inflation system that is depicted in Figure 3-2. The equi-biaxial test system cycles disc rubber samples by hydraulically inflating and deflating them. Deformation of the bubble that is created during cycling is captured using a vision system comprising two

complementary metal-oxide semiconductor (CMOS) cameras to record the movement of the centres of specific points aligned at the pole on the surface of each sample. Stress and strain throughout the inflation/deflation cycle are simultaneously determined and recorded. A detailed description of the testing system can be found in [201]. The advantages of using the bubble inflation testing system include higher stretch ratios, controlled region of failure, elimination of stress concentration and friction effects.

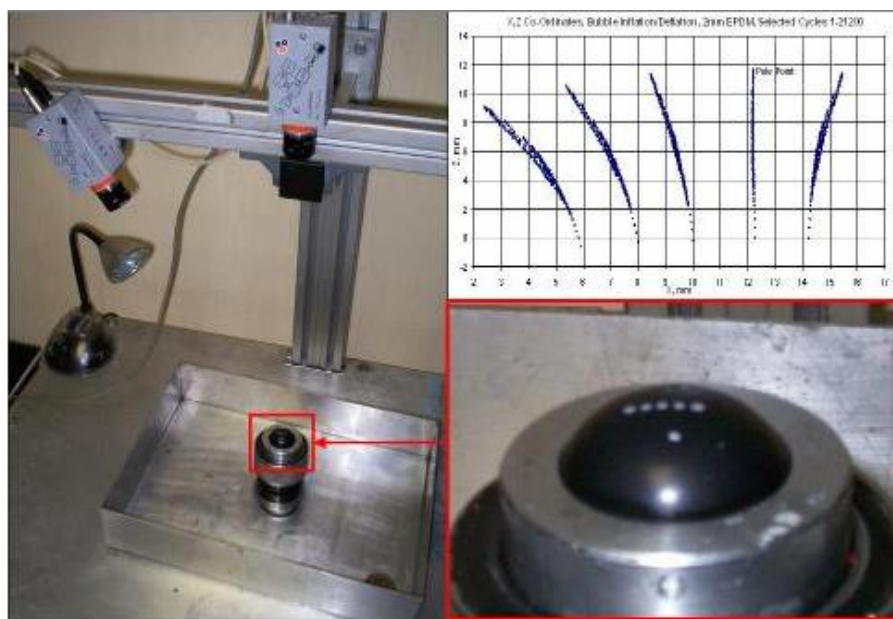


**Figure 3-2 The equal-biaxial bubble inflation test system**

### 3.3.1 Theory

Equi-biaxial stress analysis using bubble inflation is considered to comply with the theory for thin shell structures subjected to pressure (membrane theory), in which bending stiffness is assumed to be negligible. For an ideal isotropic material and an axisymmetric set-up, the bubble contour that results exhibits rotational symmetry and therefore the deformation at the pole is equi-biaxial as shown in Figure 3-3.

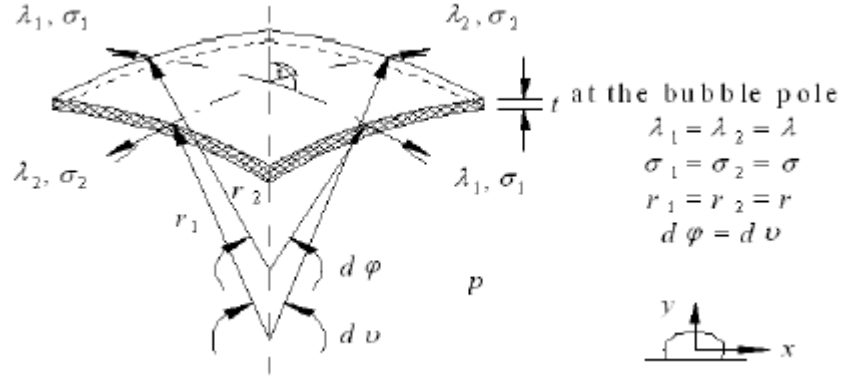


**Figure 3-3 Membrane stress at the bubble pole [202]**

Circumferential stress at the pole ( $\sigma$ ) can be determined using the relation given in Eqn. 3.1, where  $P$  is the applied pressure to inflate a thin sheet,  $r$  is the radius of curvature of the bubble and  $t$  is the specimen thickness.

$$\sigma = P \cdot (r / 2t) \quad (3.1)$$

For the bubble inflation case applied to an elastomer, Murphy [203] showed that the formula for engineering stress ( $\sigma_{Eng}$ ) should be modified to include the increased loading experienced by the bubble as it enlarged and can be expressed as in Eqn. 3.2. Hence, the expression for Cauchy stress ( $\sigma_{True}$ ) is as shown in Eqn. 3.3.

$$\sigma_{Eng} = P(r / 2t_0) \cdot \lambda \quad (3.2)$$

$$\sigma_{True} = P(r / 2t_0) \cdot \lambda^2 \quad (3.3)$$

where  $P$  and  $r$  are as previously defined,  $t_0$  is the unstrained sample thickness and  $\lambda$  is the local stretch ratio which can be determined using Eqn. 3.4.

$$\lambda = \left( (X_{cir} - X_{orig}) / X_{orig} \right) + 1 \quad (3.4)$$

where  $X_{cir}$  is the circumferential point spacing at the bubble pole and  $X_{orig}$  is the

original point spacing. Using Eqns. 3.2 and 3.4, plots of engineering stress versus stretch ratio can be generated.

### 3.3.2 Testing methods

Disc specimens as shown in Figure 3-4 (a) were used for all the tests. Figure 3-4 (b) shows a test specimen in the bubble inflation system's inflation orifice. The nominal diameter of the test piece was 50 mm and the thickness was approximately 1 mm. The diameter of the inflation orifice was approximately 38 mm.

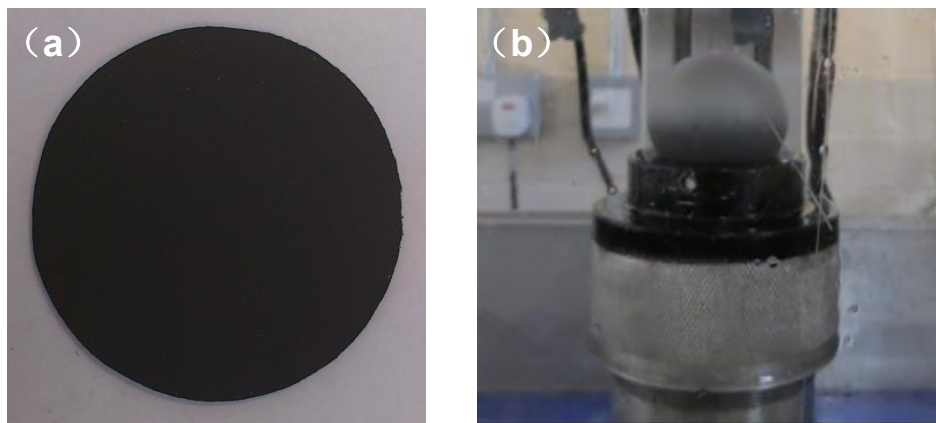


**Figure 3-4 (a) A disc test specimen; (b) An inflated disc test specimen**

Prior to fatigue tests, quasi-static tests were carried out to provide a value of ultimate tensile stress (*UTS*) and the stress-strain relationship for an initial loading. This allowed the equi-biaxial dynamic test parameters to be set.

For fatigue tests, the materials were cycled under engineering stress control. Each material was tested over a range of stress amplitudes to create Wöhler (S-N) curves. All fatigue tests were carried out at a frequency of 1 Hz. This frequency was chosen to induce failure due to crack initiation (it is assumed that the crack would be initiated from the interface between CI particles and silicone matrix [58])

and growth and represents a good compromise between a low level of heat build-up and the test time required to complete a fatigue test.

In a typical fatigue test, pressure was applied hydraulically to the samples causing them to inflate. The inflation medium used in these tests was silicone oil, DOT 5 which is incompatible with MRE samples and thus no swelling effect occurred during the testing. The vision system, which initially utilised two charge coupled device (CCD) cameras, now employs two CMOS cameras as stated at the start of this section, recorded the movement of the centres of specific points at the pole on the surface of the sample during inflation and deflation. Stress values were simultaneously calculated from the applied pressure and bubble geometry, while strain values were calculated from the change in circumferential distance between the centres of specific points on the bubble surface at the bubble pole, using three dimensional position coordinates obtained from the vision system output. In these tests, the dynamic test facility continually records dimensional changes in the bubble and corrects pressure limits to maintain constant engineering stress minima (zero stress in all the fatigue tests) and amplitudes. Concurrently, accumulated cycles are counted. At least three tests were conducted for each material and the average fatigue life was used in subsequent analyses and calculation of results.

### **3.3.3 Fatigue data analysis**

Wöhler (S-N) curves were produced by relating fatigue life to stress amplitudes. Complex modulus ( $E^*$ ) was approximated by calculating the slope of the loading curve from minimum stress and minimum strain to peak engineering stress and maximum strain for the idealised cycle depicted in Figure 3-5 [204]. Previous research into conventional elastomers (ethylene propylene diene monomer, EPDM

and styrene-butadiene rubber, SBR) by Abraham et al [178] and Alshuth et al [179] suggested that specific elastomers when subjected to uniaxial loading exhibited a limiting value of complex modulus and that this value could be used effectively to design against fatigue failure in rubber components. The concept of a limiting value of modulus was supported by Jerrams et al [201, 202] and Hanley et al [205, 206] for EPDM samples, both swollen and unswollen, subjected to equi-biaxial stress cycles. Analysis of changes in complex modulus during the fatigue process applied to MREs allows the determination of whether a limiting value of  $E^*$  is relevant for this class of material subjected to equi-biaxial cyclic loading.

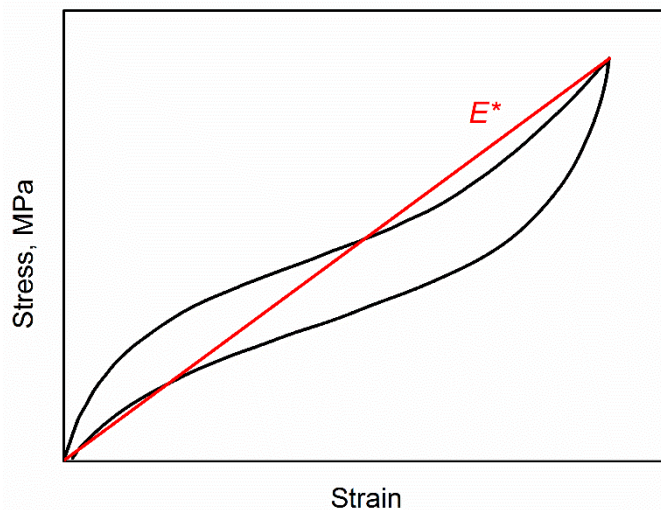


**Figure 3-5 Diagrammatic calculation of  $E^*$  from stress-strain curves**

Stored energy (per unit volume,  $W_S$ ) is defined as the strain energy available in the unloading cycle as shown in Figure 3-6. It represents the elastic stored energy in the rubber sample. Dynamic stored energy ( $W_D$ ), a term proposed by Abraham refers to the part of stored energy remaining when the value of statically stored energy is subtracted [200]. For a minimum stress equal to zero, the dynamic stored energy is equal to the overall stored energy (see Figure 3-7). Previous

analyses of uniaxial and equi-biaxial test data for EPDM found good correlation between the dynamic stored energy at failure in the specimen versus the cycles at failure and indicated that dynamic stored energy could be adopted as a plausible fatigue life predictor [170, 179, 201]. In this research, the changes in dynamic stored energy with the accumulation of cycles for MREs under various loading conditions were determined. The dynamic stored energy at failure was plotted against fatigue life to ascertain if the dynamic stored energy criterion could be applied to MREs when they are subjected to equi-biaxial cyclic loading.

Hence, Abraham et al [170] determined that under uniaxial loading the dynamic stored energy criterion was a reliable predictor and a limiting value of  $E^*$  could be used as an effective design tool. Jerrams et al [201] supported this conclusion for both swollen and unswollen rubbers subjected to equi-biaxial loading.

From an energy perspective, material damping is represented in terms of the damping loss factor,  $\eta$  [207] (Eqn. 3.5).

$$\eta = \Delta W / (2\pi W_s) \quad (3.5)$$

where,  $\Delta W$  is the dissipated energy and  $W_s$  is the stored energy during a cycle as shown in Figure 3-6.

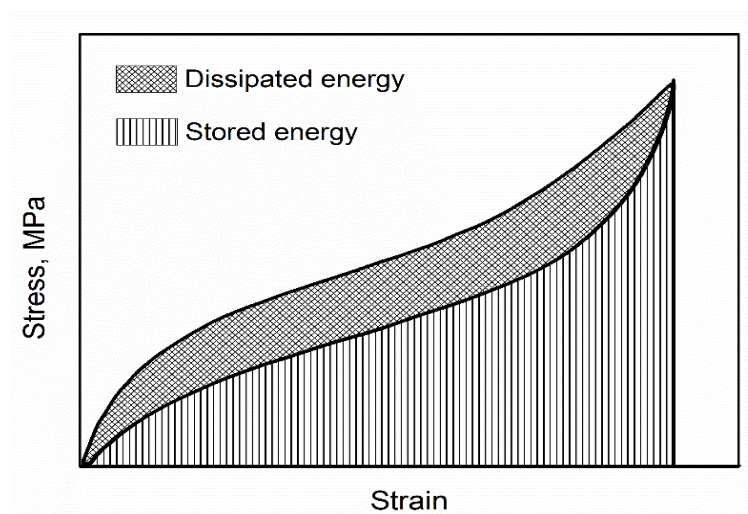


**Figure 3-6 Diagrammatic representation of stored energy from stress-strain curves**

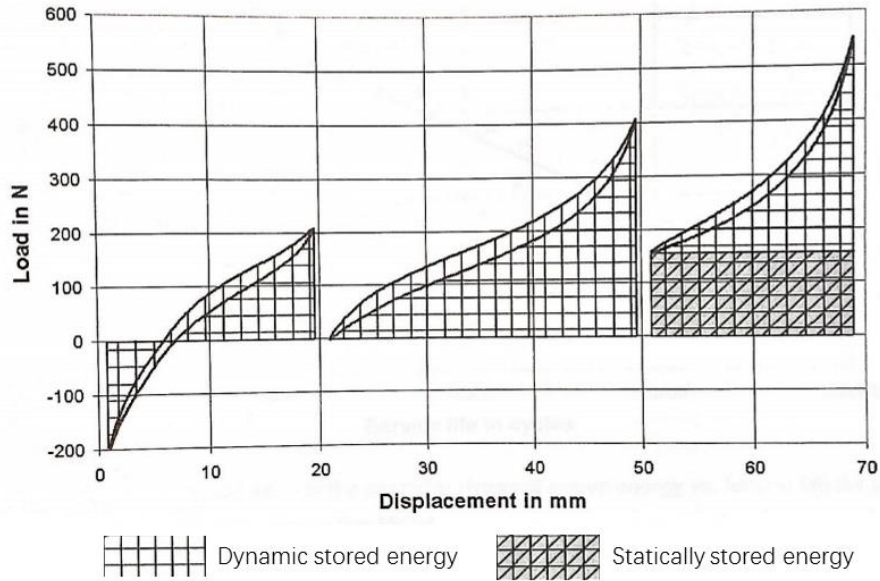


**Figure 3-7 Diagrammatic representation of dynamic stored energy for different test procedures [200]**

### **3.4 Spectroscopy and microscopy observation**

The morphological features of MREs were observed by utilising a Scanning Electron Microscope (SEM, Zeiss Supra). In particular, the use of SEM allows the observation of the distribution of magnetic particles in elastomeric matrices and also the analysis of fracture surface after fatigue failure. The cross sections were coated with a fine layer of gold to make them conductive and SEM images with various magnifications were taken with an accelerating voltage of 5 kV.

# Chapter 4 Equi-biaxial fatigue behaviour of MREs with different microstructures

## 4.1 Introduction

As MREs can be fabricated either in the absence of, or in the presence of a magnetic field during the curing process, the resultant microstructure plays an important role in determining the properties of MREs. In this chapter, the effect of microstructure on the equi-biaxial fatigue behaviour of MREs was initially investigated. Both isotropic and anisotropic MREs with a carbonyl iron content of 20 vol% were produced.

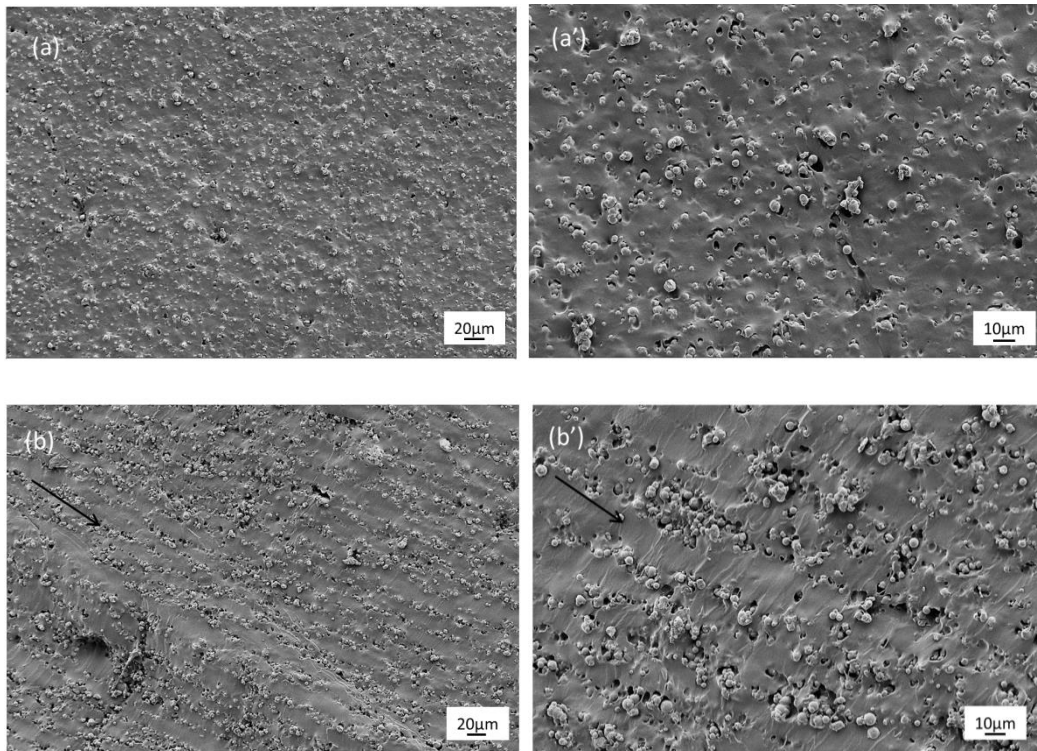


Figure 4-1 SEM images of (a and a') isotropic and (b and b') anisotropic MREs

The SEM images at different magnifications for isotropic and anisotropic MREs are shown in Figure 4-1. It can be observed that carbonyl iron particles were distributed randomly in the isotropic MREs. In contrast, they formed chain-like structures in the direction of the magnetic field in anisotropic MREs.

## 4.2 Quasi-static test

Quasi-static equi-biaxial tests to failure were carried out on both isotropic and anisotropic MRE samples. No magnetic field was applied to the samples during these tests. The average *UTS* and average maximum stretch ratios ( $\lambda_{max}$ ) achieved are shown in Table 4-1.

**Table 4-1 Quasi-static test results for isotropic and anisotropic MREs**

Sample	Average <i>UTS</i> (MPa)	Average $\lambda_{max}$
Isotropic	3.54	3.36
Anisotropic	4.12	3.21

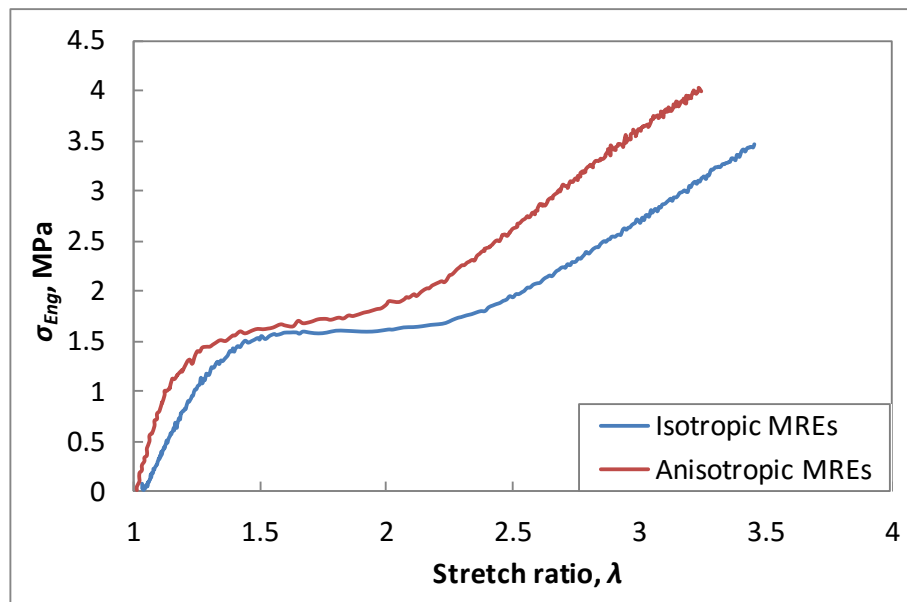


**Figure 4-2 Engineering stress-stretch ratio curves for isotropic and anisotropic MREs from quasi-static testing**

Figure 4-2 shows the typical stress-stretch ratio curves from quasi-static tests for isotropic and anisotropic MREs. As can be observed, the stress-strain curve of an equi-biaxial test results in a similar ‘S’ shaped configuration to that seen in typical uniaxial tensile tests on rubber compounds. Unsurprisingly, the stiffer anisotropic MREs exhibited lower extensibility.

### 4.3 Fatigue life

Equi-biaxial fatigue tests were then carried out at four different stress amplitudes ranging between 0.75 MPa and 1.4 MPa each with a minimum stress of zero. A minimum of three tests were carried out for each stress amplitude. The resulting fatigue lives were recorded and the average fatigue lives were used to produce standard Wöhler (S-N) curves for isotropic and anisotropic MREs, as shown in Figure 4-3. Again, no magnetic field was applied during testing.

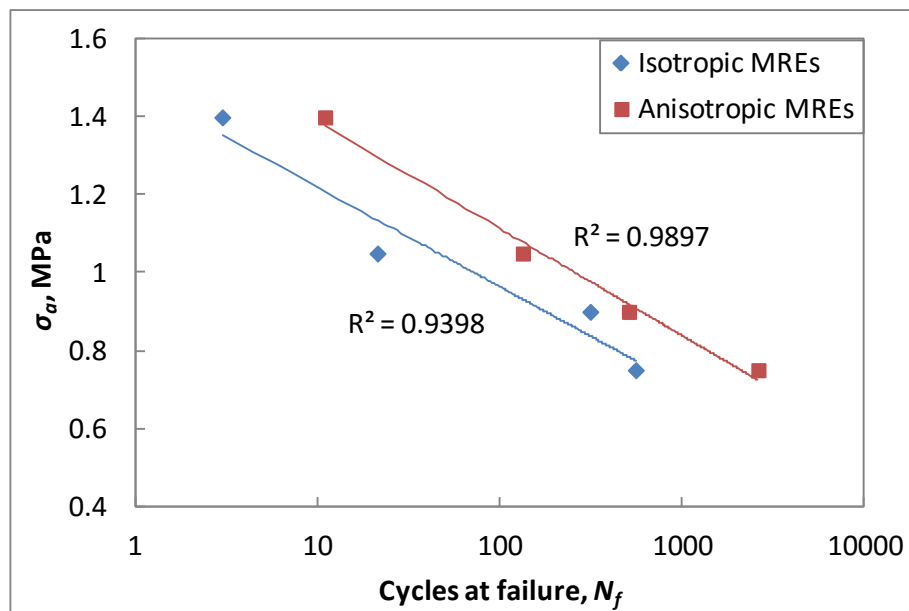


Figure 4-3 Plot of stress amplitudes versus fatigue life for isotropic and anisotropic MREs

When fatigue lives were compared at the same stress amplitudes, it was found that anisotropic MREs exhibit greater fatigue resistance than isotropic MREs. This is

because anisotropic MREs were fabricated in the presence of magnetic fields and the magnetic interactions between the iron particles are stronger in the anisotropic than in the isotropic configuration [23].

Proposing a reliable formula to allow the prediction of fatigue life for MREs was considered. Equations for fatigue life prediction, relating life ( $N_f$ ) to stress amplitude ( $\sigma_a$ ) for SR based MREs were derived as follows:

Isotropic MREs:

$$\sigma_a = -0.111 \ln(N_f) + 1.4752 \quad (4.1)$$

Anisotropic MREs:

$$\sigma_a = -0.12 \ln(N_f) + 1.6652 \quad (4.2)$$

Figure 4-4 shows the dependence of fatigue life on maximum strain for isotropic and anisotropic MREs containing 20% CI. It can be seen from Figure 4-4 that there was a good correlation between fatigue life and maximum strain for isotropic and anisotropic SR based MREs with a CI content of 20% under zero minimum engineering stress testing condition.

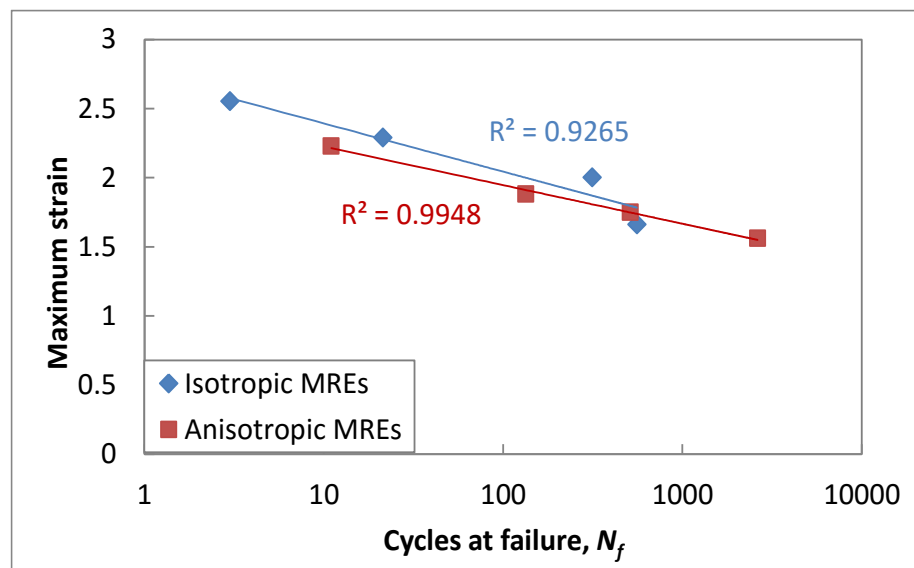


Figure 4-4 Plot of maximum strain versus fatigue life for isotropic and anisotropic MREs

## 4.4 Stress-strain behaviour

Elastomers exhibit a characteristic ‘S’ shaped stress-strain curve in both loading and unloading cycles. Hysteresis is present in the loading and unloading curves due to the continual breaking and re-formation of the weak Van der Waals bonds between the chains as they move relative to each other [208]. The presence of filler increases the stiffness and durability of elastomer but at the same time increases stress softening (the Mullins effect) [209] which results from the breakdown of the filler structure. This phenomenon comprises both the interaction between the surfaces of filler particles and the rubber as well as the breakdown of filler agglomerates. When subjected to a large number of cycles, stress softening and hysteresis in filled rubbers are significant. The stress-strain behaviour of isotropic and anisotropic MREs at a stress amplitude of 0.75 MPa is depicted in Figure 4-5.

It can be observed that stress softening continued as cycles accumulated and was most significant in the first few cycles. Furthermore, the dynamic cyclic loading induced an increase in set as each test progressed, but this increase was much greater in isotropic MREs than in anisotropic MREs, as shown in Figure 4-6. This indicates that the stiffer anisotropic MREs exhibit lower extensibility.

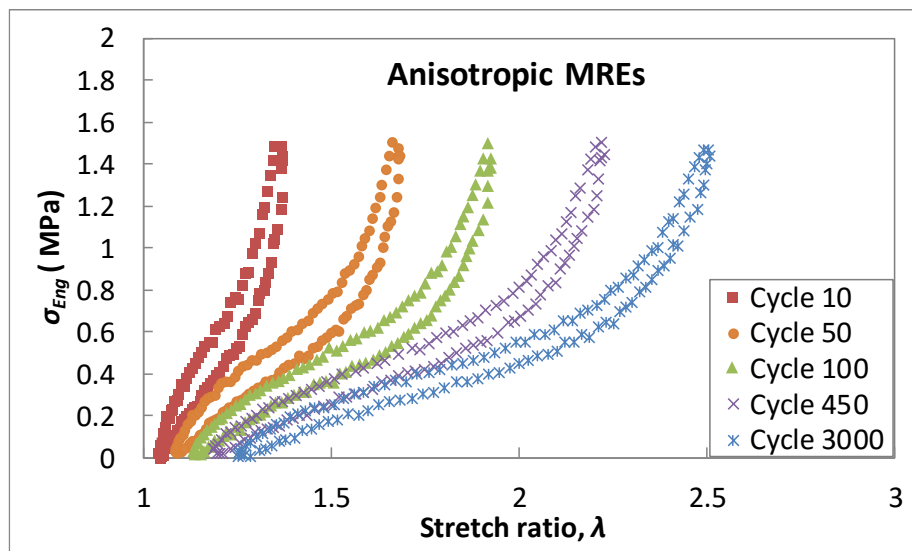
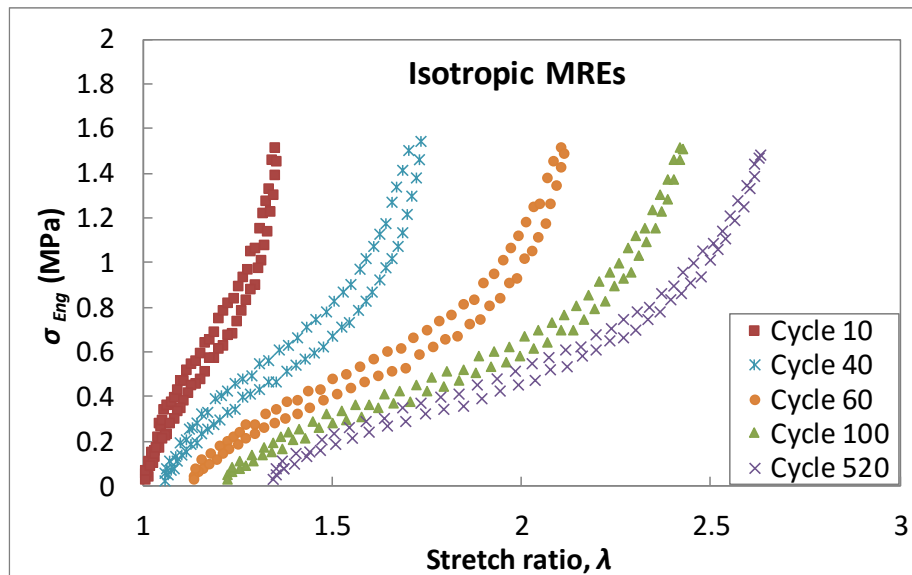


Figure 4-5 Stress-stretch ratio curves of isotropic MREs and anisotropic MREs for an engineering stress control fatigue test for selected cycles,  $\sigma_a = 0.75$  MPa

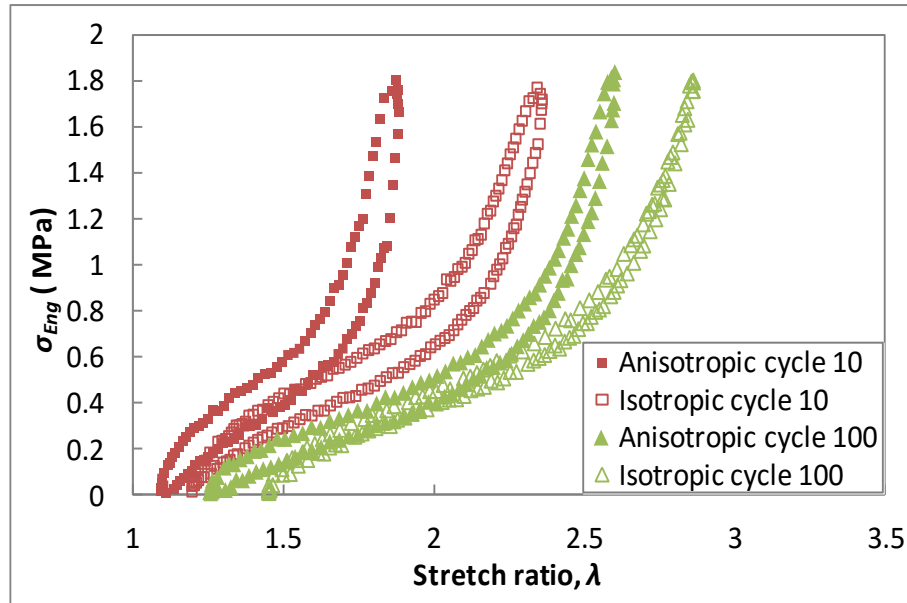


Figure 4-6 Stress-stretch ratio curves for isotropic and anisotropic MREs at  $\sigma_a = 0.9$  MPa

## 4.5 Complex modulus

It is usual for the modulus of filled rubber to decrease significantly in the first few cycles of a dynamic physical test as a result of the Mullins effect [170]. The tests on silicone based MREs described here, further strengthened the conclusion that irrespective of stress amplitude and loading method, fatigue failure occurs (within limits) at a material specific value of complex modulus ( $E^*$ ), as shown in Figure 4-7. For isotropic MREs, failure took place at  $E^*$  values between 1.16 MPa and 1.29 MPa ( $1.23 \text{ MPa} \pm 4.38\%$ ) while for anisotropic MREs, failure took place at  $E^*$  values between 1.16 MPa and 1.41 MPa ( $1.30 \text{ MPa} \pm 10.33\%$ ).

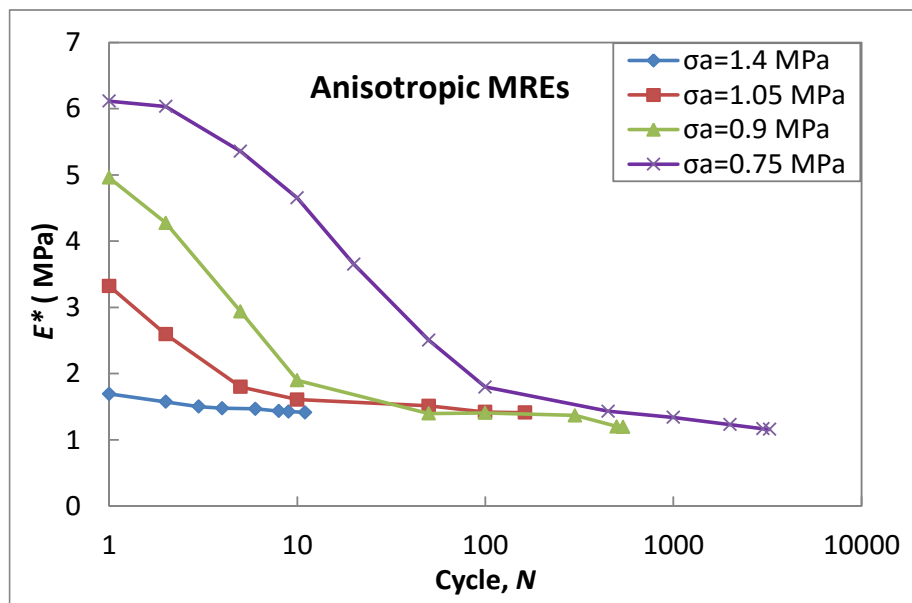
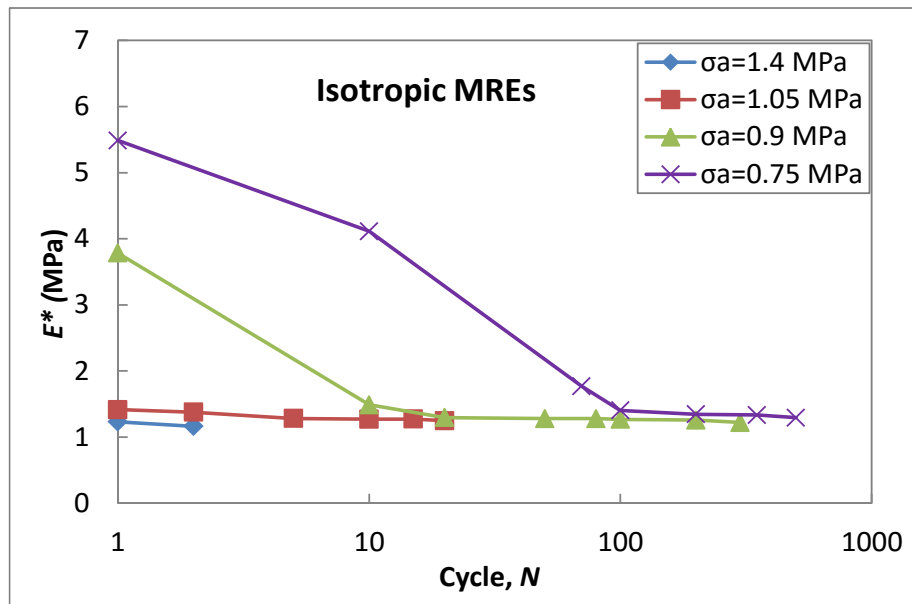


Figure 4-7  $E^*$  versus cycles for different stress amplitudes for isotropic and anisotropic MREs

## 4.6 Dynamic stored energy

The dynamic stored energy in cycles for tests on isotropic and anisotropic MREs was calculated and this parameter was plotted against cycles as shown in Figure 4-8. It can be noted that at a constant stress amplitude, the dynamic stored energy

increased with the accumulation of cycles for both isotropic and anisotropic MREs. When plotted against cycles to failure, the dynamic stored energy at failure (for different stress amplitudes) was found to decrease linearly, indicating that the dynamic stored energy hypothesis postulated by Abraham can be used as a plausible predictor of fatigue lives for isotropic and anisotropic MREs irrespective of the stress amplitudes applied.

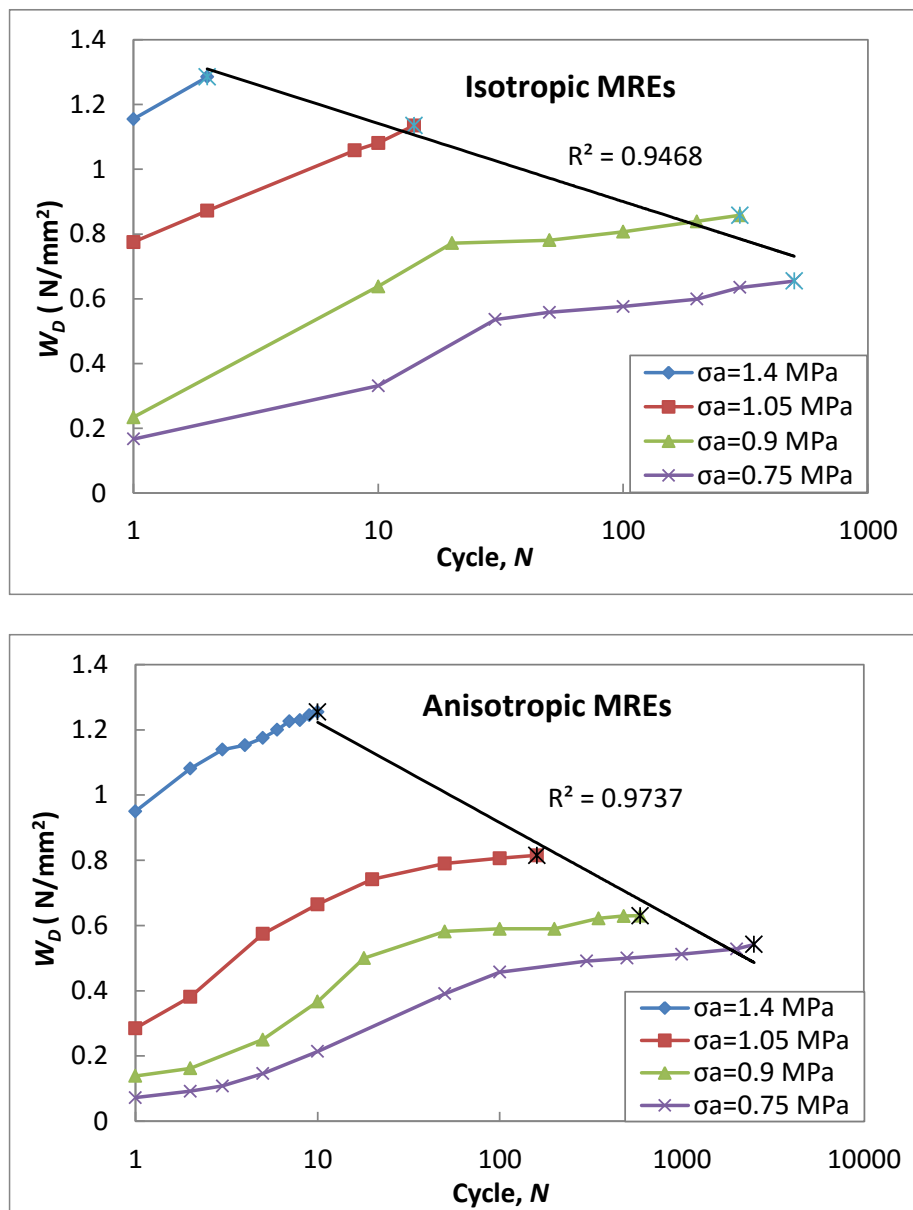
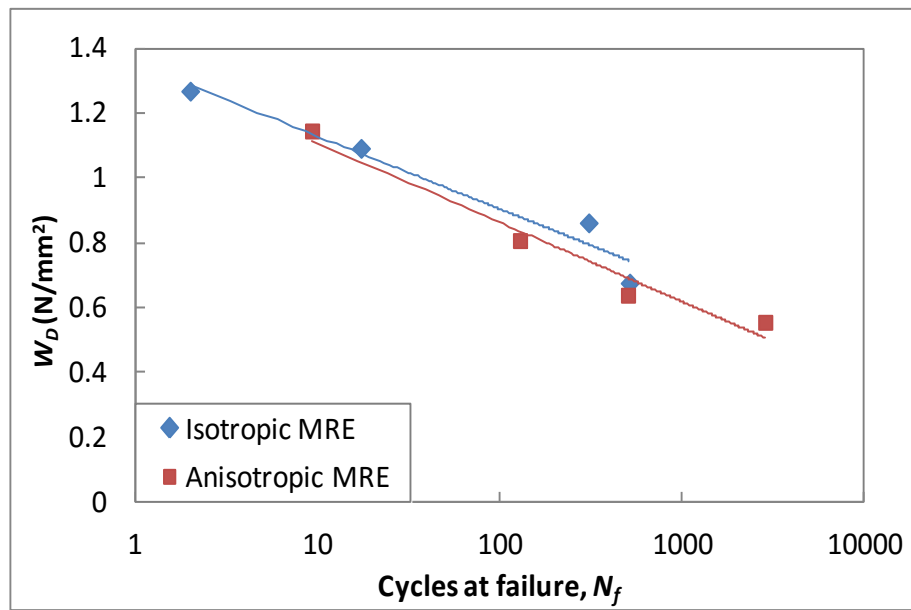


Figure 4-8 Dynamic stored energy versus cycles for isotropic MREs and anisotropic MREs

However, it should be noted that the dynamic stored energy in isotropic MREs is higher than that of anisotropic MREs for equal loading conditions. This is illustrated in Figure 4-9, where the linear plots of dynamic stored energy at failure versus cycles to failure for each are presented together. This difference can be ascribed to lower extensibility for a given applied stress due to the formation of columnar magnetic particles chains in anisotropic MREs.



**Figure 4-9 Dynamic stored energy at failure versus cycles at failure for isotropic and anisotropic MREs**

A reliable formula to allow the prediction of fatigue life for MREs based on the relation between dynamic stored energy at failure to cycles at failure was considered and equations for the materials are offered. The equations for fatigue life prediction in SR based MREs from the viewpoint of energy (relating life ( $N_f$ ) to dynamic stored energy ( $W_D$ )) are:

Isotropic MREs:

$$W_D = -0.097 \ln(N_f) + 1.353 \quad (4.3)$$

Anisotropic MREs:

$$W_D = -0.106 \ln(N_f) + 1.3521 \quad (4.4)$$

## 4.7 Damping loss factor

MREs are viscoelastic materials and the performance of MRE based devices is highly dependent on their damping capabilities [72]. The variations of damping loss factor ( $\eta$ ) with respect to cycles at different stress amplitudes for isotropic and anisotropic MREs subjected to equi-biaxial cyclic loading are shown in Figure 4-10. As can be seen, the damping loss factor decreased throughout the entire fatigue test at each stress amplitude applied to both isotropic and anisotropic MREs. However, a range of loading conditions resulted in different changes in the loss factor. It can be noted that a higher stress amplitude tended to induce a higher initial damping loss factor, but for these stress amplitudes, loss factors decreased sharply in the first few cycles, followed by a gradual degradation until failure. However, a low stress amplitude such as 0.75 MPa, induced a lower initial loss factor and a relatively constant rate of change in this loss factor during the fatigue process. It was suggested earlier [40] that the damping of MREs mainly comes from the energy dissipation induced by interfacial slippage between the elastomeric matrix and the magnetic particles. Unsurprisingly, lower loading values induced slight interfacial slippage between the magnetic particles and the silicone rubber matrices and consequently resulted in lower initial loss factors and small changes therein during the fatigue process. However, the damping due to the weakly bonded interfaces of MREs increased with the external stress [80], so the material exhibited higher initial loss factors at high stress amplitudes. High

stress probably made interfaces easy to be destroyed, so the drop of damping loss factor was more rapid at higher stress amplitudes than in lower stress amplitudes.

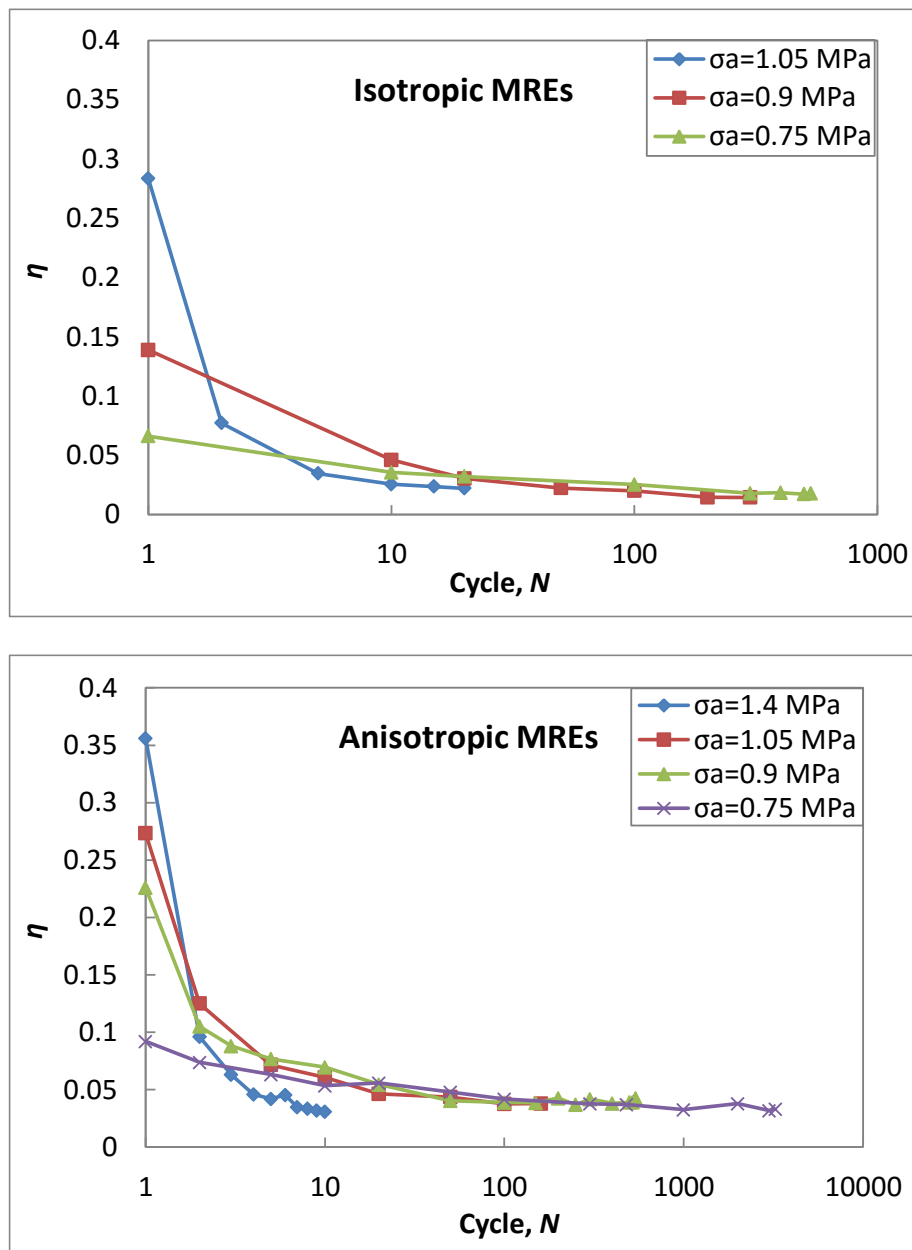


**Figure 4-10 Damping loss factor versus cycles for isotropic MREs and anisotropic MREs**

In making a comparison between isotropic and anisotropic MREs, it was found that when applying the same stress amplitudes, the damping loss factor of anisotropic MREs was higher than that of isotropic MREs. This is illustrated in Figure 4-11, where the damping loss factor  $\eta$  versus cycles was plotted for both

isotropic and anisotropic MREs fatigued at a stress amplitude of 0.9 MPa. It was suggested that the value of damping factor ( $\tan\delta$ ) of MREs was dependent on the microstructure formed during the curing process [70]. MREs cured in a field of higher intensity were characterized by higher values of  $\tan\delta$ . This is because as the strength of the magnetic field increases, the level of viscosity in the compounds is greater and so increases with the structural and magnetic anisotropy. Consequently, the material absorbs more energy which is dissipated as heat. The difference in damping loss factor between isotropic and anisotropic MREs can also be understood from this viewpoint. The damping loss factor at failure was in the range 0.014–0.022 for isotropic MREs and 0.031–0.043 for anisotropic MREs.

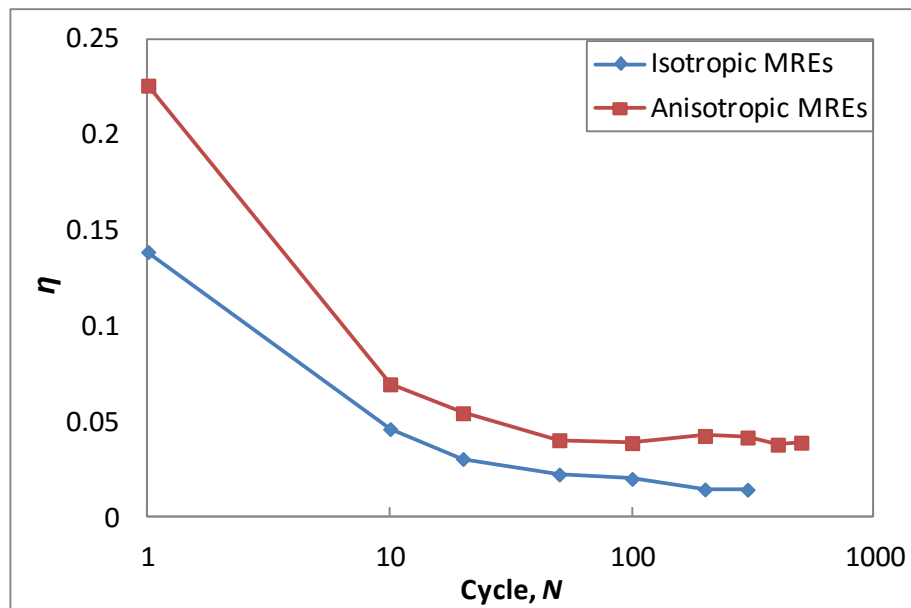
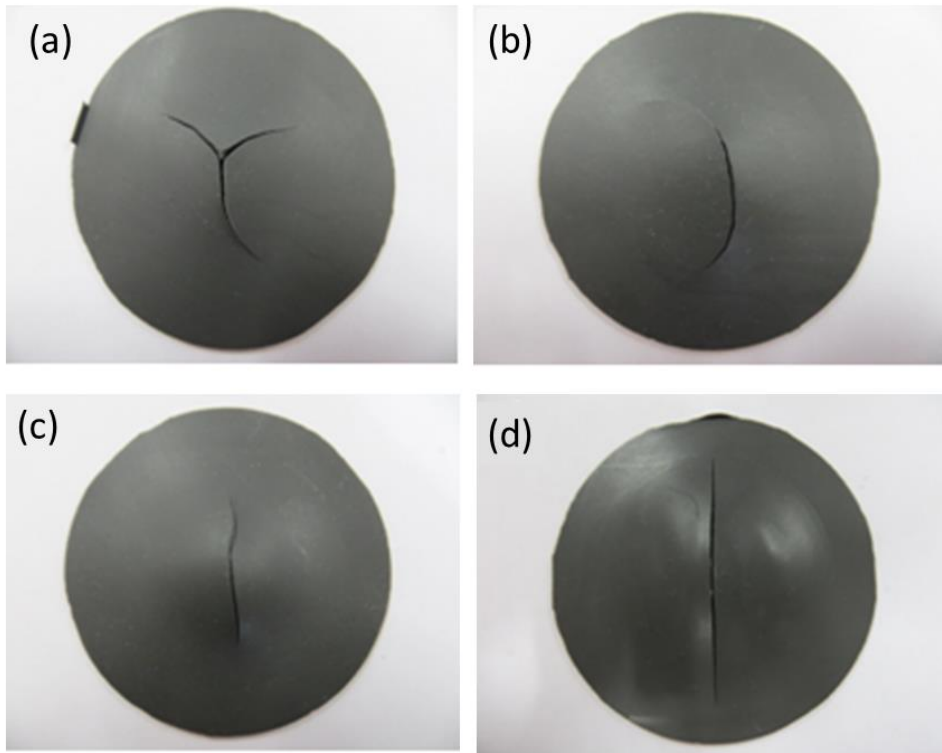


Figure 4-11 Damping loss factor for isotropic and anisotropic MREs at  $\sigma_a = 0.9$  MPa

## 4.8 Fracture surface analysis

The failure modes observed in quasi-static tests and fatigue tests at different stress amplitudes for both isotropic and anisotropic MREs were studied. It has been reported that single shot inflation to failure tended to produce a rupture in a star or

cloverleaf pattern [208]. However, as observed in the experiments described here, for isotropic MREs, quasi-static tests to failure exhibited bifurcated failures as shown in Figures 4-12 (a) and 4.12 (b). The same failure mode was observed for fatigue tests at a stress amplitude of 1.4 MPa, while fatigue tests at stress amplitudes below 1.4 MPa predominately produced a slit in a single direction running through the bubble pole as shown in Figure 4.12 (c). For anisotropic MREs, both quasi-static tests and fatigue tests for all different stress amplitudes used, induced a single slit fracture mode as shown in Figure 4.12 (d).



**Figure 4-12 Typical failure modes for isotropic and anisotropic MREs: (a) and (b) isotropic MREs, quasi-static tests and fatigue tests at  $\sigma_a = 1.4$  MPa, (c) isotropic MREs, fatigue tests at  $\sigma_a < 1.4$  MPa and (d) anisotropic MREs, quasi-static tests and fatigue tests at all  $\sigma_a$**

The surface morphologies of the crack tip of fractured anisotropic MRE samples were observed using SEM and the results suggested that this slit was in the same direction as the aligned magnetic particles chains, as shown in Figure 4-13.

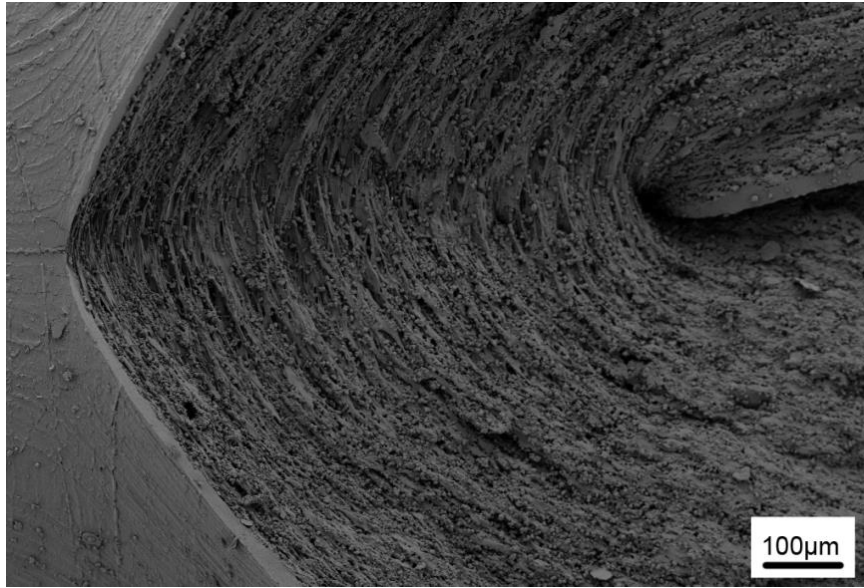


**Figure 4-13** Surface morphology of a crack tip in a fatigue failed anisotropic MRE

Thereafter, the fracture surface morphologies of isotropic and anisotropic MREs after fatigue tests at different stress amplitudes were observed by using SEM, as shown in Figures 4-14 and 4-15.

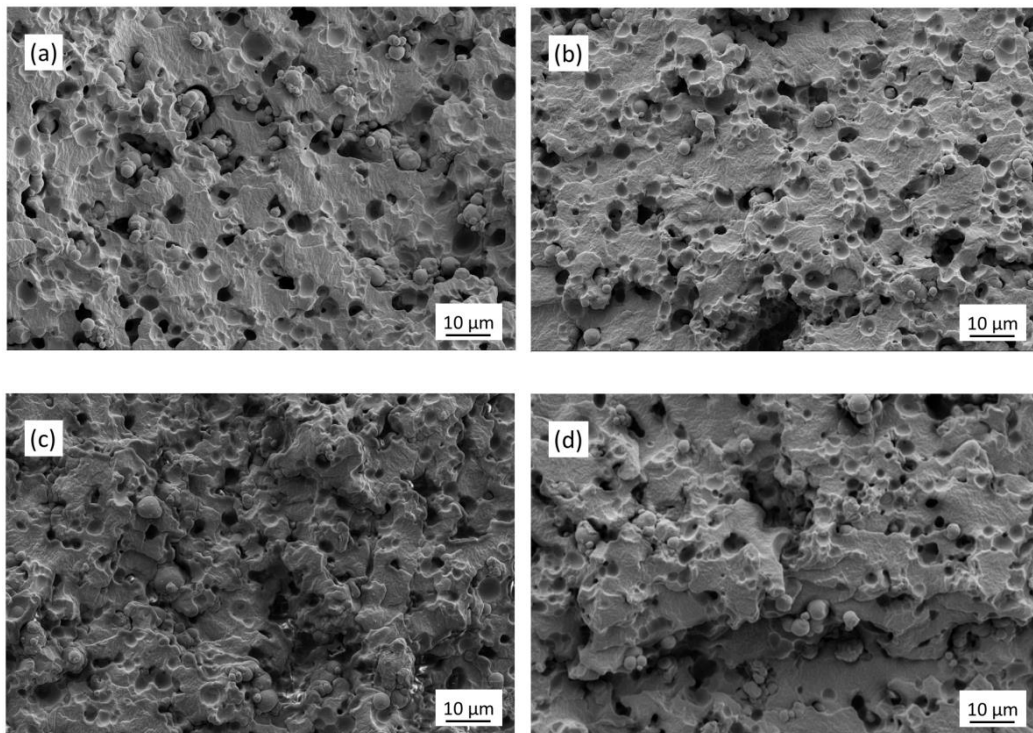


**Figure 4-14** SEM images of fracture surface for isotropic MREs at different  $\sigma_a$ : (a) 1.4 MPa, (b) 1.05 MPa, (c) 0.9 MPa and (d) 0.75 MPa

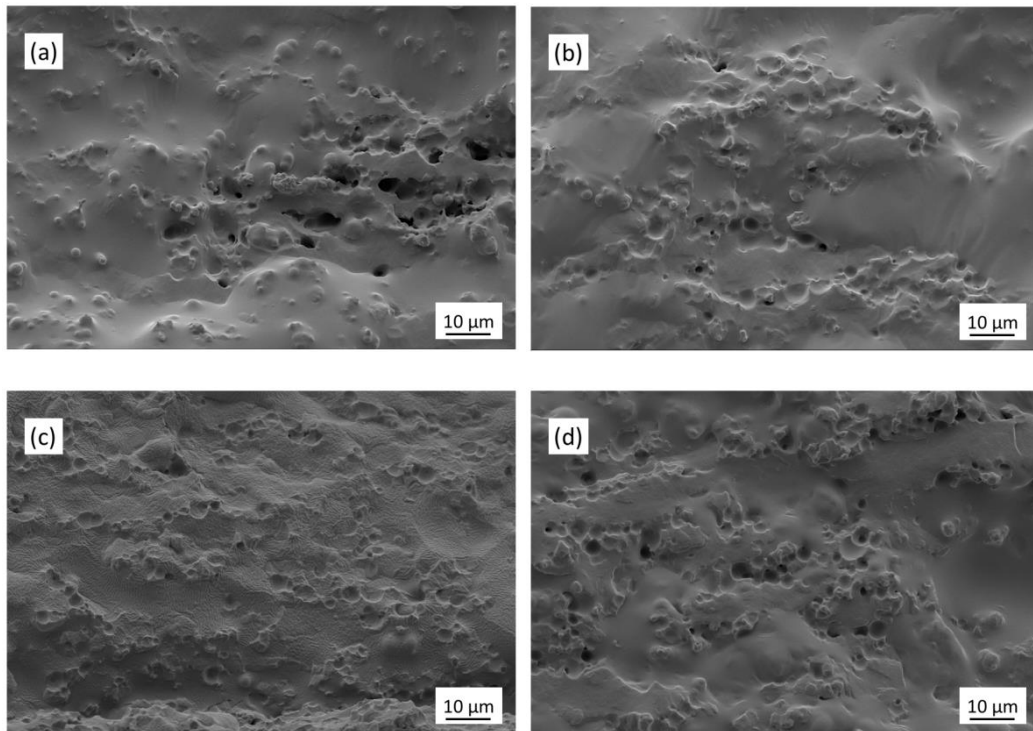


**Figure 4-15 SEM images of fracture surface for anisotropic MREs at different  $\sigma_a$ : (a) 1.4 MPa, (b) 1.05 MPa, (c) 0.9 MPa and (d) 0.75 MPa**

It was observed that at a critical stress level, debonding occurred as a distinct failure phenomenon in an elastomer containing rigid inclusions, due to stress concentrations at the weak particle-matrix interfaces [210]. For both isotropic and anisotropic MREs, voids and cavities which finally lead to failure of the material can be seen clearly from the fracture surface of samples tested at different loading conditions. These voids and cavities were induced by the debonding of the iron particles from silicone rubber matrices due to their poor adhesion with each other. The crack propagation began at the interface between the particles and the matrix [58].

When the fracture morphologies in isotropic and anisotropic MREs were compared it was seen that the fracture surface roughness of anisotropic MREs was smoother than that of isotropic MREs under the same testing condition. The

formation of chain-like structures in anisotropic MREs was destroyed by cyclic loading. It can be observed from Figure 4-15 that the remaining particles and the matrix were combined well and fewer cavities existed in the fracture surface, so anisotropic MREs exhibited superior fatigue properties as demonstrated in the earlier sections of this chapter.

## 4.9 Summary

The following conclusions can be drawn from the equi-biaxial fatigue behaviour analysis of isotropic and anisotropic MREs:

- 1) Anisotropic MREs exhibited a greater failure resistance than isotropic MREs for a given magnetic particle content for stress controlled tests due to the formation of carbonyl iron chains during the curing process.
- 2) For both isotropic and anisotropic MREs, stress softening and hysteresis continued throughout fatigue testing but these phenomena were most pronounced in the first dozen cycles and then became insignificant at lower stress amplitudes. However, the set induced by the dynamic cyclic loading was higher in isotropic MREs than in anisotropic MREs.
- 3) During the equi-biaxial fatigue tests on MREs, the complex modulus ( $E^*$ ) decreased throughout the entire test and attained a limiting value of approximately  $1.23 \text{ MPa} \pm 4.38\%$  for isotropic MREs and  $1.30 \text{ MPa} \pm 10.33\%$  for anisotropic MREs. Structured MREs had a higher initial modulus but the rate of decrease in modulus was more rapid than that in isotropic MREs.
- 4) The dynamic stored energy hypothesis can be used as a plausible predictor of fatigue lives for isotropic and anisotropic MREs. The dynamic loading induced an overall decrease in the damping loss factor for both isotropic and

anisotropic MREs. However, the damping loss factor of anisotropic MREs was higher than that of isotropic MREs at the same stress amplitudes due to more energy dissipation in anisotropic samples.

- 5) It was observed that the failure mode of isotropic MREs showed a dependence on the stress amplitudes applied. Fatigue tests at a stress amplitude of 1.4 MPa exhibited bifurcated failures while fatigue tests at stress amplitudes below 1.4 MPa predominately produced a slit in a single direction running through the bubble pole. Nevertheless, fatigue tests on anisotropic MREs, at all different stress amplitudes used, induced a single slit fracture mode and this slit was in the same direction as the aligned magnetic particle chains.

# **Chapter 5    Equi-biaxial fatigue behaviour of isotropic MREs with a range of magnetic particle contents**

## **5.1 Introduction**

The concentration of filler has a great influence on the properties of elastomer based composites. Hence, it is of great importance to investigate the equi-biaxial fatigue behaviour of MREs with various magnetic particle contents in order to provide a comprehensive understanding of the properties of MREs. In this chapter, the fabrication of isotropic silicone based MREs containing different volume fractions (15%, 20%, 25%, 30% and 35%) of carbonyl iron particles and the analysis of their equi-biaxial fatigue behaviour in the absence of external magnetic fields are described. Wöhler curves for each material were derived by cycling test samples to failure over a range of stress amplitudes. Changes in physical properties including complex modulus ( $E^*$ ) and the damping loss factor ( $\eta$ ) were observed during the fatigue process. A dynamic stored energy based criterion has been developed for predicting fatigue life of MREs with various magnetic particle contents.

The surface morphologies of the range of MREs fabricated are shown in Figure 5-1. It can be seen that spherically shaped iron particles were dispersed randomly in the silicone resin for all test samples. As the filler content increased, the distance between iron particles became proportionally smaller. When the particle content was very high, some agglomeration of particles could be observed.

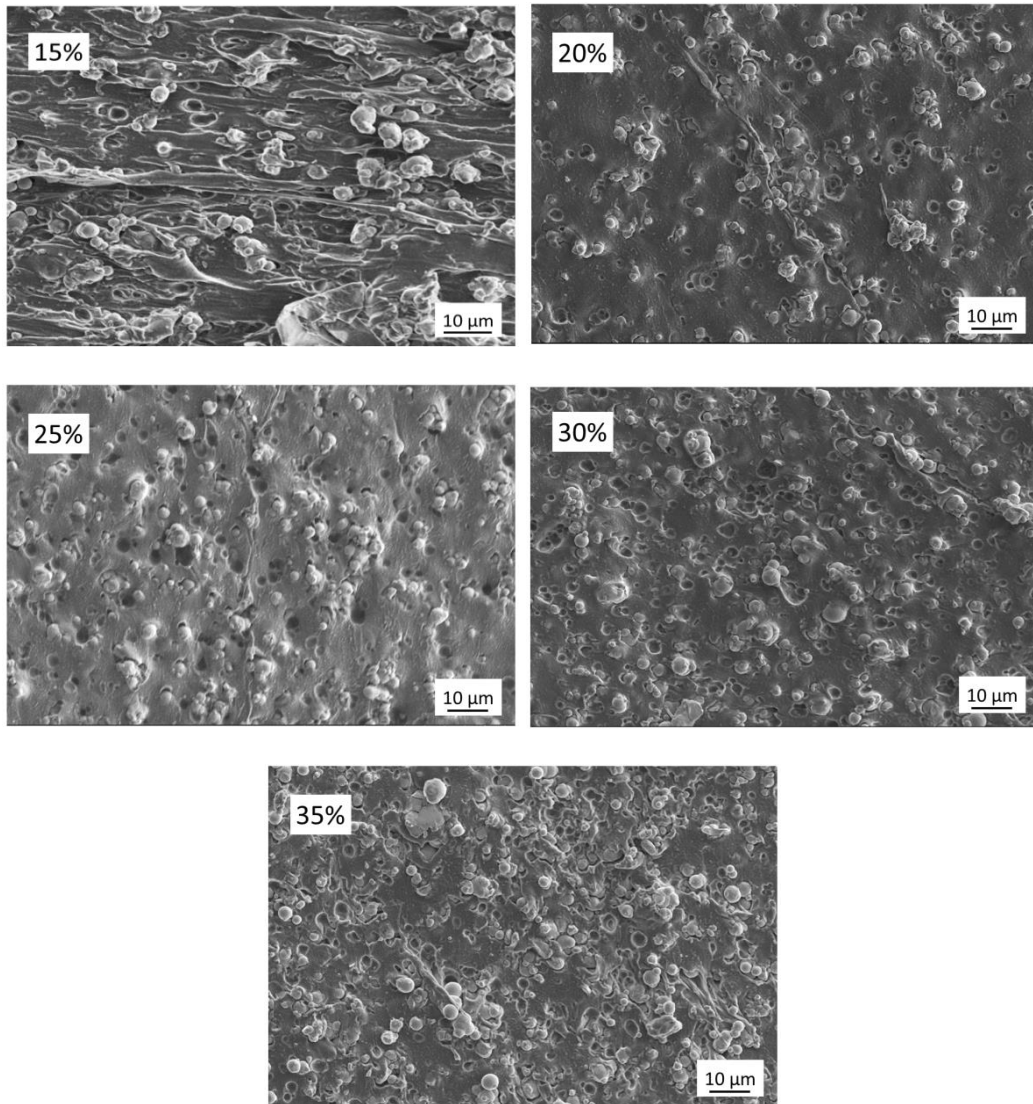
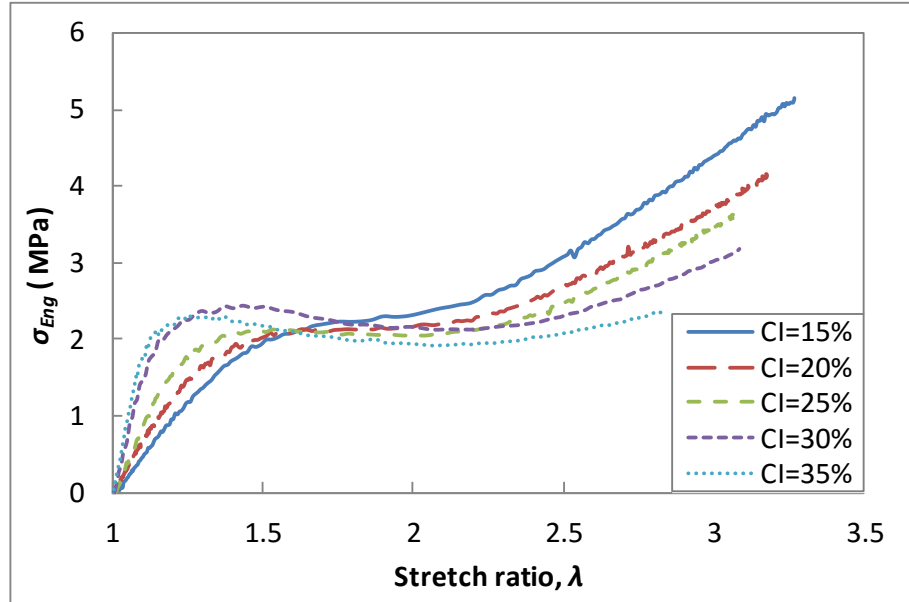


Figure 5-1 Surface morphologies of isotropic MREs containing different volume fractions of CI

## 5.2 Quasi-static test

Quasi-static stress-stretch ratio curves for each sample are depicted in Figure 5-2 and the values of  $UTS$  and  $\lambda_{max}$  are shown in Table 5-1. It can be seen that the  $UTS$  and  $\lambda_{max}$  of MREs decreased as particle content increased. This indicates that the mechanical properties of MREs in this range deteriorated with increased quantities of CI particles. However, for lower stretch ratios (below 1.1, as shown

in Figure 5-3), MREs with high particle concentrations exhibited higher stresses indicating higher moduli of elasticity. The same findings were obtained from uniaxial testing on silicone based MREs [19].



**Figure 5-2 Equi-biaxial quasi-static stress-stretch ratio curves of MREs with various CI contents. Samples were tested in the absence of a magnetic field**

**Table 5-1  $UTS$  and  $\lambda_{max}$  for MREs with various CI contents**

<b>CI content</b>	<b><math>UTS</math> (MPa)</b>	<b><math>\lambda_{max}</math></b>
15%	5.10	3.33
20%	4.10	3.19
25%	3.43	3.09
30%	3.10	3.08
35%	2.37	2.85

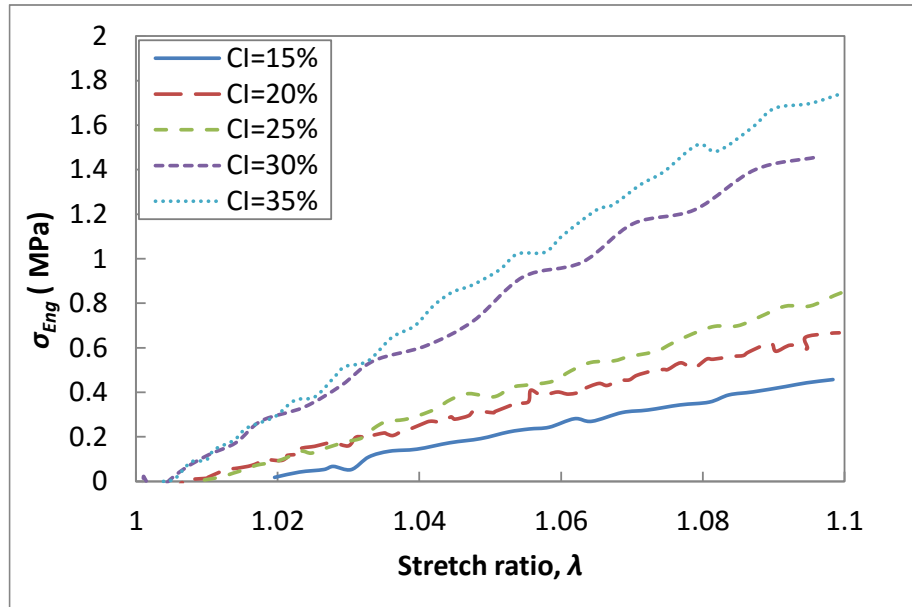
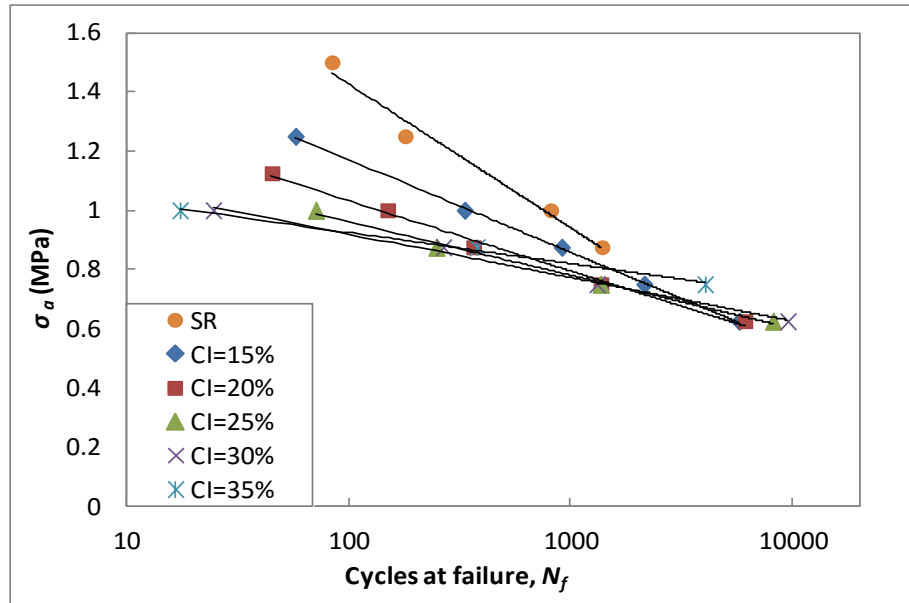


Figure 5-3 Equi-biaxial quasi-static stress-stretch ratio curves of MREs at stretch ratio below 1.1

### 5.3 Fatigue life

Figure 5-4 shows the Wöhler (S-N) curves for SR and SR based MREs with different CI contents varying between 15% and 35%. Unsurprisingly, irrespective of the carbonyl iron particles content, for a minimum stress of zero, fatigue life of MREs decreased as stress amplitude increased. However, the dependence of fatigue life on stress amplitude varied for MREs with different particle contents. This can be seen from the slopes of S-N curves for each sample which are given in Table 5-2. It can be noted that the gradient of the S-N curves decreased as particle content increased. This indicates that the decrease of fatigue life as stress amplitude increased was more rapid for MREs with lower particle contents. It is reasonable to assume that the matrix rubber plays a dominant role in controlling the fatigue of MREs when they contain fewer magnetic particles, e.g. 15% by volume. However, the fatigue behaviour of MREs is probably more dependent on

the particle networks when the magnetic particle content is increased beyond this level. The particle networks are very easily broken down in conditions of high loadings, but exhibit strength at low loadings which consequently lead to higher fatigue lives.



**Figure 5-4 Wöhler curves for SR and SR based MREs with different CI contents. Samples were tested in the absence of a magnetic field**

**Table 5-2 The gradient of S-N curves of each sample**

CI content	Gradient
15%	-0.1358
20%	-0.1031
25%	-0.0779
30%	-0.0638
35%	-0.0456

Equations for fatigue life prediction, relating life ( $N_f$ ) to engineering stress amplitudes ( $\sigma_a$ ) for SR based MREs were derived as follows:

$$\sigma_a = A_1 \ln(N_f) + A_2 \quad (5.1)$$

$$\ln(N_f) = \frac{\sigma_a - A_2}{A_1} \quad (5.2)$$

where  $A_1$  and  $A_2$  are material specific constants dependent on magnetic particle content. The values of  $A_1$  and  $A_2$  for MREs with various CI contents are listed in Table 5-3.

**Table 5-3 Values for  $A_1$  and  $A_2$  for a series of MREs with different CI contents**

CI content	$A_1$ (N/mm <sup>2</sup> )	$A_2$ (N/mm <sup>2</sup> )
15%	-0.1358	1.7961
20%	-0.1031	1.5071
25%	-0.0779	1.3191
30%	-0.0638	1.2132
35%	-0.0456	1.1348

If  $A_1$  is related to magnetic particle content ( $C_p$ ) a second order polynomial relationship can be found between them:

$$A_1 = -1.1457(C_p)^2 + 1.0123(C_p) - 0.261 \quad (R^2 = 0.9963) \quad (5.3)$$

$$\text{And assuming } A_2 = \sigma_{FCon}/2 \quad (5.4)$$

where  $\sigma_{FCon}$  is the stress amplitude of the cycles after the material has been conditioned. The cycles to achieve conditioning will be different for different rubbers. However, as 10 conditioning cycles is a typical value applied in industry [211], the stress amplitude at 10 cycles was chosen as a reasonable value for  $\sigma_{FCon}$ .  $\sigma_{FCon}$  for MREs with various CI contents are shown in Table 5-4.

**Table 5-4  $\sigma_{FCon}$  for MREs with various CI contents**

CI content	$\sigma_{FCon}$ (MPa)
15%	1.4834
20%	1.2699
25%	1.1395
30%	1.0658
35%	1.0289

Consequently, the equation for fatigue life prediction based on the failure stress of a conditioned test piece and particle content (vol%) for SR and CI based MREs can be stated as:

$$\ln(N_f) = \frac{\sigma_a - 0.5\sigma_{FCon}}{-0.1457(C_p)^2 + 1.0123(C_p) - 0.261} \quad (5.5)$$

where  $N_f$  is the cycles to failure;  $\sigma_a$  is the stress amplitude (MPa);  $\sigma_{FCon}$  is the stress amplitude for the sample to have a fatigue life of 10 cycles (MPa) and  $C_p$  is the volume fraction of the CI particles.

Hence it is suggested that Eqn. 5.5 can be used to determine the fatigue lives of silicone based MRE components subjected to complex loading, provided the principal alternating stresses at the points of failure are known. Further, it is suggested that Eqn. 5.5 can be used in its general form (Eqn. 5.6) for MREs based on other rubber compounds, where material constants  $D$ ,  $E$  and  $F$  (units MPa) are determined from equi-biaxial fatigue testing.

$$\ln(N_f) = \frac{\sigma_a - 0.5\sigma_{FCon}}{D(C_p)^2 + E(C_p) + F} \quad (5.6)$$

The maximum strain dependence of the fatigue life is shown in Figure 5-5 where the fatigue life of isotropic MREs with each CI content was plotted against the average maximum strain experienced by the material before failure. As can be seen from Figure 5-5, there was a good correlation between fatigue life and maximum strain for MREs containing 15% and 20% CI particles. However, for MREs with higher CI contents (25%, 30% and 35%), the fatigue life did not correlate well with the maximum strain. This indicates that maximum strain can not be used as a general fatigue life predictor for isotropic SR based MREs when particle content is taken into consideration.

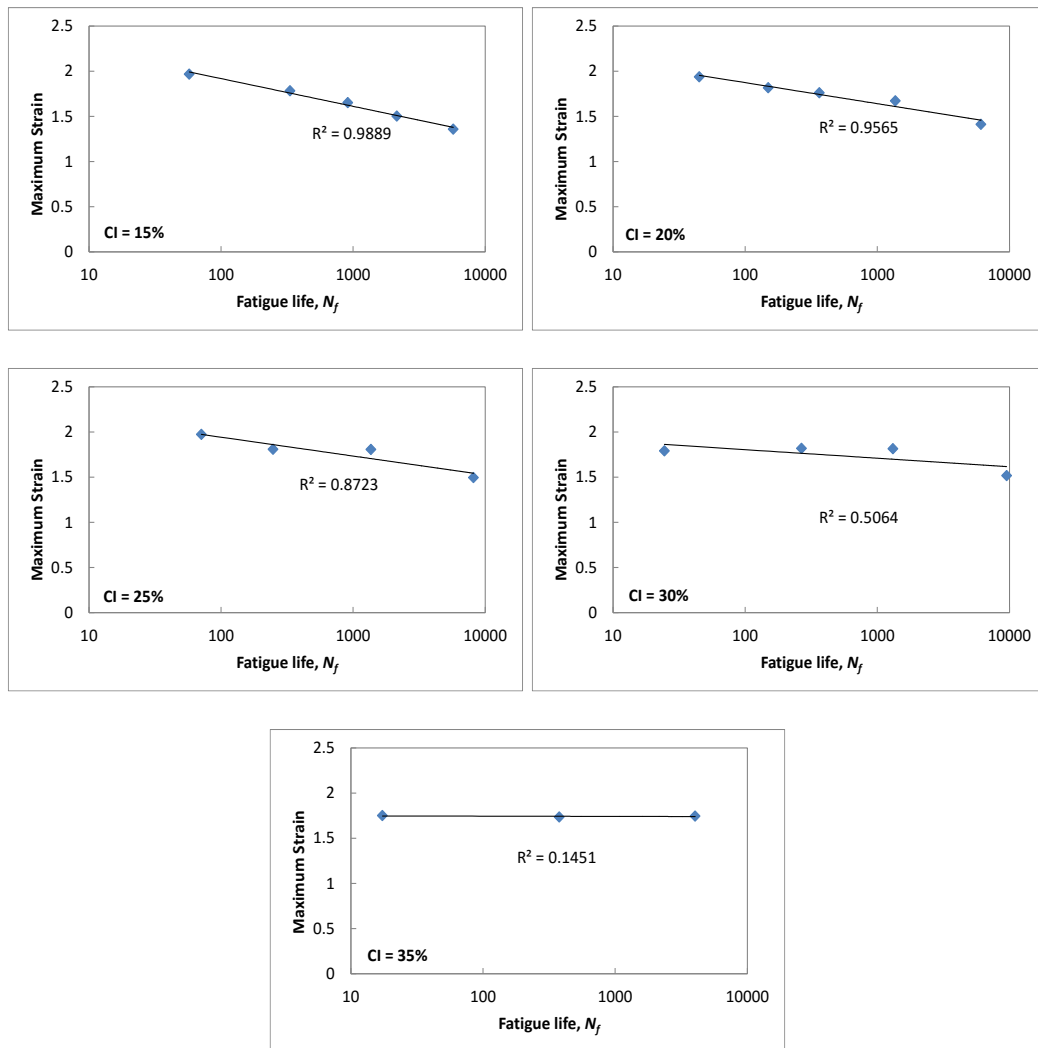


**Figure 5-5 Plot showing dependence of fatigue life on maximum strain for isotropic MREs with different CI contents. Samples were tested in the absence of a magnetic field**

## 5.4 Complex modulus

Figure 5-6 depicts the changes in complex modulus with the accumulation of equi-biaxial fatigue cycles for isotropic MREs containing different volume fractions of carbonyl iron particles. It can be seen that for each material,  $E^*$  decreased due to stress softening induced by the cyclic loading as cycles accumulated. The increases in hysteresis with increases in stress amplitude can be

observed from the first stress-strain cycles at stress amplitudes of 1 MPa, 0.875 MPa, 0.75 MPa and 0.625 MPa as shown in Figure 5-7.

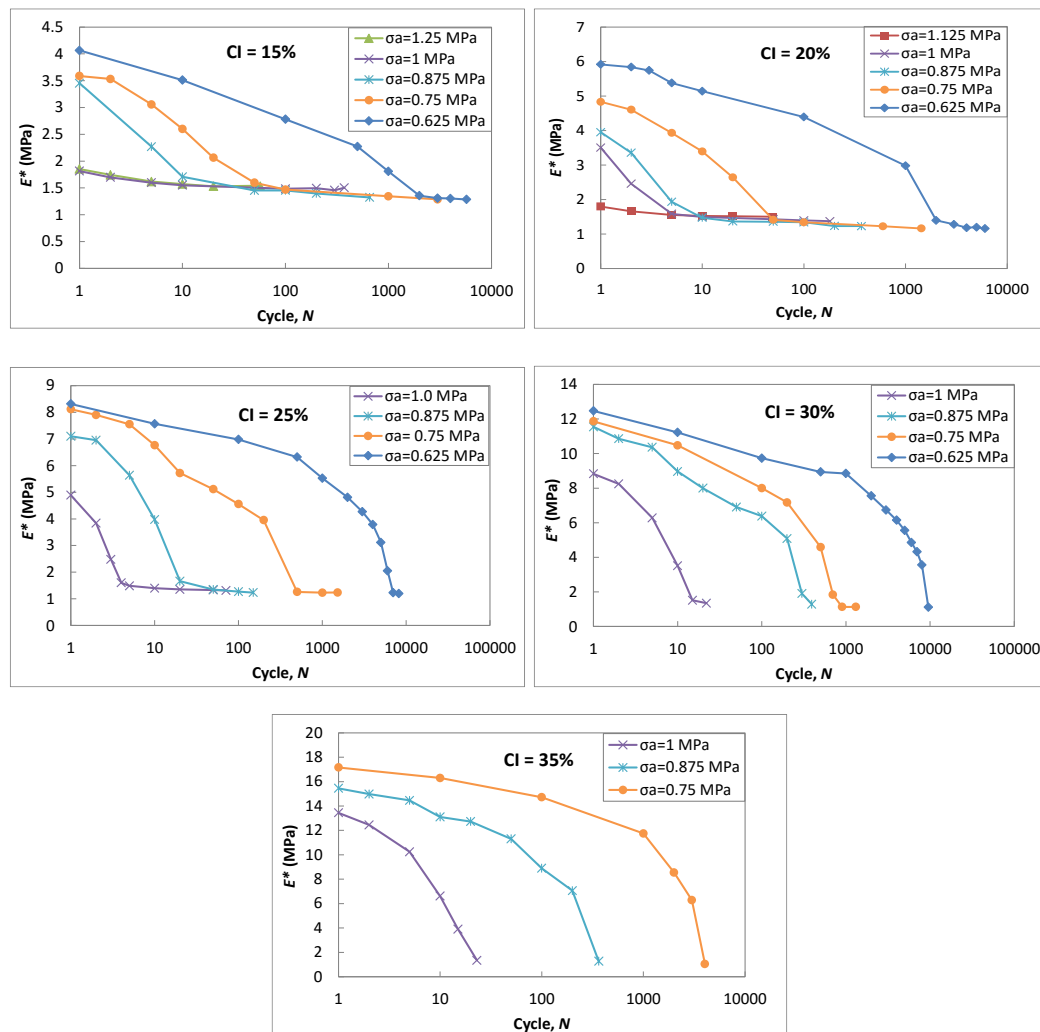


**Figure 5-6 Changes in  $E^*$  during the fatigue process for isotropic MREs containing different volume fractions of CI. Samples were tested in the absence of a magnetic field**

The higher the magnetic particle content in an MRE then the higher will be the material's elastic modulus. Rheological tests for PU and CI based anisotropic MREs tested in the absence of magnetic fields also found that the increase of particle content caused an increase in both the storage shear modulus and loss shear modulus (and consequently an increase in complex shear modulus) [70].

This is to be expected since the incorporation of rigid fillers typically increases the stiffness of an elastomeric material due to hydrodynamic reinforcement [212].

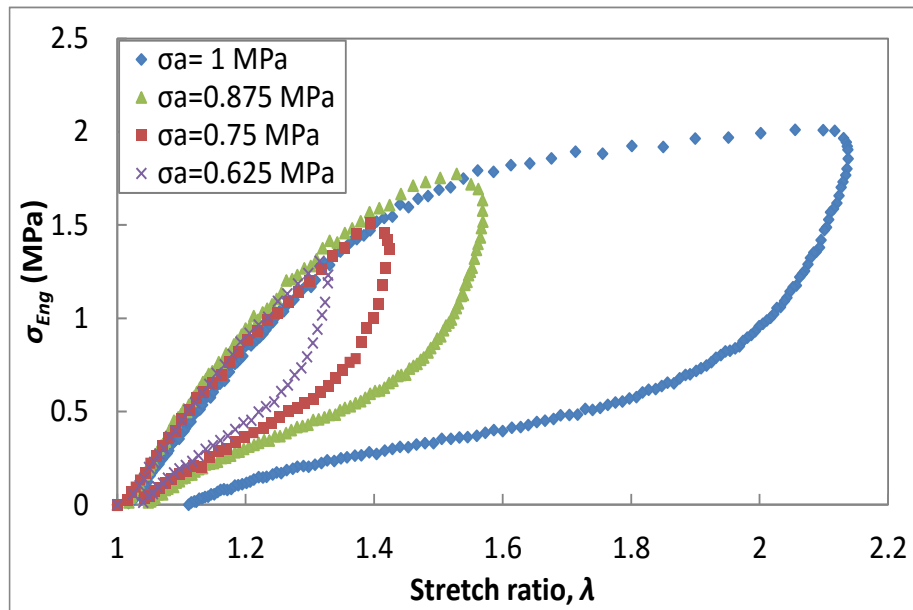
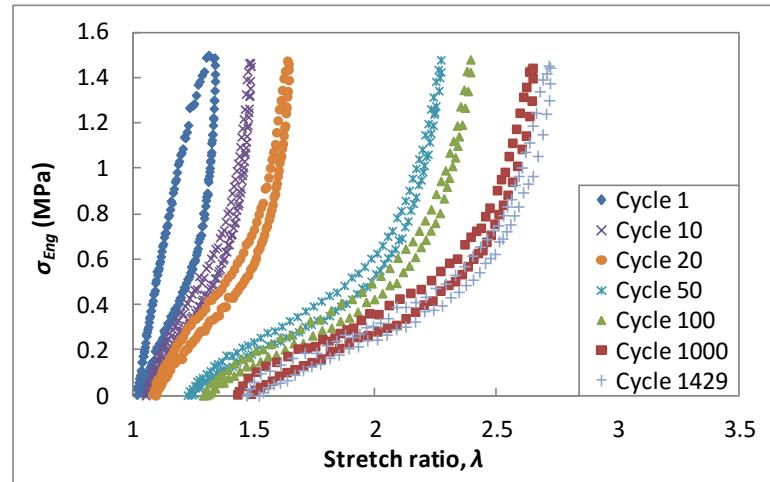


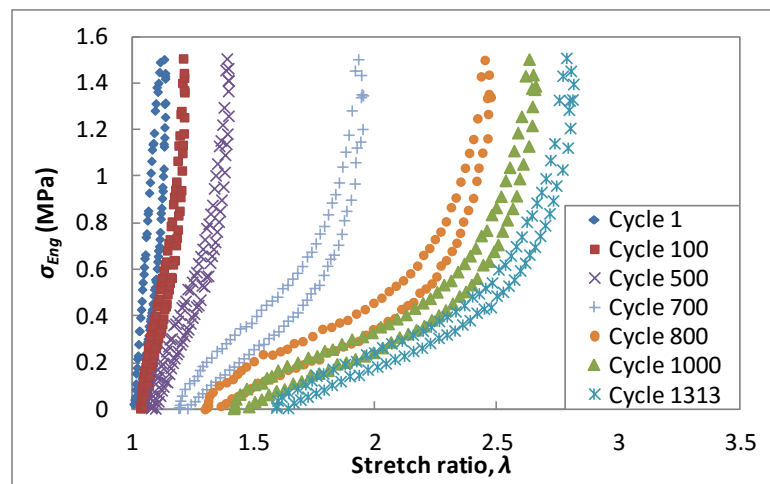
**Figure 5-7 Stress-strain curves for the first cycle induced by different stress amplitudes (CI = 15%)**

It is also worth noting that although the reductions in modulus were most significant in the first few cycles for MREs with lower particle contents, the rate of reduction was less when the samples were close to failure. However, for MREs with higher particle contents (30% and 35%),  $E^*$  decreased gradually with the accumulation of cycles and the materials subsequently failed after a rapid drop of  $E^*$  in the last few cycles. To assist in understanding this behaviour, stress-stretch ratio relations for MREs with 20% and 30% carbonyl iron particles during fatigue tests at a stress amplitude of 0.75 MPa are presented in Figure 5-8. It can be noted that both the samples failed after about 1400 cycles but they exhibited quite different stress-strain behaviour throughout the fatigue process. For MRE samples with 20% carbonyl iron particles, stress softening was most pronounced in the first dozens cycles and became insignificant afterwards. However, for MREs

containing 30% carbonyl iron particles, the stress-strain curves altered little in the first 100 cycles and large deformation predominantly occurred in the last few cycles before failure.



(a) CI = 20%



(b) CI = 30%

**Figure 5-8 Stress-stretch ratio curves for SR based MREs with 20% and 30% CI during a fatigue test at  $\sigma_a = 0.75$  MPa: (a) 20% CI, sample failed at 1430 cycles and (b) 30% CI, sample failed at 1314 cycles**

It is known that the total life of a rubber component subjected to fatigue loading comprises three stages: crack nucleation, crack propagation and rapid failure [213]. Crack nucleation plays a very important role in determining fatigue life because

the presence of a crack damages the structural integrity of a component and the hyperelastic field surrounding the crack offers little resistance to its growth [214]. During the fatigue tests on MREs, the cyclic loading induced continuous damage to the filler networks which resulted in a drop in  $E^*$ . For MREs containing fewer particles, after the filler networks were broken down, the matrix rubber reacted to the loading, producing large deformation, so the material eventually failed at a life depending on the stress amplitude applied. However, for MREs with higher particle contents, the breakdown of particle agglomerates and the debonding of particles from matrices induced high levels of crack nucleation and cavities in the matrix rubber. This deterioration in the matrix material led to a diminished ability to resist external loading. As a result, the samples underwent sudden failures after material specific drops in  $E^*$ .

Nonetheless, for each MRE sample tested, it was found that fatigue failure took place at a limiting value of  $E^*$  regardless of the stress amplitudes applied. As can be seen from Table 5-5, these values are very similar for each CI content and are generally lower than the measured values of  $E^*$  at failure for pure silicone rubber. It suggests that the weakening of the rubber matrix is the controlling parameter in respect of complex modulus at fatigue failure. However, the dissimilarity of the limiting value of  $E^*$  for pure silicone rubber and MREs as well as the dependence of changes in  $E^*$  on carbonyl iron content during the fatigue process indicate that separation and crack initiation at interfacial layers has a great influence on the fatigue process of MREs.

**Table 5-5  $E^*$  just prior to failure of isotropic MREs with different CI contents (without magnetic fields)**

<b>CI contents</b>	<b><math>E^*</math> (MPa)</b>
0%	$1.75 \pm 6.58\%$
15%	$1.38 \pm 8.19\%$
20%	$1.32 \pm 10.05\%$
25%	$1.26 \pm 8.12\%$
30%	$1.24 \pm 6.84\%$
35%	$1.22 \pm 9.13\%$

## 5.5 Dynamic stored energy

The evolution of stored energy density against cycles for MREs with different CI contents is depicted in Figure 5-9. For each sample, the stored energy density increased with the accumulation of cycles at each constant stress amplitude. However, the change of stored energy density during the entire fatigue process differed for MREs with various particle contents. It can be seen that the stored energy density increased significantly in the first few cycles before becoming stable for MREs with lower carbonyl iron contents (15%, 20% and 25%). However, dependent on stress amplitude, for high particle contents (30% and 35%) dynamic stored energy remained virtually unchanged in the first few cycles and increased rapidly in the last few cycles before material failure. This is because with the increase of the particle content, the distance between the particles became smaller and consequently restrained rubber could form between the particles [40]. The deformation of the restrained rubber was inhibited, so the material deformed little with the accumulation of cycles which resulted in small changes in dynamic stored energy. However, after the particle agglomerates and networks were broken down, the material experienced large deformation and consequently rapid increase in dynamic stored energy just prior to failure. As for the observed changes in

complex modulus, the differences in dynamic stored energy for MREs with different particle contents could be attributed to quite different fatigue mechanisms for each material.

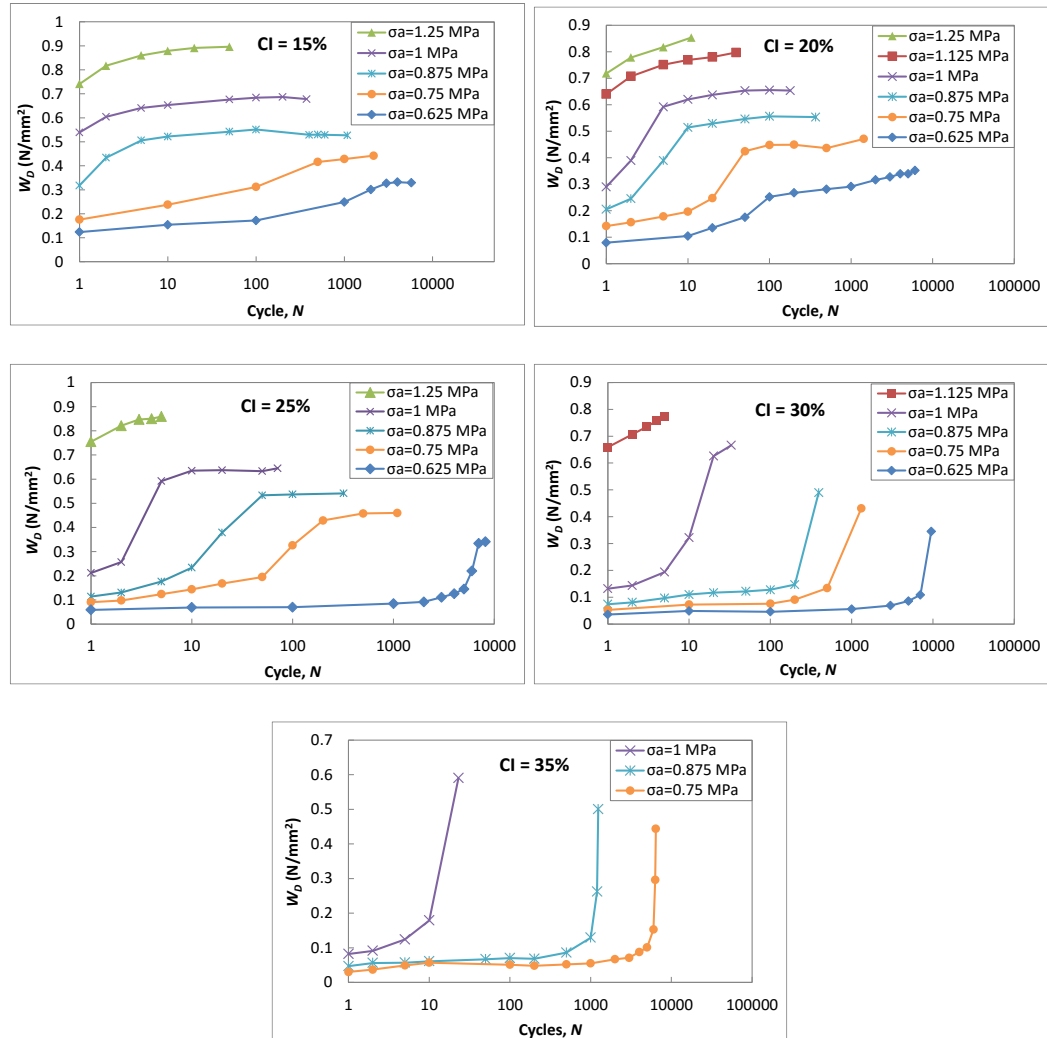


**Figure 5-9 Evolution of dynamic stored energy against cycles for isotropic MREs with different CI contents. Samples were tested in the absence of a magnetic field**

As shown in Figure 5-10, when plotted against cycles to failure, the stored energy density at failure for a range of stress amplitudes was found to decrease linearly regardless of the particle content. This indicates that the stored energy criterion can be used as a plausible fatigue life predictor for isotropic SR based MREs irrespective of the magnetic particle content and the stress amplitudes applied. A

stored energy density based equation for fatigue life prediction can be written by relating life ( $N_f$ ) to dynamic stored energy ( $W_D$ ) as shown:

$$W_D = B_1 \ln(N_f) + B_2 \quad (5.7)$$

$$\ln(N_f) = \frac{W_D - B_2}{B_1} \quad (5.8)$$

where  $B_1$  and  $B_2$  are material specific constants dependent on the magnetic particle content. The values for  $B_1$  and  $B_2$  for MREs with various CI contents are given in Table 5-6.

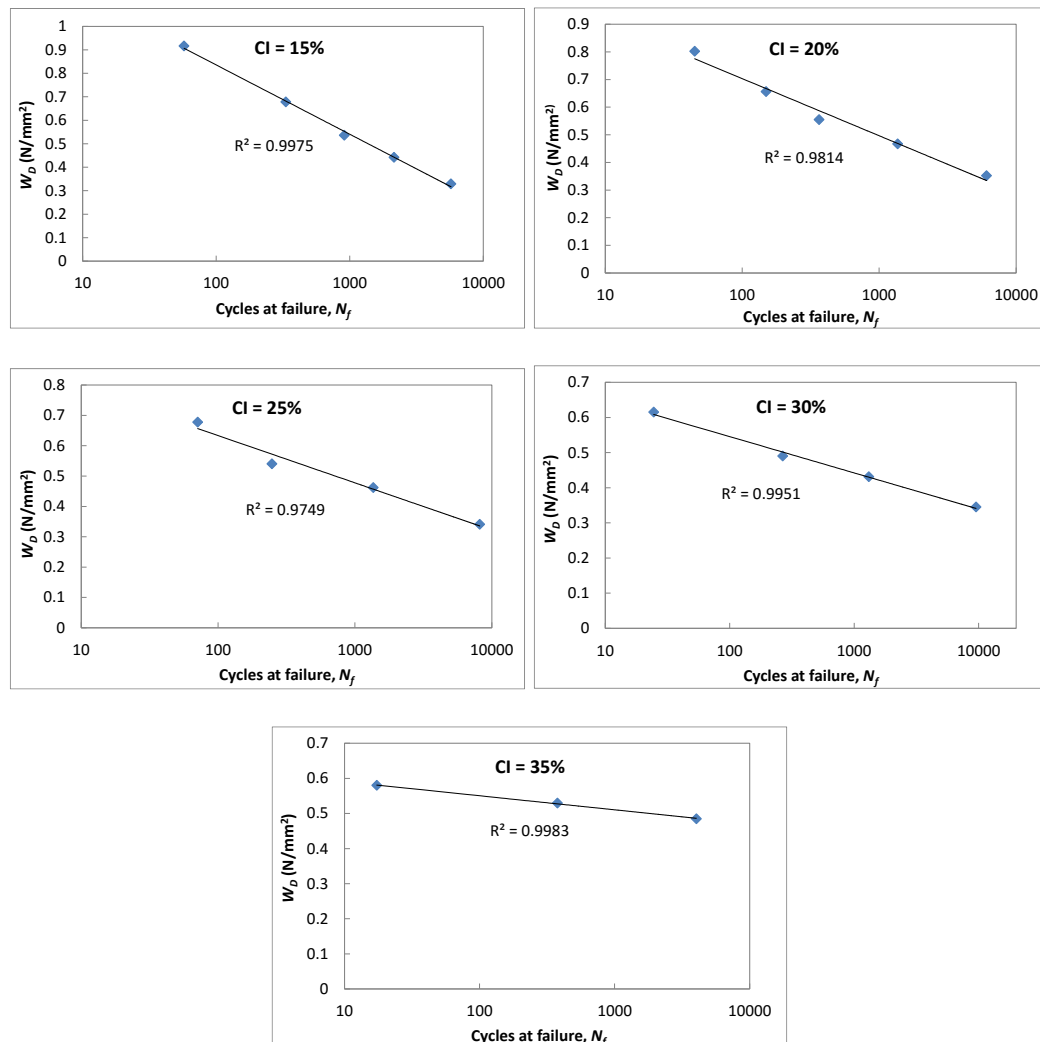


**Figure 5-10** Plots of stored energy density at failure versus cycles at failure for isotropic SR based MREs with different CI contents. Samples were tested in the absence of a magnetic field

**Table 5-6 Values for  $B_1$  and  $B_2$  for a series of MREs with different CI contents**

CI content	$B_1$ (mm <sup>2</sup> /N)	$B_2$ (mm <sup>2</sup> /N)
15%	-0.1282	1.4262
20%	-0.0898	1.1168
25%	-0.0676	0.9449
30%	-0.0448	0.7519
35%	-0.0174	0.6306

Relating  $B_1$  to magnetic particle content ( $C_p$ ) and a second order polynomial relationship can be found between them:

$$B_1 = -0.6114(C_p)^2 + 0.8389(C_p) - 0.238 \quad (R^2 = 0.9937) \quad (5.9)$$

$$B_2 = W_{DCon} \quad (5.10)$$

where  $W_{DCon}$  is the dynamic stored energy (per unit volume) of the cycles at failure after the material is conditioned (N/mm<sup>2</sup>). As in Section 5.3, 10 conditioning cycles was chosen and  $W_{DCon}$  for MREs with various CI contents are shown in Table 5-7.

**Table 5-7 Values for  $W_{DCon}$  for MREs with various CI contents**

CI content	$W_{DCon}$ (N/mm <sup>2</sup> )
15%	1.1310
20%	0.9100
25%	0.7892
30%	0.6487
35%	0.5905

As  $W_D$  is a function of  $\sigma$  and  $\lambda$

$$W_D = \int \sigma \lambda d\lambda \quad (5.11)$$

An equation for fatigue life prediction based on dynamic stored energy can be derived as:

$$\ln(N_f) = \frac{\int \sigma \lambda d\lambda - (\int \sigma \lambda d\lambda)_{Con}}{-0.6114(C_p)^2 + 0.8389(C_p) - 0.238} \quad (5.12)$$

where  $\sigma$  is the engineering stress;  $\lambda$  is the stretch ratio;  $\left(\int \sigma \lambda \partial \lambda\right)_{Con}$  is the dynamic stored energy of the cycles at failure after the material is conditioned and  $C_p$  is the volume fraction of the CI particles.

As in Section 5.3, a general equation (Eqn. 5.13) relating fatigue life to dynamic stored energy can be written for MREs based on other elastomer matrices provided the material constants  $L$ ,  $M$  and  $N$  (units  $\text{N}/\text{mm}^2$ ) are derived from equibiaxial dynamic testing.

$$\ln(N_f) = \frac{\int \sigma \lambda \partial \lambda - \left(\int \sigma \lambda \partial \lambda\right)_{Con}}{L(C_p)^2 + M(C_p) + N} \quad (5.13)$$

## 5.6 Damping loss factor

The performance of MRE devices are very dependent on the damping capabilities of MRE materials, so it is crucial that during the fatigue process these properties are investigated. The variations of damping loss factor  $\eta$  with respect to cycles at different stress amplitudes for isotropic SR based MREs with different CI contents are shown in Figure 5-11 and the absolute values of dissipated energy are shown in Figure 5-12.

As can be seen from Figure 5-11, the cyclic loading at various loading levels induced an overall decrease in the damping loss factor throughout the entire fatigue test for MREs containing different volume fractions of carbonyl iron particles. However, for each material,  $\eta$  decreased primarily in the first few cycles and reached a limiting value at failure irrespective of the stress amplitudes applied. This indicates that the damping properties of MREs can be maintained at stable levels during the entire service life after conditioning has taken place. The value

of  $\eta$  at failure was between 0.019–0.079 although MREs with higher CI contents generally exhibited a slightly higher  $\eta$  as shown in Table 5-8.

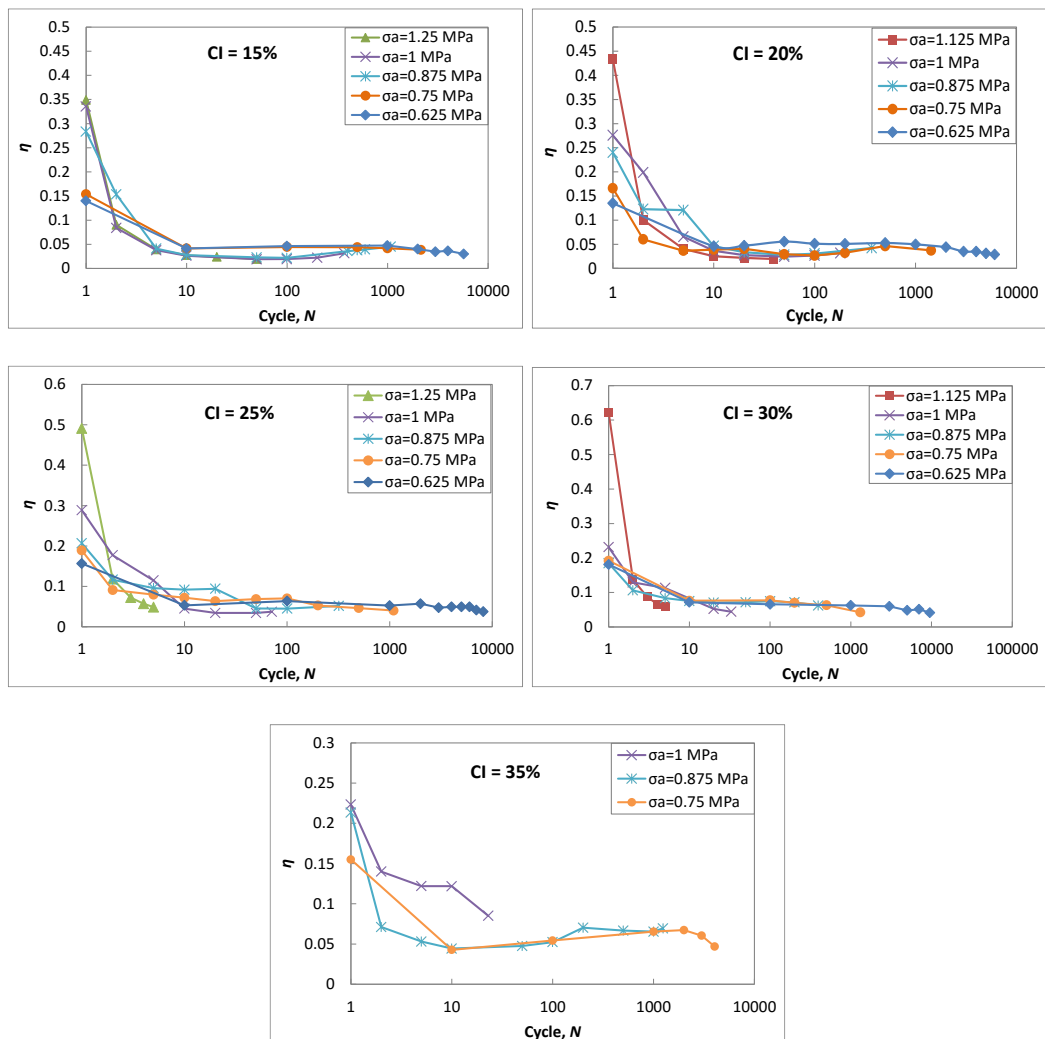


**Figure 5-11 Damping loss factor versus cycles for isotropic MREs with different CI contents.**

**Samples were tested in the absence of a magnetic field**

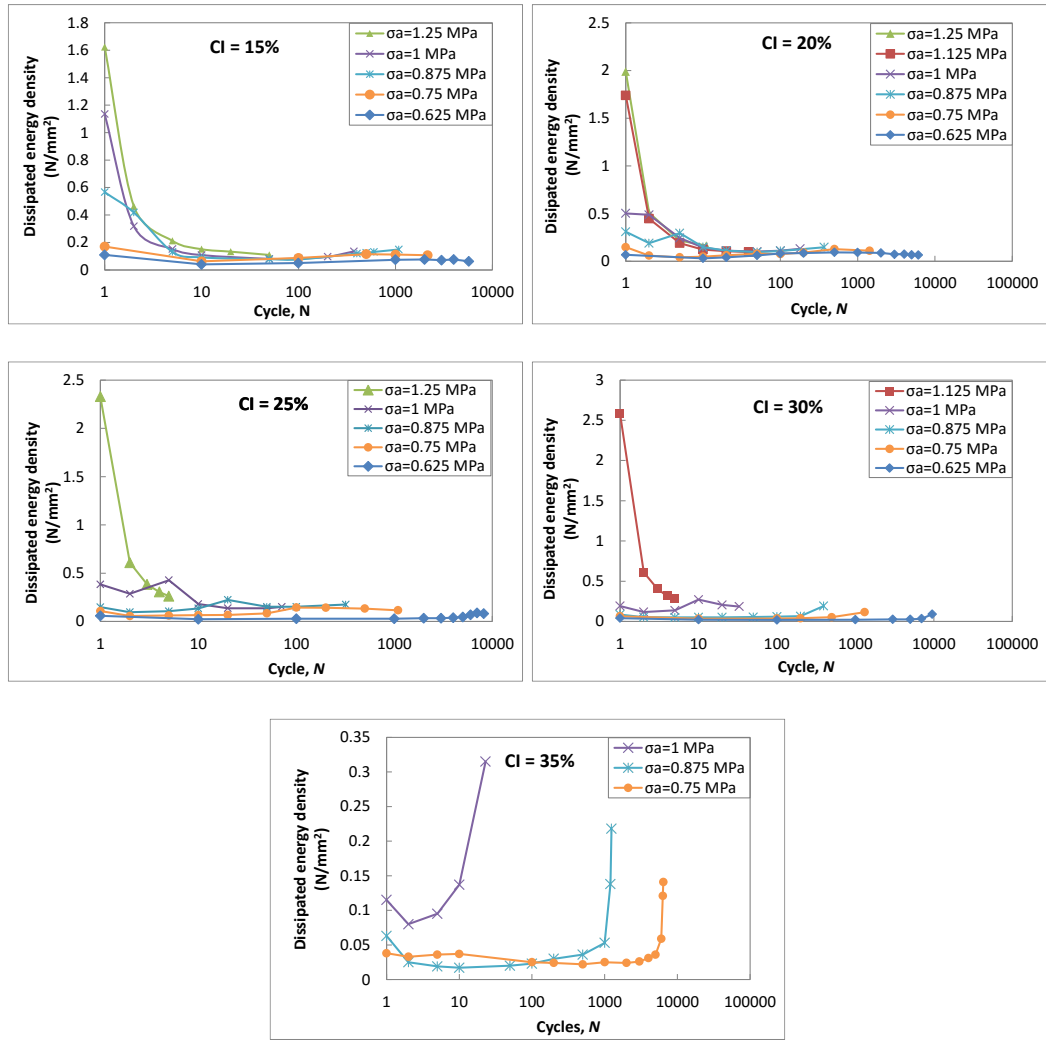


Figure 5-12 Plots of dissipated energy density versus cycles for isotropic MREs with different CI contents. Samples were tested in the absence of a magnetic field

Table 5-8 Values of  $\eta$  at failure for MREs with different CI contents (without magnetic fields)

CI content	$\eta$
15%	0.019–0.045
20%	0.019–0.046
25%	0.033–0.051
30%	0.042–0.062
35%	0.045–0.079

## 5.7 Summary

In this chapter, equi-biaxial fatigue behaviour of isotropic silicone based MREs with various carbonyl iron contents was investigated. It was found that MREs with lower particle content exhibit higher fatigue resistance to higher loadings whereas MREs with higher particle content show higher fatigue resistance at lower loadings due to the complex particle networks formed in their structure. As the content of carbonyl iron particles increased, the fatigue life of MREs generally decreased at stress amplitudes above 1 MPa but increased at stress amplitude of 0.625 MPa. For stress amplitudes between 0.625 MPa and 1 MPa, MREs with very low (15%) and very high (35%) particle content higher fatigue lives were exhibited than those of MREs with medium particle contents (20%–30%).

Changes in physical properties which can be observed by evaluating complex modulus ( $E^*$ ) during the fatigue process were also studied for MREs with different particle contents. It was shown that for each material,  $E^*$  decreased as cycles accumulated. Tests at lower stress amplitudes generally exhibited longer times (more cycles) for stress softening to reach a minimum. For the same loading conditions, MREs with lower particle content failed after  $E^*$  had stabilised while MREs containing more particles failed after a rapid drop in  $E^*$  just prior to failure. However, for each material tested, fatigue failure took place at a limiting value of  $E^*$  between 1.22 MPa and 1.38 MPa regardless of the particle content and the stress amplitudes applied.

Dynamic stored energy was found to decrease with the accumulation of cycles for each material tested over a range of stress amplitudes. When plotted against cycles to failure, the dynamic stored energy was found to decrease linearly, which indicates that dynamic stored energy can be used as a plausible predictor in

determining the fatigue life of MREs irrespective of particle content. This builds significantly on the conclusion gleaned from the dynamic tests described in Chapter 4 that dynamic stored energy can be used as a reliable predictor in determining the fatigue life of isotropic and anisotropic MREs containing 20% magnetic particles.

Damping loss factor generally decreased throughout the entire fatigue process for MREs containing different volume fractions of carbonyl iron particles. The value of  $\eta$  at failure was between 0.019–0.079 although MREs with higher CI contents generally exhibited a slightly higher  $\eta$  due to more interfacial slippages [215] at the magnetic particle-silicone matrix interfaces.

It was noticed that there were some variations between the results quoted in this chapter (the second series) and those obtained in the previous tests (the first series) as described in Chapter 4 for isotropic MREs containing 20% CI particles. The stretch ratios at failure in the static tests were very similar in both series, though the material in the second series did seem stiffer as the *UTS* was 16% higher on average. There is always scatter in fatigue life results for the most homogeneous materials (such as metals with carefully controlled content of alloying elements, grain size and heat treatments), so discrepancies in fatigue results for silicone based MREs made in small batch sizes is to be expected. Importantly, the limiting complex moduli are similar for both tests and trends are comparable for different amplitudes.

The minor dissimilarities between two batches of tests could be attributed to the compounds differing due to variations in time and room temperature during curing, though every attempt was made to keep these variations to a minimum. Small changes in the silicone due to aging occurring during storage and minor difference

in the distribution and contiguity of the ferromagnetic particles could also have influenced the dissimilarities between the two batches. The continuous improvement in the development of the equi-biaxial testing rig also could have also contributed to the increased *UTS* and fatigue lives predicted in the second series of tests. As the correlation coefficient ( $R^2$ ) between fatigue life and stress amplitude in the second series (0.9924) was noticeably higher than that in the first series (0.9398), it is reasonable to suggest that the results described in this chapter are more reliable.

# Chapter 6 Equi-biaxial fatigue behaviour of MREs subjected to magnetic fields during cyclic testing

## 6.1 Introduction

In the previous chapters, the equi-biaxial fatigue behaviour of silicone based MREs in the absence of magnetic fields was described. However, in their engineering applications, MREs are intended to be used where magnetic fields are switched off and on. Hence it is crucial that the fatigue behaviour of MREs in the presence of magnetic fields is also investigated. For this to occur, a Halbach Array (as shown in Appendix B which was used to produce magnetic fields during the material fabrication) was positioned around the bubble inflation testing orifice as depicted schematically in Figure 6-1. The position of the Halbach Array ensured the tested specimens were subjected to a relatively uniform mean magnetic field strength of about 400 mT during inflation and deflation.

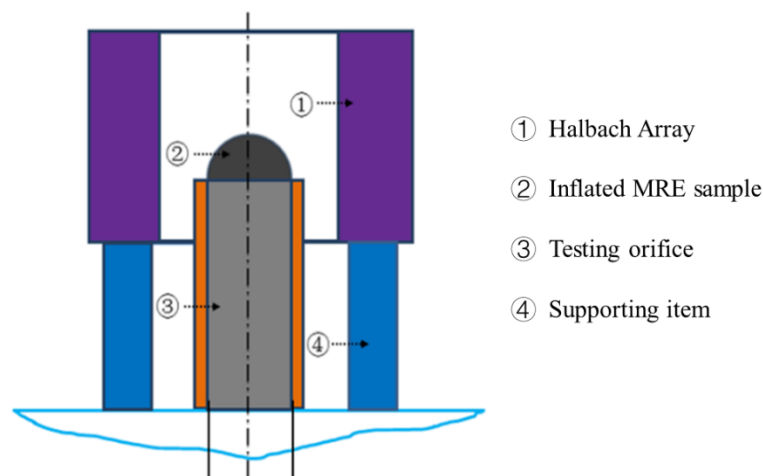


Figure 6-1 Equi-biaxial fatigue test setup for fatigue testing in the presence of an external magnetic field provided by Halbach Array

## 6.2 Effect of magnetic fields on fatigue life of MREs

Figure 6-2 shows the Wöhler curves of MREs containing different volume fractions of carbonyl iron particles tested in the absence and in the presence of the magnetic field provided by the Halbach array. The values of fatigue life are shown in Table 6-1.

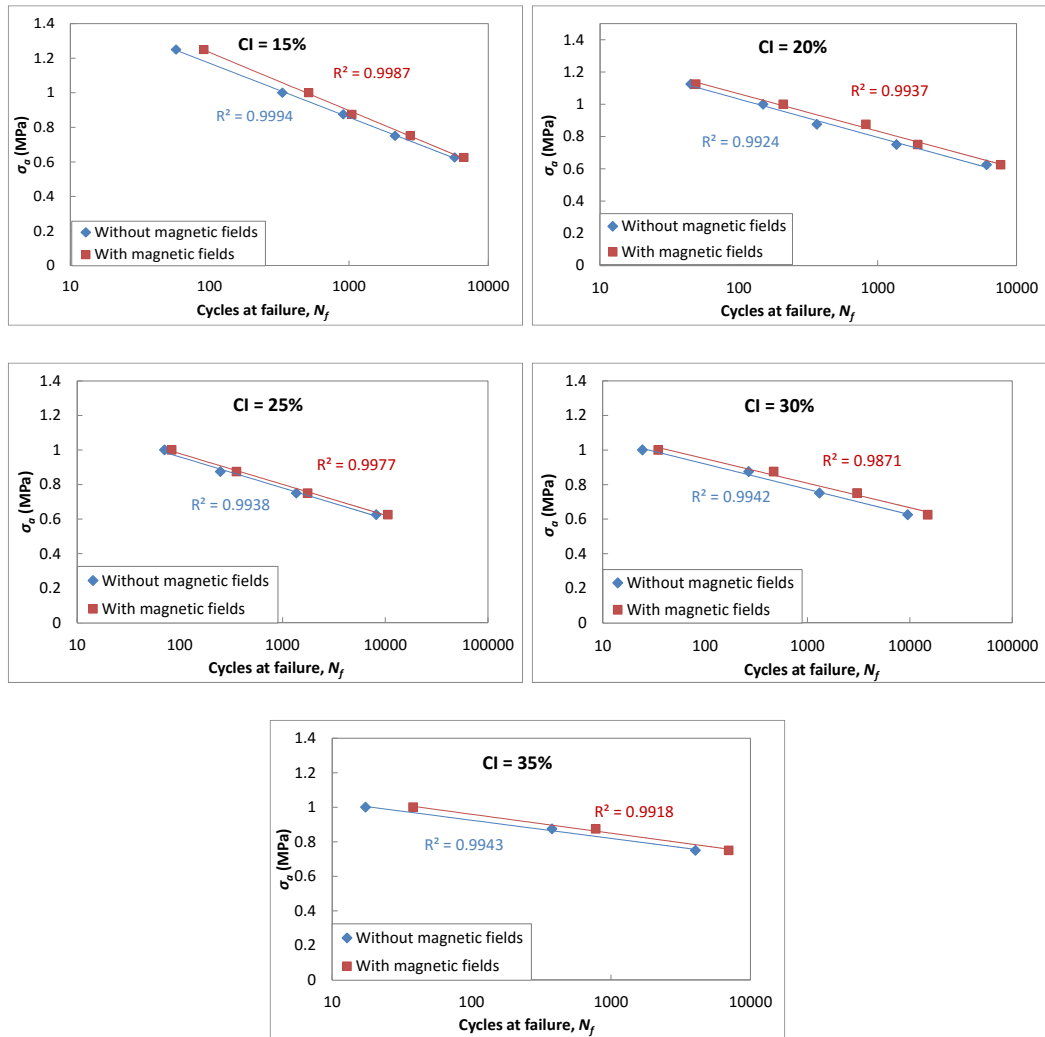


Figure 6-2 Wöhler curves of MREs with various CI contents tested without and with a magnet

**Table 6-1 Fatigue life of MREs tested with and without magnetic fields**

CI content	$\sigma_a$ / MPa	$N_f$ (Average cycles to failure)	
		with magnetic fields	without magnetic fields
15%	1.25	91	58
	1	514	333
	0.875	1051	911
	0.75	2756	2146
	0.625	6684	5735
20%	1.125	49	45
	1	209	150
	0.875	822	365
	0.75	1945	1368
	0.625	7679	6093
25%	1	84	71
	0.875	356	248
	0.75	1758	1364
	0.625	10603	8167
30%	1	35	25
	0.875	468	267
	0.75	3055	1314
	0.625	14935	9528
35%	1	38	17
	0.875	777	378
	0.75	6982	4033

As can be seen from Figure 6-2 and Table 6-1, for MREs with the same CI content, the fatigue life was higher when the samples were tested in the magnetic field. When a magnetic field was applied to MREs, the interaction between particles increased and the enhanced inter-particle magnetic force acted as a magnetic loading to compress the silicone matrix [63]. It was also reported that the application of a magnetic field induced an overall compression on the MR solids consisting of random, statistically homogeneous distributions of ferromagnetic inclusions within an elastic matrix, in the direction of and in directions orthogonal to the magnetic field [216]. So when subjected to the equibiaxial tension loading in the bubble inflation testing, MREs exhibited higher

fatigue resistance in the presence of magnetic fields than in the absence of magnetic fields.

Eqns. 5.1 and 5.2 can also be used for fatigue life prediction for MREs subjected to external magnetic fields. The values of  $A_1$  and  $A_2$  for MREs with various CI contents are listed in Table 6-2.

**Table 6-2 Values for  $A_1$  and  $A_2$  for MREs tested in magnetic fields**

CI content	$A_1$ (N/mm <sup>2</sup> )	$A_2$ (N/mm <sup>2</sup> )
15%	-0.146	1.9061
20%	-0.101	1.5285
25%	-0.077	1.3352
30%	-0.064	1.2332
35%	-0.048	1.1785

Similar to that described in Section 5.3, the equation for fatigue life prediction in the presence of magnetic fields based on the failure stress of a conditioned test piece can be derived as:

$$\ln(N_f) = \frac{\sigma_a - 0.5\sigma_{FCon}}{-1.9714(C_p)^2 + 1.4517(C_p) - 0.3171} \quad (6.1)$$

where  $N_f$ ,  $\sigma_a$  and  $\sigma_{FCon}$  are as previously defined.

The values of  $\sigma_{FCon}$  for MREs with various CI contents are shown in Table 6-3.

**Table 6-3 Values of  $\sigma_{FCon}$  for MREs in the presence of magnetic fields**

CI content	$\sigma_{FCon}$ (MPa)
15%	1.5697
20%	1.2959
25%	1.1579
30%	1.0904
35%	1.0680

Eqn. 5.6 can also be used as a general equation for MREs based on other rubber compounds when they are subjected to external magnetic fields, where material

constants  $D$ ,  $E$  and  $F$  (units MPa) are determined from equi-biaxial fatigue testing in the presence of magnetic fields.

The maximum strain dependence of the fatigue life for isotropic MREs subjected to external magnetic fields is shown in Figure 6-3. As for the case when the samples were tested in the absence of magnetic fields, there was not a good correlation between fatigue life and maximum strain when the particle content was above 30%.

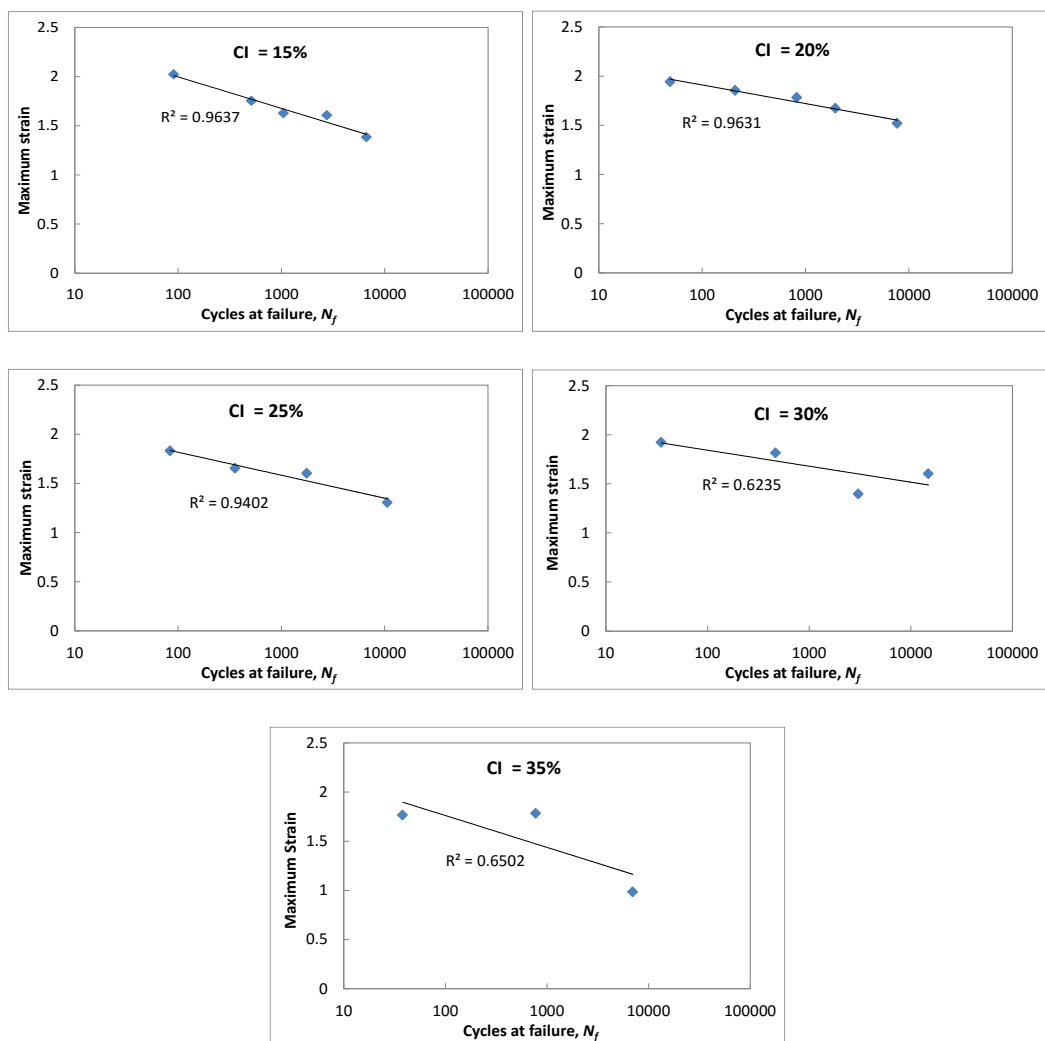
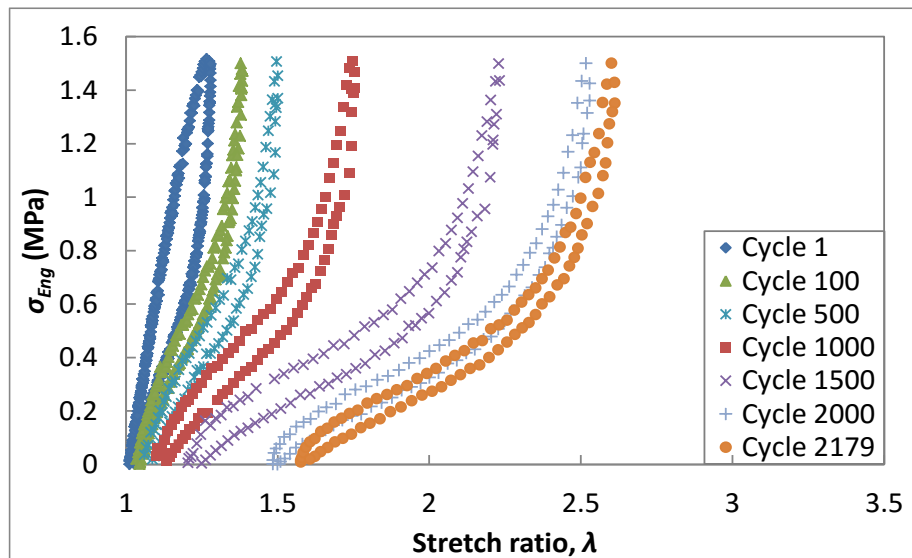


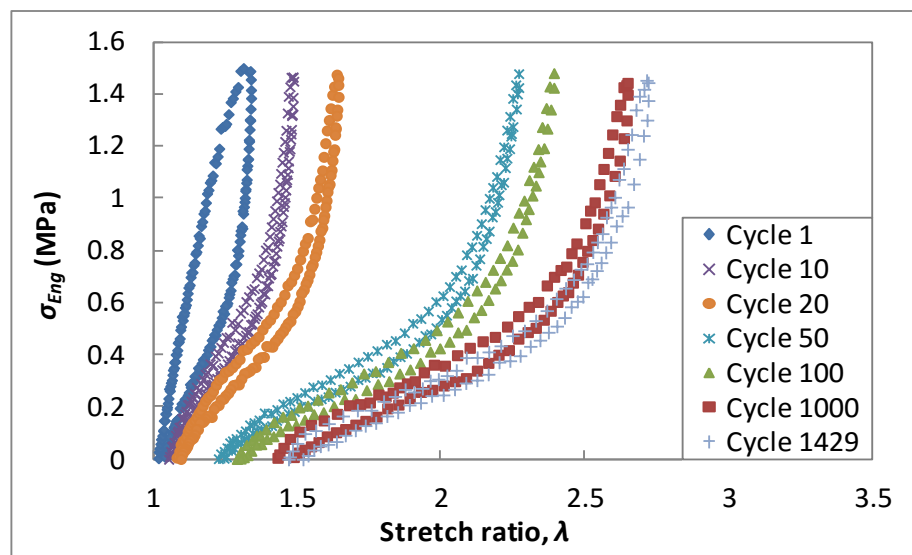
**Figure 6-3 Plot showing dependence of fatigue life on maximum strain for isotropic MREs with different CI content. Samples were tested in the presence of a magnetic field**

### 6.3 Stress-strain behaviour

Figure 6-4 shows the stress-strain behaviour of MRE samples during fatigue tests in the presence and in the absence of magnetic fields. In this figure, the behaviour of the 20% CI content samples is depicted, but curves were similar for all CI contents.



(a)



(b)

Figure 6-4 Stress-stretch ratio curves for MREs with 20% CI during a fatigue test at  $\sigma_a = 0.75$  MPa, (a) with and (b) without magnetic fields applied

The plots clearly indicate that the algorithm employed to maintain constant engineering stress limits as the bubble material softened, kept the stress range within acceptable limits. Stress softening and hysteresis continued as cycles accumulated in both cases. However, the stress-strain behaviour of MRE samples was greatly influenced by the application of external magnetic fields. As can be noted from Figure 6-4, at the same maximum engineering stress of 1.5 MPa, the stretch ratio for the same cycle was significantly lower when the sample was tested in a magnetic field (with the exception of the first loading), e.g. at 100 cycles, the maximum stretch ratio was 2.39 when the sample was tested without a magnetic field while it was only 1.38 in the presence of a magnetic field. It is known that an external magnetic field causes the interaction between particles to increase, hence their attractions to each other clearly became greater [13]. However, compared with when the field was absent, these enhanced interactions between magnetic particles restricted the mobility of the elastomer chains, leading to smaller deformations for the same number of cycles.

## **6.4 Complex modulus**

Changes in complex modulus ( $E^*$ ) at various stress amplitudes for MRE samples tested in the presence of magnetic fields are shown in Figure 6-5. It was found that, as was the case with samples tested in the absence of magnetic fields,  $E^*$  of MREs subjected to magnetic fields decreased with accumulated cycles regardless of the stress levels applied. However, the decrease in  $E^*$  was more gradual when the samples were tested in magnetic fields and this was more evident in MREs with lower CI contents and in tests at lower stress amplitudes. This result coincided with the stress-strain behaviour described in Section 6.3. When an

external magnetic field was applied to the MREs sample, the magnetic interaction force between the particles was enhanced and this consequently obstructed the movement of elastomer molecular chains [40], so it took longer for specimens to undergo large deformations and for  $E^*$  to reach the failure limit at a similar engineering stress.

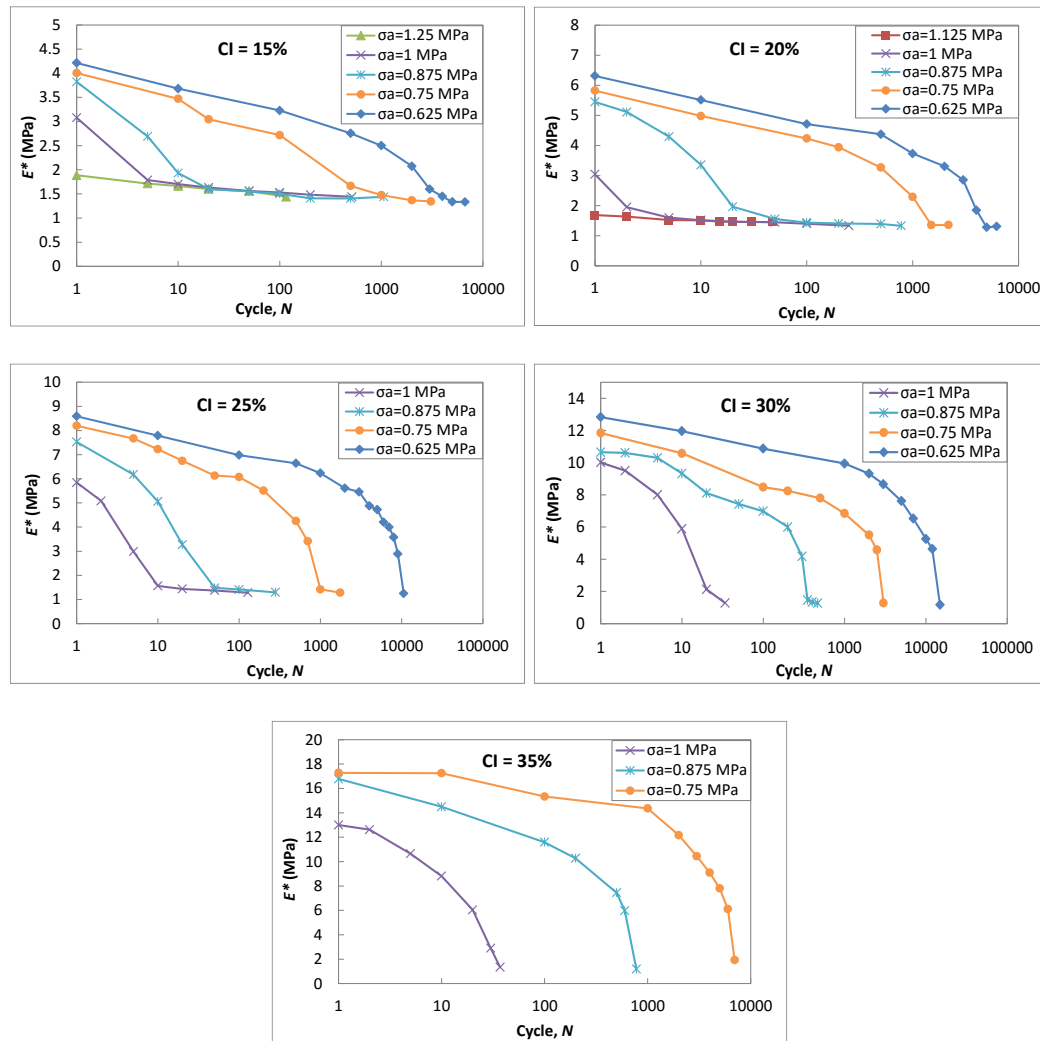


**Figure 6-5 Evolution of  $E^*$  during testing for MREs with various CI contents. Samples were tested in the presence of a magnetic field**

Regardless of the stress amplitude applied, all samples failed at a limiting value of  $E^*$  ranging between 1.28 and 1.44 MPa (refer to Table 6-4). When compared with previous results without magnetic fields, it was found that  $E^*$  at failure for MREs

with various particle contents were slightly higher in the presence of magnetic fields, but this was in a relatively small range.

**Table 6-4  $E^*$  at failure for MREs tested with magnetic fields applied**

<b>CI content</b>	<b><math>E^*</math> at failure (MPa)</b>
15%	$1.44 \pm 5.58\%$
20%	$1.37 \pm 3.25\%$
25%	$1.33 \pm 6.12\%$
30%	$1.27 \pm 4.24\%$
35%	$1.28 \pm 5.99\%$

## 6.5 Dynamic stored energy

The evolution of dynamic stored energy against cycles for the tests on isotropic MREs subjected to magnetic fields is shown in Figure 6-6. When plotted against cycles to failure, the stored energy density at failure for a range of stress amplitudes was found to decrease linearly for each sample as shown in Figure 6-7. This indicates that the stored energy criterion can also be used as a plausible fatigue life predictor for MREs when they are subjected to external magnetic fields. A stored energy-based equation for fatigue life prediction can be written by relating life ( $N_f$ ) to dynamic stored energy density ( $W_D$ ) as represented by Eqns. 5.7 and 5.8. The values for  $B_1$  and  $B_2$  for MREs with various CI contents subjected to magnetic fields are given in Table 6-5.

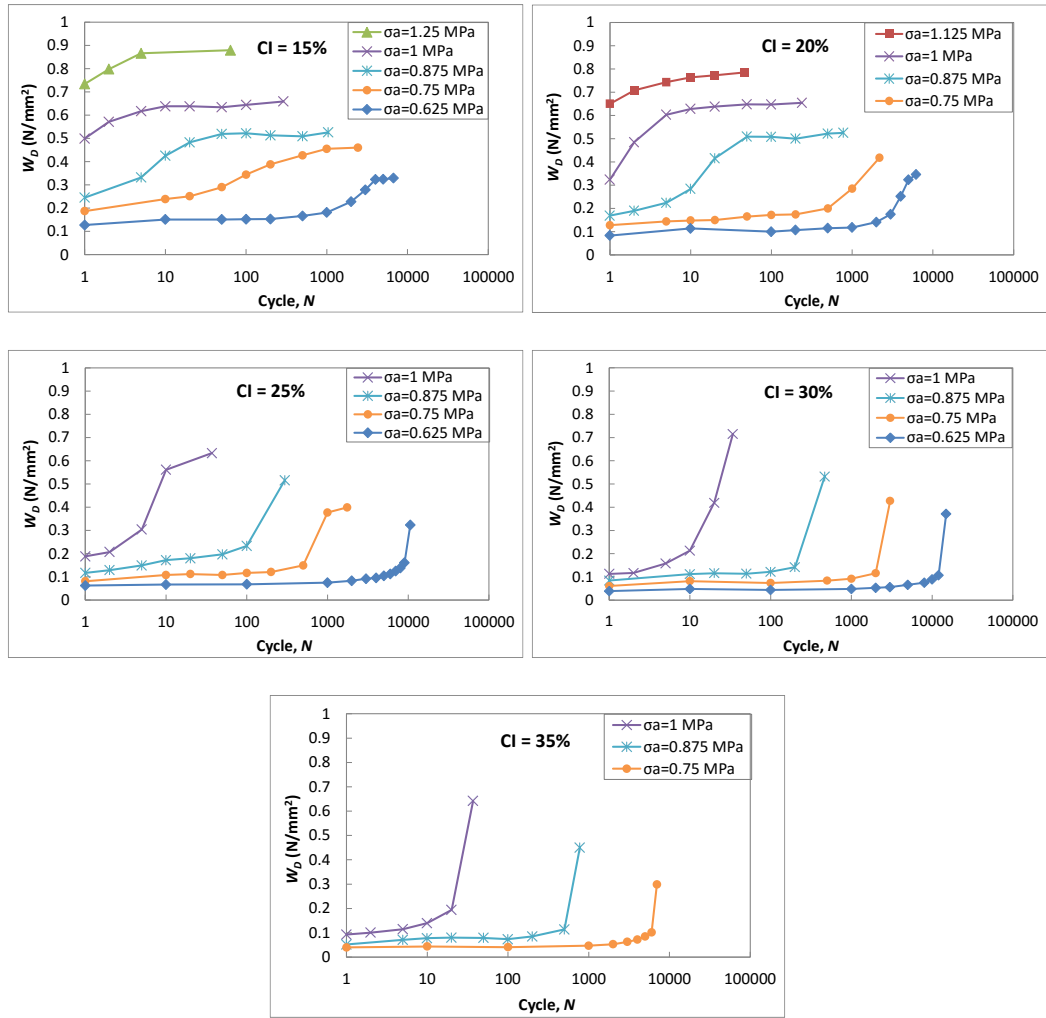


Figure 6-6 Evolution of stored energy density versus cycles for isotropic MREs with different CI contents. Samples were tested in the presence of a magnetic field

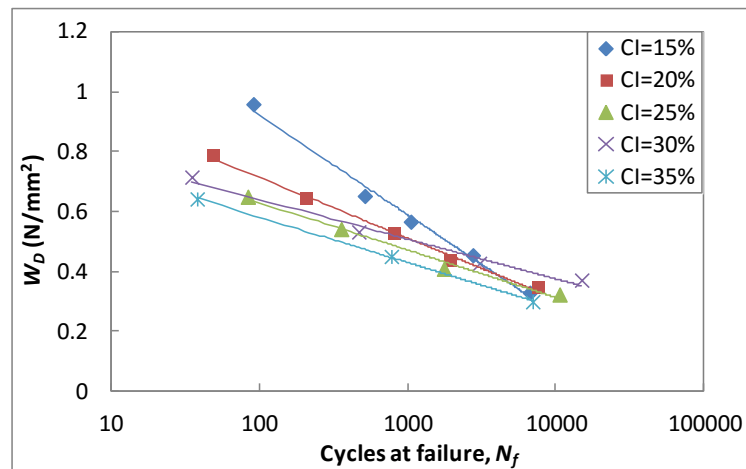


Figure 6-7 Stored energy density at failure versus cycles at failure for isotropic MREs with different CI contents. Samples were tested in the presence of a magnetic field

**Table 6-5 Values for  $B_1$  and  $B_2$  for MREs tested with magnetic fields applied**

CI content	$B_1$ (mm <sup>2</sup> /N)	$B_2$ (mm <sup>2</sup> /N)
15%	-0.144	1.584
20%	-0.088	1.1174
25%	-0.069	0.9448
30%	-0.058	0.9049
35%	-0.066	0.8827

Similar to the situation described in Section 5.5, the equation for fatigue life prediction based on dynamic stored energy for MREs subjected to external magnetic fields can be derived as:

$$\ln(N_f) = \frac{\int \sigma \lambda \partial \lambda - W_{DCon}}{-3.8857(C_p)^2 + 2.3149(C_p) - 0.4014} \quad (6.2)$$

where  $\sigma$ ,  $\lambda$ ,  $W_{DCon}$  and  $C_p$  are as previously defined. The values of  $W_{DCon}$  for MREs subjected to external magnetic fields are shown in Table 6-6.

**Table 6-6 Values for  $W_{DCon}$  for MREs with various CI contents subjected to magnetic fields**

CI content	$W_{DCon}$ (N/mm <sup>2</sup> )
15%	1.2524
20%	0.9147
25%	0.7859
30%	0.7714
35%	0.7307

Eqn. 5.13 can also be used as a general equation relating fatigue life to dynamic stored energy for MREs based on other elastomer matrices when they are subjected to external magnetic fields, provided the material constants  $L$ ,  $M$  and  $N$  (units N/mm<sup>2</sup>) are derived from equi-biaxial dynamic testing in the presence of magnetic fields.

## 6.6 Damping loss factor

The variations of damping loss factor with respect to cycles are shown in Figure 6-8. The values of dissipated energy with accumulated cycles in the fatigue process are shown Figure 6-9.

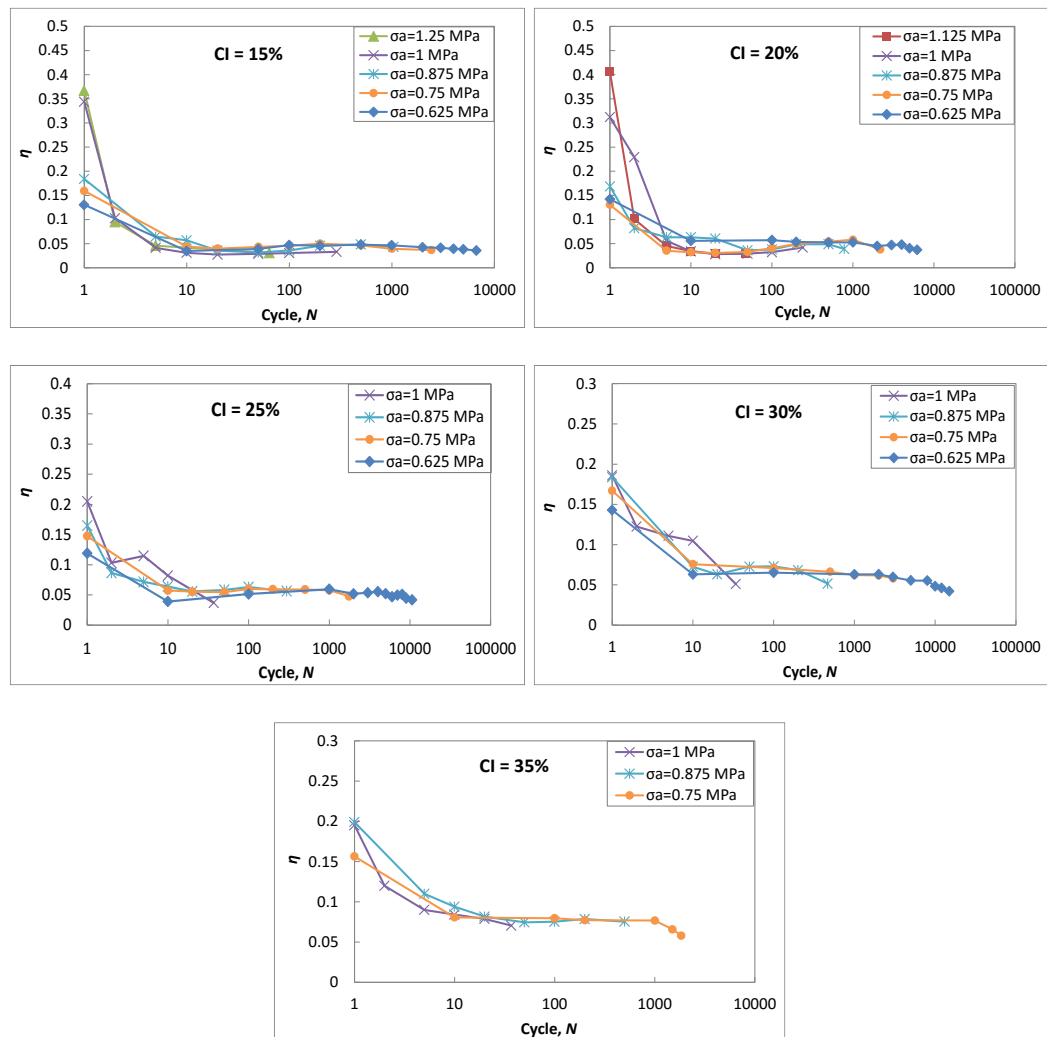
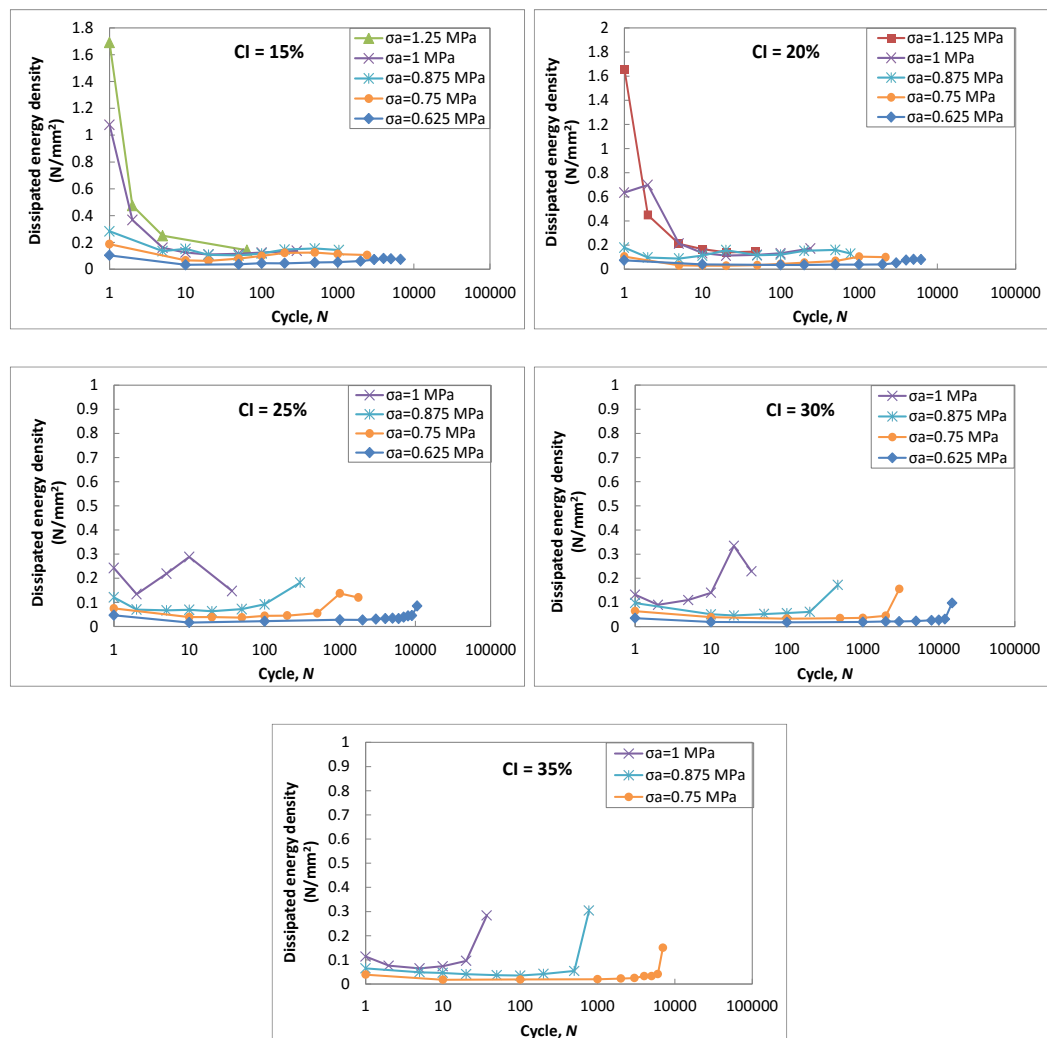


Figure 6-8 Damping loss factor versus cycles for isotropic MREs with different CI contents.

Samples were physically tested in magnetic fields

From Figure 6-8 it can be seen that dynamic loading induced an overall decrease in the damping loss factor throughout the entire fatigue process. When  $\eta$  was compared for MREs tested with and without magnetic fields applied, it was found

that the presence of a magnetic field did not have significant influence on the damping loss factor during the entire fatigue process, although the value of  $\eta$  at failure (refer to Table 6-7) was generally slightly higher in the presence of an external magnetic field. This was a similar result to outcomes obtained in other studies which indicated that the influence of the magnetic fields on the damping properties of MREs was small [54, 63, 85]. This was probably because the molecular chains of the MRE matrix are highly crosslinked and the magnetic particles are restricted in the matrix even under an applied magnetic field [81].



**Figure 6-9 Plots of dissipated energy density versus cycles for isotropic MREs with different CI contents. Samples were physically tested in magnetic fields**

**Table 6-7 Values of  $\eta$  at failure for MREs with different CI contents (with magnetic fields applied)**

<b>CI content</b>	<b><math>\eta</math></b>
15%	0.025–0.043
20%	0.030–0.048
25%	0.036–0.056
30%	0.042–0.062
35%	0.058–0.080

## 6.7 Summary

In this chapter, equi-biaxial fatigue behaviour of silicone based MREs in the presence of external magnetic fields was investigated. The results were compared with those obtained in the absence of magnetic fields. It was found that for the same carbonyl iron content and testing conditions, the fatigue life of silicone based MREs in magnetic fields was higher than that without magnetic fields. Magnetic fields have a great influence on the stress-strain behaviour of MREs. More cycles were accumulated for the samples to undergo large deformation when they were tested in magnetic fields. The decrease in the rate of  $E^*$  was more gradual in the presence of magnetic fields and this was particularly evident for MREs with lower CI contents and at lower stress amplitudes. A limiting value of  $E^*$  at failure was reached for each material and the values of  $E^*$  at failure were within a quite small range when the samples were tested both with and without a magnetic field applied. As previously found, the dynamic stored energy criterion can also be used as a plausible predictor in determining the fatigue life of MREs when they are subjected to external magnetic fields. However, the magnetic field did not have a significant influence on the damping loss factor for the range of MREs tested. The experimentation showed that the damping properties of MREs

can be maintained at a stable level during their entire service lives after conditioning has taken place.

# **Chapter 7 Preliminary research into interfacial layer design in MREs**

## **7.1 Introduction**

As for other elastomer based composites with various fillers, the properties of MREs depend not only on the types of elastomer matrix and magnetic particles, but also on the level of adhesion between the particles and the matrix [57, 97, 217]. However, the incompatibility of the inorganic magnetic fillers and the matrix usually leads to poor wettability and adhesion between them and consequently results in diminished mechanical strength of the MRE [96]. The surfaces of magnetic particles can be coated with various organic materials prior to mixing to provide interfacial layers between particles and the matrix in an attempt to obtain MREs with improved properties [85, 100]. In this chapter, the preparation of polysiloxane coated magnetic particles to provide improved dispersion in silicone rubber matrices was preliminarily explored.

## **7.2 Coating process**

Polysiloxane encapsulated CI particles were prepared by hydrolysis-condensation reaction of tetraethyl orthosilicate (TEOS) employing a sol-gel method. Firstly, TEOS was hydrolysed in deionised water at 80 °C using nitric acid as the catalyst. After 1 hour of stirring, the carbonyl iron particles were gradually added to the sol and continually stirred for a further 4 hours. Finally, the treated particles were separated using a magnet, washed with methanol followed by deionised water and then dried immediately in a vacuum oven at 100 °C for 4 hours.

### 7.3 Chemical structure

The chemical structure of the pure and coated CI particles was investigated using a Perkin Elmer Spotlight 400N Fourier transform infrared (FTIR) Microscope. The FTIR spectra of uncoated and polysiloxane coated CI particles are presented in Figure 7-1. In the spectrum of coated CI particles, a sharp absorption peak appeared at 1100–1000  $\text{cm}^{-1}$ , this was ascribed to the antisymmetric stretching vibration of Si-O-Si bonds [218]. The peaks that appeared at around 969  $\text{cm}^{-1}$  and 787  $\text{cm}^{-1}$  were the bending vibrations of Si-O-Si bonds.

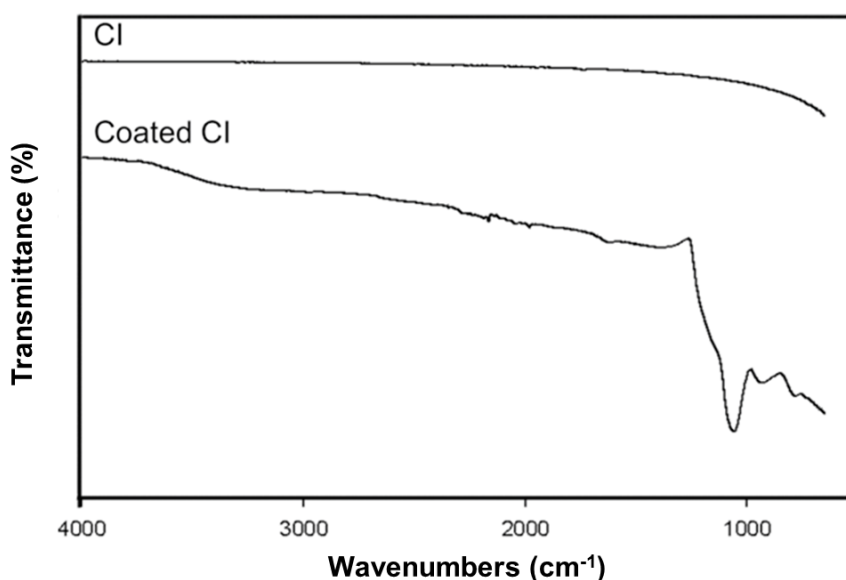
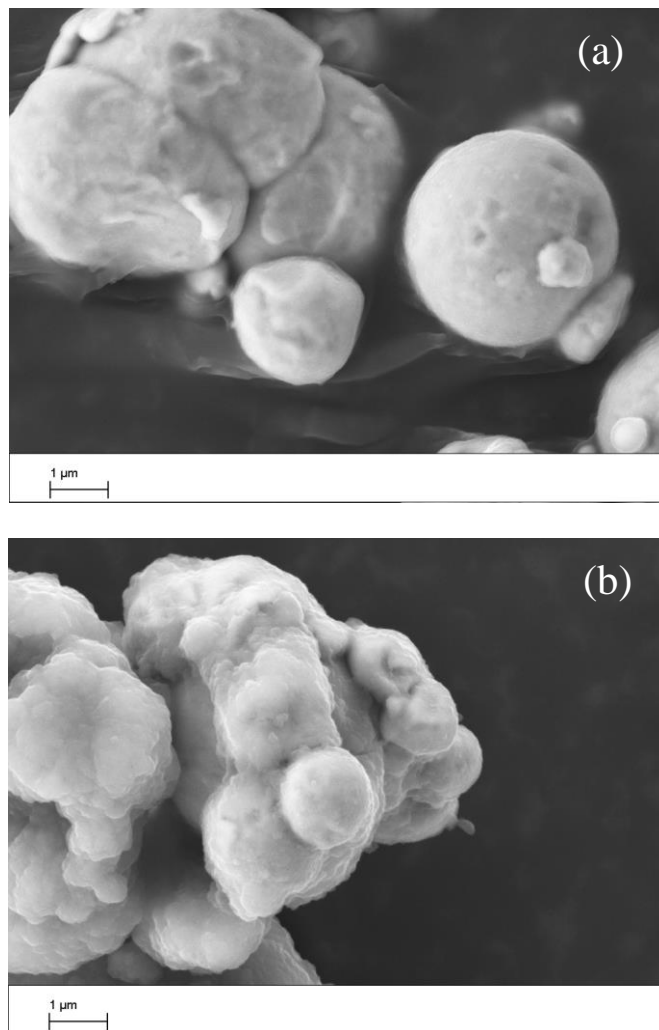


Figure 7-1 FTIR of CI and coated CI

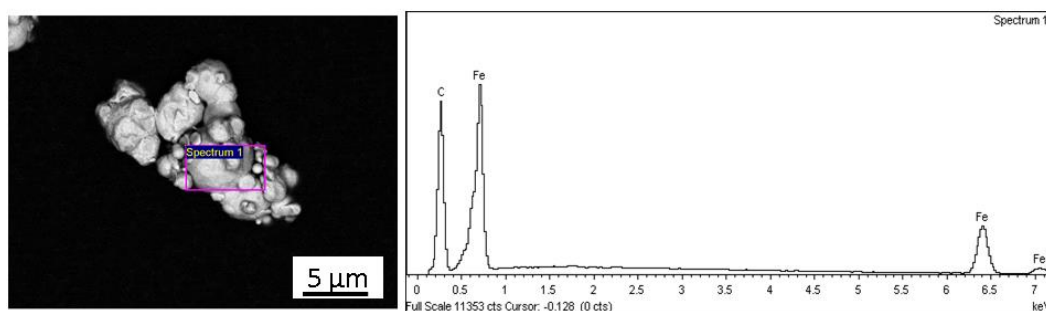
### 7.4 Surface morphology

Morphological features of the coated particles were observed by utilising a Scanning Electron Microscope (SEM, Zeiss Supra), which was also equipped with an energy-dispersive X-ray spectrometer (EDS, Oxford Inca Xmax) to enable

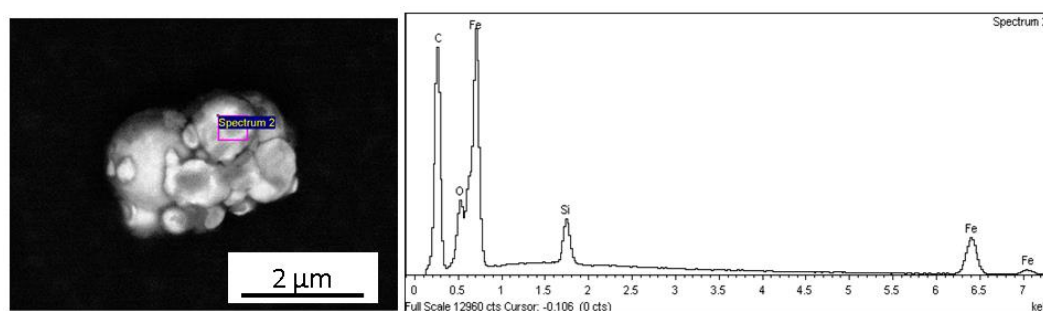
surface element analysis of the samples. The specimens were coated with a very thin (2 nm) carbon layer prior to testing in order to improve surface conductivity. The surface morphologies of uncoated and polysiloxane coated CI particles are shown in Figure 7-2. It was found that the surfaces of uncoated CI particles are slightly coarse and the inter-particle contact between each particle was quite distinct. In stark contrast, the surfaces of the coated particles showed layers of soft material and the contact between two particles was blurred by the coating layer. EDS analysis (see Figure 7-3) indicated the existence of Si on the surface of the coated particles, confirming that the coating process had indeed taken place.



**Figure 7-2 Photo micrographs showing the surface morphologies of (a) uncoated and (b) coated CI particles**



(a) Uncoated CI



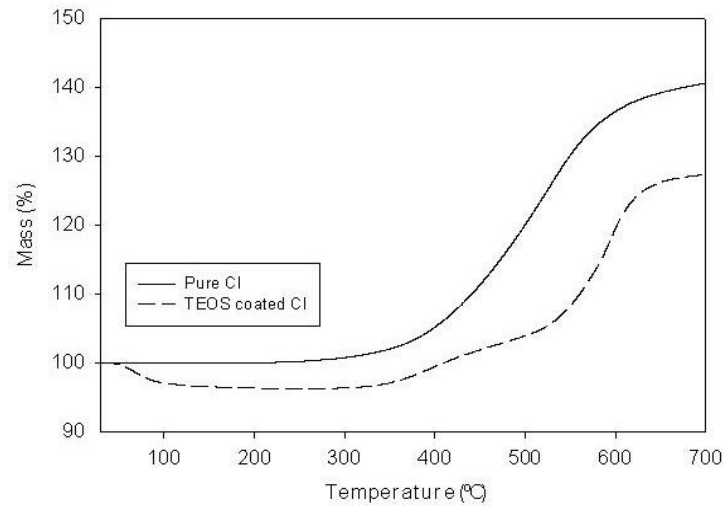
(b) coated CI

Figure 7-3 EDS analysis of uncoated and TEOS coated CI particles

## 7.5 Thermal stability

The coating layer plays an important role in protecting the particles from oxidation and thus enhances the thermal stability of the particles [219]. The effect of TEOS coating on the thermal resistance of CI particles was studied and is depicted in Figure 7-4. In the case of the coated particles, an initial mass loss was assumed to be caused by the polycondensation of the hydroxyl group which was also previously observed in zirconia-coated CI particles [220]. Thereafter, the iron oxidation caused a significant weight increase above 400 °C which can be seen in the figure. There was a marked difference in the increase in mass between pure CI particles and treated CI particles. The mass of the pure CI particles increased by 41% at 700 °C. However, the mass increase was merely 27% at the same

temperature for particles coated with a layer of polysiloxane, indicating that the resistance to thermal oxidation of polysiloxane encapsulated CI particles was greatly improved.



**Figure 7-4 TGA curves of pure and TEOS coated CI particles**

## 7.6 Effect of coating on surface morphology of MREs

The surface appearance of isotropic MREs fabricated using unmodified and TEOS modified CI particles is shown in Figure 7-5. It is evident that the uncoated carbonyl iron agglomerated in the silicone rubber matrix. The interface between carbonyl iron particles and silicone rubber was distinct, which indicates the interaction between the two phases was weak. In contrast, the dispersion of polysiloxane encapsulated carbonyl iron in silicone rubber was observed to be more homogeneous. This improved dispersion can be attributed to the presence of a coating layer derived from the hydrolysis and condensation of TEOS which can act as interfacial layers to bond the carbonyl iron particles and the silicone rubber and consequently increase their interaction.

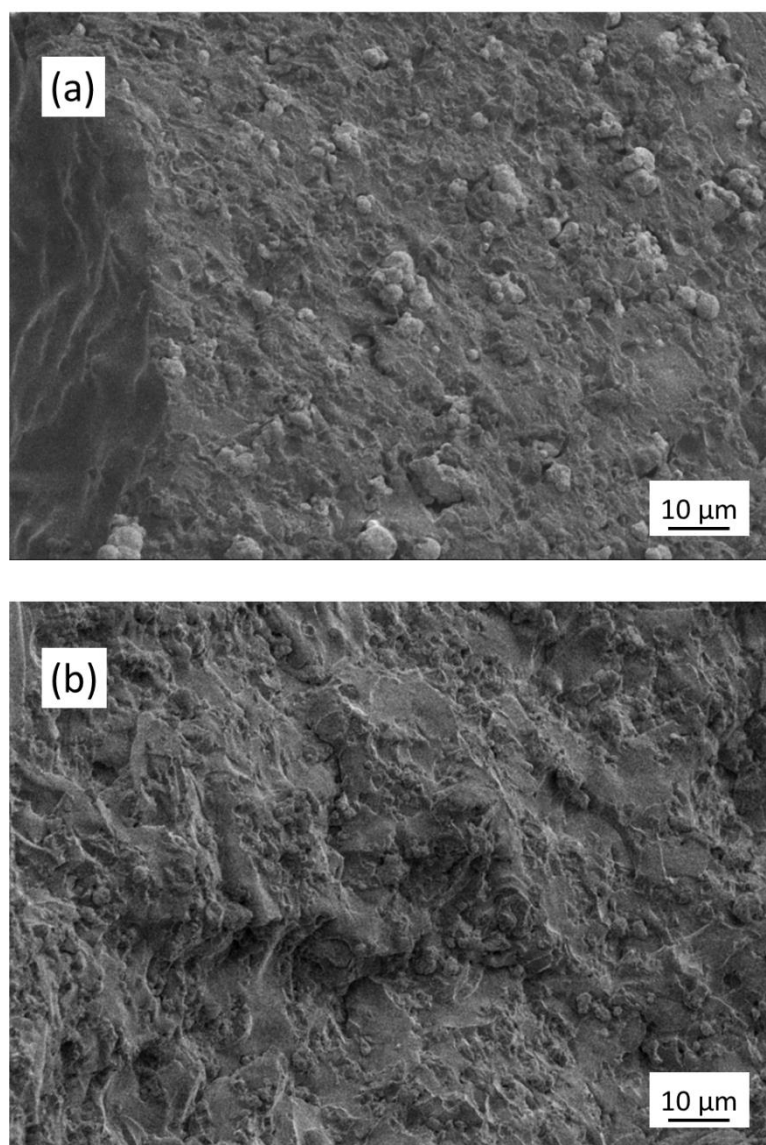


**Figure 7-5 Surface morphologies of MREs fabricated using (a) pure CI particles and (b) TEOS coated CI particles**

## **7.7 Summary**

Polysiloxane encapsulated carbonyl iron magnetic particles were prepared by hydrolysis-condensation polymerisation of tetraethyl orthosilicate (TEOS) using a sol-gel method. The chemical structure of the coated particles was confirmed by FTIR with bands due to Si-O-Si and -OH. SEM confirmed the existence of the coating layer on the surface of the coated particles by exhibiting a surface

morphology with less roughness than the uncoated particles. The presence of silicon was confirmed by EDS analysis. Thermal analysis showed that the resistance to thermal oxidation of TEOS encapsulated CI particles was greatly improved by comparison with uncoated particles. The mass of the pure CI particles increased by 41% at 700 °C, but only increased by 27% for particles coated with a layer of polysiloxane. The coated particles were used to fabricate isotropic magnetorheological elastomers by incorporating them into silicone rubber matrices and the results showed that the dispersion of carbonyl iron in silicone rubber was greatly improved after polysiloxane encapsulation.

# Chapter 8 Conclusions and proposed future work

## 8.1 Conclusions

The novel analyses described in this text provide the first critical insight into the fatigue properties of MREs under complex dynamic loading.

As well as being stiffer and stronger, anisotropic MREs exhibit higher fatigue resistance than isotropic MREs. Also, MREs have higher fatigue lives in the presence of magnetic fields than they have in the absence of magnetic fields.

Equi-biaxial fatigue behaviour of silicone based MREs were investigated by using the bubble inflation testing method. Wöhler (S-N) curves relating fatigue life to stress amplitude were produced by subjecting the compounds to cycling over a range of stress amplitudes. Changes in physical properties, including variation in stress-strain relations, complex modulus and damping loss factor during the fatigue process were analysed. The influence of varying a range of parameters, including microstructure, magnetic particle content and external magnetic fields, on the equi-biaxial fatigue behaviour of MREs were analysed and discussed.

It was found that for the same carbonyl iron content of 20%, anisotropic MREs exhibited a greater fatigue resistance than isotropic MREs due to the formation of carbonyl iron chains during the curing process. For isotropic MREs, the samples with lower particle content exhibit higher fatigue resistance to higher loadings whereas MREs with higher particle content show higher fatigue resistance at lower loadings due to the complex particle networks formed in their structure. As the content of carbonyl iron particles increased, the fatigue life of MREs generally

decreased at stress amplitudes above 1 MPa but increased at a stress amplitude of 0.625 MPa. For stress amplitudes between 0.625 MPa and 1 MPa, MREs with very low (15%) and very high (35%) particle content exhibited higher fatigue lives than those of MREs with medium particle contents (20%–30%). The fatigue lives of MREs with various carbonyl iron content ranging between 15% and 35% increased when the materials were cycled in the presence of external magnetic fields.

The complex modulus ( $E^*$ ) decreased throughout the entire fatigue process as a result of stress softening induced by cyclic loading. Structured MREs were found to have higher initial moduli but the rate of decrease in moduli was more rapid than that in isotropic MREs. Isotropic MREs with various carbonyl iron contents exhibited quite different changes in  $E^*$ . For the same loading conditions, MREs with lower particle content failed after  $E^*$  had stabilized while MREs containing more particles failed after a rapid drop in  $E^*$  just prior to failure. For MREs with the same carbonyl iron content, the decrease in the rate of  $E^*$  was more gradual when the samples were subjected to external magnetic fields and this was particularly evident for MREs with lower CI contents and at lower stress amplitudes. Nonetheless, a limiting value of  $E^*$  at failure was reached for each material regardless of the stress amplitudes applied. For isotropic MREs with various carbonyl iron contents,  $E^*$  at failure was between 1.22 MPa and 1.38 MPa when the samples were tested in the absence of magnetic fields and between 1.28 MPa and 1.44 MPa when they were subjected to external magnetic fields. Fatigue failure took place at a limiting value of 1.30 MPa for anisotropic silicone based MREs with a carbonyl iron content of 20%. Overall,  $E^*$  at failure for each material was within a quite small range irrespective of the stress amplitude

applied, the carbonyl iron content, the directionality of the particles and whether an external magnetic field was applied or not. Thus complex modulus can provide an indicator in respect of preventative maintenance which will allow MRE based rubber components to be replaced prior to costly failure.

Dynamic cyclic loading at various levels induced an overall decrease in the damping loss factor ( $\eta$ ) throughout the entire fatigue process for MREs. However, for each material,  $\eta$  decreased primarily in the first few cycles and then was maintained at a stable level until fatigue failure took place. Hence it is evident that MREs can be successfully employed in damping applications provided the MRE components are adequately conditioned before they are used in service.

The dynamic stored energy criterion can be used as a plausible predictor of fatigue lives for silicone based MREs irrespective of the loading level, the directionality and content of the ferromagnetic particles and whether an external magnetic field was applied or not.

General equations for equi-biaxial fatigue life prediction for MREs relating life to both alternating stress and dynamic stored energy were derived. The dynamic stored energy criterion has been shown to be a plausible fatigue life predictor for MREs and it is likely that this is the case for all elastomers containing hard particles. The parameters obtained provide a useful reference for the development of constitutive models for characterising the complex dynamic behaviour of MREs.

Preliminary research into interfacial layers design for MREs was carried out in order to improve the interaction between magnetic particles and the silicone matrix and consequently to enhance the property of MREs. The carbonyl iron particles were coated by using a sol-gel method. FTIR, SEM and EDS analysis

confirmed the existence of coating layers around the carbonyl iron particles. When the coated particles were incorporated into silicone rubber, SEM observation suggested that the dispersion of particles in silicone rubber was greatly improved after polysiloxane encapsulation.

Overall, by studying equi-biaxial fatigue behaviour of silicone based MREs using the bubble inflation testing method, the influence of a wide range of parameters, including microstructure, magnetic particle content and external magnetic fields, on the equi-biaxial fatigue behaviour of MREs was determined. Stress-strain behaviour during the fatigue process for a series of MREs was investigated, allowing limiting values of complex modulus at failure to be obtained and general equations relating fatigue life to stress amplitude and dynamic stored energy to be derived. Consequently, the research question posed in Section 1.1 has been answered by achieving the aims and objectives set out in Section 1.2.

## **8.2 Proposed future work**

Due to testing limitations, the equi-biaxial loadings were generally set at stress amplitudes that induced medium fatigue lives in this research. To fully characterise the property of MREs, dynamic equi-biaxial fatigue behaviour of MREs during long-term fatigue testing should be carried out. Measurement of the mechanical performance of MREs with various fatigue lives will allow a theoretical fatigue mechanism for MREs subjected to equi-biaxial cyclic loading to be postulated. A model emanating from this theoretical fatigue mechanism would need to be evaluated for MREs based on a range of elastomeric matrix materials.

A method was provided for coating of carbonyl iron particles and thus improving the interactions between particles and the matrix. However, this is only an initial attempt to design interfacial layers for silicone based MREs. More work needs to be done to optimise the coating process and obtain interfacial layers with improved properties. Uniaxial and equi-biaxial fatigue tests on MREs with coated magnetic particles should be carried out to investigate the effect of interfacial layers on the fatigue behaviour of MREs. Moreover, a more detailed study of the nature of the resulting fatigue failures and the fracture surfaces should be undertaken.

In addition, due to the asymmetry in equi-biaxial bubble inflation of anisotropic MREs, it will be necessary to reconsider the determination of stress, strain and dynamic stored energy in two mutually perpendicular planes [221]. The equi-biaxial bubble inflation of an anisotropic MRE will result in the formation of an ellipsoidal bubble, irrespective of whether or not a magnetic field is applied during dynamic testing. The MRE sample will have its smallest stretch in the direction parallel to the particle chains and largest stretch in the plane at right angles to the particle chains. This will also be true to a lesser extent for the behaviour of an isotropic MRE sample inflated in a magnetic field. Consider Figure 8-1.

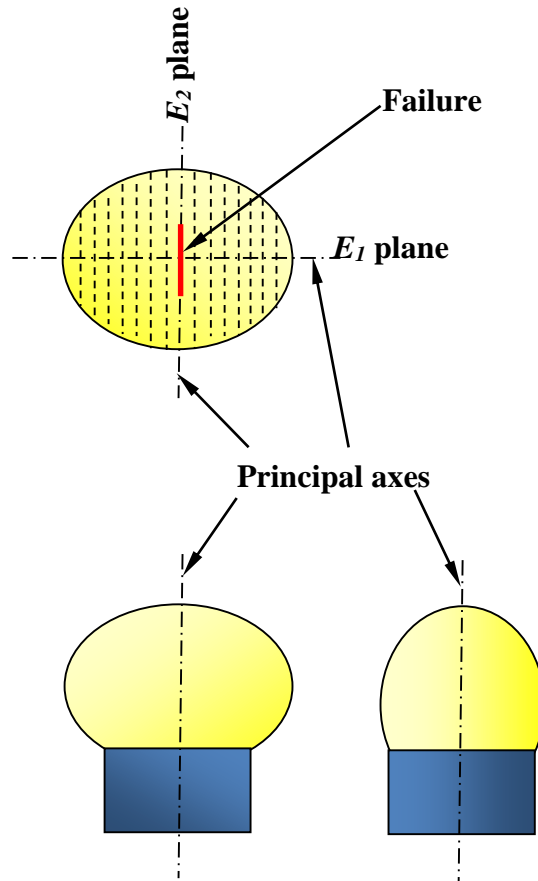


Figure 8-1 The inflation of an anisotropic MRE showing inflation ellipses and failure direction diagrammatically

From Eqns. 8.1 and 8.2, an expression for the elastic modulus ‘ $E$ ’ in each of the principal planes for a point at the pole of an inflated MRE sample can be written:

$$E_1 = \frac{\sigma_1}{\lambda_1 - 1} \quad (8.1)$$

$$E_2 = \frac{\sigma_2}{\lambda_2 - 1} \quad (8.2)$$

At failure the elastic modulus in each principal plane will be given by:

$$E_F = \frac{\sigma_F}{\lambda_F - 1} = \frac{P_{FF} r_F \lambda_F}{2t(\lambda - 1)} \quad (8.3)$$

Eqn. 8.3 will allow  $E_F$  to be determined in each of the principal planes at failure (or for any other cycle) and from  $E_F$  in each plane,  $\sigma_1$  and  $\sigma_2$  at failure can be calculated.

It will be necessary to measure stretch ratios in the two principal planes, hence three instead of two CMOS cameras will need to be employed or alternatively two dynamic test procedures will have to take place for each compound and stress amplitude: i) with the particle direction in the plane of the cameras and ii) with the particle direction at right angles to the plane of the cameras.

## References

- [1] P. Ponte Castañeda, E. Galipeau, Homogenization-based constitutive models for magnetorheological elastomers at finite strain, *Journal of the Mechanics and Physics of Solids*, 59 (2011) 194-215.
- [2] E. Galipeau, P. Ponte Castañeda, A finite-strain constitutive model for magnetorheological elastomers: Magnetic torques and fiber rotations, *Journal of the Mechanics and Physics of Solids*, 61 (2013) 1065-1090.
- [3] W.M. Winslow, Method and means for translating electrical impulses into mechanical force, US Patent 2,417,850, 1947.
- [4] J. Rabinow, The magnetic fluid clutch, *Electrical Engineering*, 67 (1948) 1167-1167.
- [5] J.D. Carlson, D.M. Catanzarite, K.A.S. Clair, Magneto-rheological Suspensions and Associated Technology, 5th Int. Conf. on Electroheological, Sheffield, 1995.
- [6] J.D. Carlson, M.J. Chrzan, Magnetorheological fluid dampers, US, 1994.
- [7] J.D. Carlson, M.J. Chrzan, F.O. James, Magnetorheological fluid devices, US, 1994.
- [8] Anon, Brake cuts exercise-equipment cost, *Design News*, 4 (1995).
- [9] J.D. Carlson, M.J. Chrzan, F.O. James, Magnetorheological fluid devices, US, 1995.
- [10] V.D. Chase, Cutting Edge, Appliance Manufacturer, 1996, pp. 6.
- [11] Audi A1 Sportback concept, Efficient and dynamic driving fun, [http://www.audi.co.za/za/brand/en/experience/design\\_studies/audi\\_a1\\_sportback.html](http://www.audi.co.za/za/brand/en/experience/design_studies/audi_a1_sportback.html).
- [12] H.X. Deng, X.L. Gong, L.H. Wang, Development of an adaptive tuned vibration absorber with magnetorheological elastomer, *Smart Materials and Structures*, 15 (2006) N111.
- [13] H. Böse, R. Röder, Magnetorheological elastomers with high variability of their mechanical properties, *Journal of Physics: Conference Series*, IOP Publishing, 2009, pp. 012090.
- [14] H. Böse, Viscoelastic properties of silicone-based magnetorheological elastomers, *International Journal of Modern Physics B*, 21 (2007) 4790-4797.
- [15] X.C. Guan, X.F. Dong, J.P. Ou, Magnetostrictive effect of magnetorheological elastomer, *Journal of Magnetism and Magnetic Materials*, 320 (2008) 158-163.
- [16] N. Kchit, G. Bossis, Piezoresistivity of magnetorheological elastomers, *Journal of Physics: Condensed Matter*, 20 (2008) 204136.
- [17] M. Farshad, A. Benine, Magnetoactive elastomer composites, *Polymer Testing*, 23 (2004) 347-353.
- [18] P.R. von Lockette, S.E. Lofland, J.H. Koo, J. Kadlowec, M. Dermond, Dynamic characterization of bimodal particle mixtures in silicone rubber magnetorheological materials, *Polymer Testing*, 27 (2008) 931-935.
- [19] G. Schubert, P. Harrison, Large-strain behaviour of Magneto-Rheological Elastomers tested under uniaxial compression and tension, and pure shear deformations, *Polymer Testing*, 42 (2015) 122-134.

- [20] G.J. Liao, X.L. Gong, S.H. Xuan, C.Y. Guo, L.H. Zong, Magnetic-Field-Induced Normal Force of Magnetorheological Elastomer under Compression Status, *Industrial & Engineering Chemistry Research*, 51 (2012) 3322-3328.
- [21] I. Agirre-Olabide, M.J. Elejabarrieta, M.M. Bou-Ali, Matrix dependence of the linear viscoelastic region in magnetorheological elastomers, *Journal of Intelligent Material Systems and Structures*, (2015).
- [22] J.B. Feng, S.H. Xuan, T.X. Liu, L. Ge, L.X. Yan, H. Zhou, X.L. Gong, The prestress-dependent mechanical response of magnetorheological elastomers, *Smart Materials and Structures*, 24 (2015) 085032.
- [23] H. Böse, R. Röder, Magnetorheological elastomers with high variability of their mechanical properties, *Journal of Physics: Conference Series*, 149 (2009) 012090.
- [24] J.M. Ginder, M.E. Nichols, L.D. Elie, S.M. Clark, Controllable-stiffness components based on magnetorheological elastomers, SPIE's 7th Annual International Symposium on Smart Structures and Materials, International Society for Optics and Photonics, 2000, pp. 418-425.
- [25] L. Chen, X.L. Gong, W.Q. Jiang, J.J. Yao, H.X. Deng, W.H. Li, Investigation on magnetorheological elastomers based on natural rubber, *Journal of Materials Science*, 42 (2007) 5483-5489.
- [26] J.M. Ginder, M.E. Nichols, L.D. Elie, J.L. Tardiff, Magnetorheological elastomers: properties and applications, 1999 Symposium on Smart Structures and Materials, International Society for Optics and Photonics, 1999, pp. 131-138.
- [27] J.K. Wu, X.L. Gong, Y.C. Fan, H.S. Xia, Anisotropic polyurethane magnetorheological elastomer prepared through in situ polycondensation under a magnetic field, *Smart Materials and Structures*, 19 (2010) 105007.
- [28] A. Boczkowska, S.F. Awietjan, Urethane magnetorheological elastomers-manufacturing, microstructure and properties, *Solid State Phenomena, Trans Tech Publ*, 2009, pp. 107-112.
- [29] B. Wei, X. Gong, W. Jiang, Influence of polyurethane properties on mechanical performances of magnetorheological elastomers, *Journal of Applied Polymer Science*, 116 (2010) 771-778.
- [30] A. Boczkowska, S. Awietjan, T. Wejrzanowski, K. Kurzydłowski, Image analysis of the microstructure of magnetorheological elastomers, *Journal of Materials Science*, 44 (2009) 3135-3140.
- [31] Y. Shen, M.F. Golnaraghi, G. Hepler, Experimental research and modeling of magnetorheological elastomers, *Journal of Intelligent Material Systems and Structures*, 15 (2004) 27-35.
- [32] Y. Hu, Y.L. Wang, X.L. Gong, X.Q. Gong, X.Z. Zhang, W.Q. Jiang, P.Q. Zhang, Z.Y. Chen, New magnetorheological elastomers based on polyurethane/Si-rubber hybrid, *Polymer Testing*, 24 (2005) 324-329.
- [33] W. Zhang, X. Gong, S. Xuan, W. Jiang, Temperature-Dependent Mechanical Properties and Model of Magnetorheological Elastomers, *Industrial & Engineering Chemistry Research*, 50 (2011) 6704-6712.
- [34] Y.L. Wang, Y. Hu, X.L. Gong, W.Q. Jiang, P.Q. Zhang, Z.Y. Chen, Preparation and properties of magnetorheological elastomers based on silicon rubber/polystyrene blend matrix, *Journal of Applied Polymer Science*, 103 (2007) 3143-3149.
- [35] P. Zając, J. Kaleta, D. Lewandowski, A. Gasperowicz, Isotropic magnetorheological elastomers with thermoplastic matrices: structure, damping properties and testing, *Smart Materials and Structures*, 19 (2010) 045014.

- [36] W. Zhang, X.L. Gong, W.Q. Jiang, Y.C. Fan, Investigation of the durability of anisotropic magnetorheological elastomers based on mixed rubber, *Smart Materials and Structures*, 19 (2010) 085008.
- [37] L. Ge, X.L. Gong, Y.C. Fan, S.H. Xuan, Preparation and mechanical properties of the magnetorheological elastomer based on natural rubber/rosin glycerin hybrid matrix, *Smart Materials and Structures*, 22 (2013) 115029.
- [38] X.S. Lu, X.Y. Qiao, H. Watanabe, X.L. Gong, T. Yang, W. Li, K. Sun, M. Li, K. Yang, H.E. Xie, Q. Yin, D. Wang, X.D. Chen, Mechanical and structural investigation of isotropic and anisotropic thermoplastic magnetorheological elastomer composites based on poly(styrene-*b*-ethylene-co-butylene-*b*-styrene) (SEBS), *Rheologica Acta*, 51 (2012) 37-50.
- [39] X.S. Lu, M. Li, K. Yang, H.E. Xie, Q. Yin, D. Wang, SEBS Based Magnetorheological Elastomer: Preparation and Property, (2011).
- [40] Y.C. Fan, X.L. Gong, S.H. Xuan, W. Zhang, J. Zheng, W.Q. Jiang, Interfacial friction damping properties in magnetorheological elastomers, *Smart Materials and Structures*, 20 (2011) 035007.
- [41] K. Danas, S.V. Kankanala, N. Triantafyllidis, Experiments and modeling of iron-particle-filled magnetorheological elastomers, *Journal of the Mechanics and Physics of Solids*, 60 (2012) 120-138.
- [42] K.L. Pickering, S. Raa Khimi, S. Ilanko, The effect of silane coupling agent on iron sand for use in magnetorheological elastomers Part 1: Surface chemical modification and characterization, *Composites Part A: Applied Science and Manufacturing*, 68 (2015) 377-386.
- [43] G.V. Stepanov, S.S. Abramchuk, D.A. Grishin, L.V. Nikitin, E.Y. Kramarenko, A.R. Khokhlov, Effect of a homogeneous magnetic field on the viscoelastic behavior of magnetic elastomers, *Polymer*, 48 (2007) 488-495.
- [44] Z. Varga, G. Filipcsei, M. Zr ńnyi, Smart composites with controlled anisotropy, *Polymer*, 46 (2005) 7779-7787.
- [45] H.J. Song, N.M. Wereley, R.C. Bell, J.L. Planinsek, J.A. Filer II, Field dependent response of magnetorheological elastomers utilizing spherical Fe particles versus Fe nanowires, *Journal of Physics: Conference Series*, IOP Publishing, 2009, pp. 012097.
- [46] N. Kchit, G. Bossis, Electrical resistivity mechanism in magnetorheological elastomer, *Journal of Physics D: Applied Physics*, 42 (2009) 105505.
- [47] R.A. Landa, P. Soledad Antonel, M.M. Ruiz, O.E. Perez, A. Butera, G. Jorge, C.L.P. Oliveira, R.M. Negri, Magnetic and elastic anisotropy in magnetorheological elastomers using nickel-based nanoparticles and nanochains, *Journal of Applied Physics*, 114 (2013) 213912.
- [48] N. Dishovsky, K. Ruskova, I. Radulov, "In situ" magnetic modification of polar elastomers, *Materials Research Bulletin*, 36 (2001) 35-45.
- [49] E.Y. Kramarenko, A.V. Chertovich, G.V. Stepanov, A.S. Semisalova, L.A. Makarova, N.S. Perov, A.R. Khokhlov, Magnetic and viscoelastic response of elastomers with hard magnetic filler, *Smart Materials and Structures*, 24 (2015) 035002.
- [50] M. Hansaka, Preparation and properties of magnetic vibration-damper, INTER-NOISE and NOISE-CON Congress and Conference Proceedings, Institute of Noise Control Engineering, 1993, pp. 859-862.
- [51] I. Kim, S. Bae, J. Kim, Composition effect on high frequency properties of carbonyl-iron composites, *Materials Letters*, 62 (2008) 3043-3046.

- [52] M. Lokander, T. Reitberger, B. Stenberg, Oxidation of natural rubber-based magnetorheological elastomers, *Polymer Degradation and Stability*, 86 (2004) 467-471.
- [53] X.L. Gong, X.Z. Zhang, P.Q. Zhang, Fabrication and characterization of isotropic magnetorheological elastomers, *Polymer Testing*, 24 (2005) 669-676.
- [54] M. Lokander, B. Stenberg, Improving the magnetorheological effect in isotropic magnetorheological rubber materials, *Polymer Testing*, 22 (2003) 677-680.
- [55] M. Farshad, M. Le Roux, Compression properties of magnetostrictive polymer composite gels, *Polymer Testing*, 24 (2005) 163-168.
- [56] Y.L. Wang, Y. Hu, Y.L. Wang, H.X. Deng, X.L. Gong, P.Q. Zhang, W.Q. Jiang, Z.Y. Chen, Magnetorheological elastomers based on isobutylene–isoprene rubber, *Polymer Engineering & Science*, 46 (2006) 264-268.
- [57] Y.L. Wang, Y. Hu, L. Chen, X.L. Gong, W.Q. Jiang, P.Q. Zhang, Z.Y. Chen, Effects of rubber/magnetic particle interactions on the performance of magnetorheological elastomers, *Polymer Testing*, 25 (2006) 262-267.
- [58] W. Zhang, X. Gong, W. Jiang, Y. Fan, Investigation of the durability of anisotropic magnetorheological elastomers based on mixed rubber, *Smart Materials and Structures*, 19 (2010) 085008.
- [59] D. Borin, D. Günther, C. Hintze, G. Heinrich, S. Odenbach, The level of cross-linking and the structure of anisotropic magnetorheological elastomers, *Journal of Magnetism and Magnetic Materials*, 324 (2012) 3452-3454.
- [60] E. Coquelle, G. Bossis, Mullins effect in elastomers filled with particles aligned by a magnetic field, *International Journal of Solids and Structures*, 43 (2006) 7659-7672.
- [61] L. Chen, X.L. Gong, W.H. Li, Microstructures and viscoelastic properties of anisotropic magnetorheological elastomers, *Smart Materials and Structures*, 16 (2007) 2645.
- [62] A. Boczkowska, S.F. Awietjan, R. Wroblewski, Microstructure–property relationships of urethane magnetorheological elastomers, *Smart Materials and Structures*, 16 (2007) 1924.
- [63] G.Y. Zhou, Shear properties of a magnetorheological elastomer, *Smart Materials and Structures*, 12 (2003) 139.
- [64] S. Rudykh, K. Bertoldi, Stability of anisotropic magnetorheological elastomers in finite deformations: A micromechanical approach, *Journal of the Mechanics and Physics of Solids*, 61 (2013) 949-967.
- [65] L.C. Davis, Model of magnetorheological elastomers, *Journal of Applied Physics*, 85 (1999) 3348-3351.
- [66] X.Z. Zhang, S.L. Peng, W.J. Wen, W.H. Li, Analysis and fabrication of patterned magnetorheological elastomers, *Smart Materials and Structures*, 17 (2008) 045001.
- [67] M. Kallio, T. Lindroos, S. Aalto, E. Järvinen, T. Kärrä, T. Meinander, Dynamic compression testing of a tunable spring element consisting of a magnetorheological elastomer, *Smart Materials and Structures*, 16 (2007) 506.
- [68] A. Boczkowska, S.F. Awietjan, Effect of the processing conditions on the mechanical properties of urethane magnetorheological elastomers, *Materials Science Forum*, Trans Tech Publ, 2008, pp. 630-634.
- [69] W.J. Choi, Dynamic analysis of magnetorheological elastomer configured sandwich structures, University of Southampton, 2009.

- [70] A. Boczkowska, S. Awietjan, *Microstructure and Properties of Magnetorheological Elastomers*, *Advanced Elastomers–Technology, Properties and Applications* 2012.
- [71] M.R. Jolly, J.D. Carlson, B.C. Muñoz, A model of the behaviour of magnetorheological materials, *Smart Materials and Structures*, 5 (1996) 607.
- [72] T.L. Sun, X.L. Gong, W.Q. Jiang, J.F. Li, Z.B. Xu, W.H. Li, Study on the damping properties of magnetorheological elastomers based on cis-polybutadiene rubber, *Polymer Testing*, 27 (2008) 520-526.
- [73] W.H. Li, Y. Zhou, T.F. Tian, Viscoelastic properties of MR elastomers under harmonic loading, *Rheologica Acta*, 49 (2010) 733-740.
- [74] W. Zhang, X.L. Gong, L. Chen, A Gaussian distribution model of anisotropic magnetorheological elastomers, *Journal of Magnetism and Magnetic Materials*, 322 (2010) 3797-3801.
- [75] M. Lokander, B. Stenberg, Performance of isotropic magnetorheological rubber materials, *Polymer Testing*, 22 (2003) 245-251.
- [76] S.A. Demchuk, V.A. Kuz'min, Viscoelastic properties of magnetorheological elastomers in the regime of dynamic deformation, *Journal of Engineering Physics and Thermophysics*, 75 (2002) 396-400.
- [77] G.Y. Zhou, Z.Y. Jiang, Deformation in magnetorheological elastomer and elastomer–ferromagnet composite driven by a magnetic field, *Smart Materials and Structures*, 13 (2004) 309.
- [78] A. Dorfmann, R.W. Ogden, Magnetoelastic modelling of elastomers, *European Journal of Mechanics - A/Solids*, 22 (2003) 497-507.
- [79] R.K. Gupta, *Polymer and composite rheology*, CRC Press 2000.
- [80] J. Yang, X.L. Gong, H.X. Deng, L.J. Qin, S.H. Xuan, Investigation on the mechanism of damping behavior of magnetorheological elastomers, *Smart Materials and Structures*, 21 (2012) 125015.
- [81] X.L. Gong, Y.C. Fan, S.H. Xuan, Y.G. Xu, C. Peng, Control of the Damping Properties of Magnetorheological Elastomers by Using Polycaprolactone as a Temperature-Controlling Component, *Industrial & Engineering Chemistry Research*, 51 (2012) 6395-6403.
- [82] H.L. Sun, P.Q. Zhang, X.L. Gong, H.B. Chen, A novel kind of active resonator absorber and the simulation on its control effort, *Journal of Sound and Vibration*, 300 (2007) 117-125.
- [83] N. Hoang, N. Zhang, H. Du, A dynamic absorber with a soft magnetorheological elastomer for powertrain vibration suppression, *Smart Materials and Structures*, 18 (2009) 074009.
- [84] C. Bellan, G. Bossis, Field dependence of viscoelastic properties of MR elastomers, *International Journal of Modern Physics B*, 16 (2002) 2447-2453.
- [85] Y.C. Fan, X.L. Gong, W.Q. Jiang, W. Zhang, B. Wei, W.H. Li, Effect of maleic anhydride on the damping property of magnetorheological elastomers, *Smart Materials and Structures*, 19 (2010) 055015.
- [86] F. Gordaninejad, X. Wang, P. Mysore, Behavior of thick magnetorheological elastomers, *Journal of Intelligent Material Systems and Structures*, 23 (2012) 1033-1039.
- [87] I. Bica, Compressibility modulus and principal deformations in magneto-rheological elastomer: The effect of the magnetic field, *Journal of Industrial and Engineering Chemistry*, 15 (2009) 773-776.

- [88] J.H. Koo, F. Khan, D.D. Jang, H.J. Jung, Dynamic characterization and modeling of magneto-rheological elastomers under compressive loadings, *Smart Materials and Structures*, 19 (2010) 117002.
- [89] G.Y. Zhou, J.R. Li, Dynamic behavior of a magnetorheological elastomer under uniaxial deformation: I. Experiment, *Smart Materials and Structures*, 12 (2003) 859.
- [90] L. Chen, X. Gong, W. Li, Microstructures and viscoelastic properties of anisotropic magnetorheological elastomers, *Smart Materials and Structures*, 16 (2007) 2645.
- [91] B.X. Ju, R. Tang, D.Y. Zhang, B.L. Yang, M. Yu, C.R. Liao, Temperature-dependent dynamic mechanical properties of magnetorheological elastomers under magnetic field, *Journal of Magnetism and Magnetic Materials*, 374 (2015) 283-288.
- [92] A. Boczkowska, S.F. Awietjan, S. Pietrzko, K.J. Kurzydłowski, Mechanical properties of magnetorheological elastomers under shear deformation, *Composites Part B: Engineering*, 43 (2012) 636-640.
- [93] M. Yu, B.X. Ju, J. Fu, X.Q. Liu, Q. Yang, Influence of composition of carbonyl iron particles on dynamic mechanical properties of magnetorheological elastomers, *Journal of Magnetism and Magnetic Materials*, 324 (2012) 2147-2152.
- [94] L. Chen, X.L. Gong, W.H. Li, Effect of carbon black on the mechanical performances of magnetorheological elastomers, *Polymer Testing*, 27 (2008) 340-345.
- [95] J.K. Wu, X.L. Gong, Y.C. Fan, H.S. Xia, Improving the magnetorheological properties of polyurethane magnetorheological elastomer through plasticization, *Journal of Applied Polymer Science*, 123 (2012) 2476-2484.
- [96] J.K. Wu, X.L. Gong, L. Chen, H.S. Xia, Z.G. Hu, Preparation and characterization of isotropic polyurethane magnetorheological elastomer through in situ polymerization, *Journal of Applied Polymer Science*, 114 (2009) 901-910.
- [97] J.F. Li, X.L. Gong, H. Zhu, W.Q. Jiang, Influence of particle coating on dynamic mechanical behaviors of magnetorheological elastomers, *Polymer Testing*, 28 (2009) 331-337.
- [98] A. Fuchs, J. Sutrisno, F. Gordaninejad, M.B. Caglar, L. Yanming, Surface polymerization of iron particles for magnetorheological elastomers, *Journal of Applied Polymer Science*, 117 (2010) 934-942.
- [99] Y.D. Liu, F.F. Fang, H.J. Choi, Core-shell-structured silica-coated magnetic carbonyl iron microbead and its magnetorheology with anti-acidic characteristics, *Colloid and Polymer Science*, 289 (2011) 1295-1298.
- [100] T. Pössinger, C. Bolzmacher, L. Bodelot, N. Triantafyllidis, Interfacial adhesion between the iron fillers and the silicone matrix in magneto-rheological elastomers at high deformations, 2013, pp. 87631Y.
- [101] J.M. Ginder, S.M. Clark, W.F. Schlotter, M.E. Nichols, Magnetostrictive Phenomena in Magnetorheological Elastomers, *International Journal of Modern Physics B*, 16 (2002) 2412-2418.
- [102] V.V. Sorokin, E. Ecker, G.V. Stepanov, M. Shamonin, G.J. Monkman, E.Y. Kramarenko, A.R. Khokhlov, Experimental study of the magnetic field enhanced Payne effect in magnetorheological elastomers, *Soft Matter*, 10 (2014) 8765-8776.
- [103] T. Shiga, A. Okada, T. Kurauchi, Magnetroviscoelastic behavior of composite gels, *Journal of Applied Polymer Science*, 58 (1995) 787-792.

- [104] H.X. Deng, X.L. Gong, Application of magnetorheological elastomer to vibration absorber, *Communications in Nonlinear Science and Numerical Simulation*, 13 (2008) 1938-1947.
- [105] A. Fuchs, F. Gordaninejad, G.H. Hitchcock, Controllable magnetorheological elastomer vibration isolator, Google Patents, 2006.
- [106] J.Y. Yeh, Vibration analysis of sandwich rectangular plates with magnetorheological elastomer damping treatment, *Smart Materials and Structures*, 22 (2013) 035010.
- [107] D. Miedzińska, R. Gieleta, J. Osiński, Experimental and Analytical Research on Resonance Phenomena of Vibrating Head with MRE Regulating Element, *International Journal of Applied Mechanics and Engineering*, 2015, pp. 201.
- [108] G. Liao, X. Gong, S. Xuan, Phase based stiffness tuning algorithm for a magnetorheological elastomer dynamic vibration absorber, *Smart Materials and Structures*, 23 (2014) 015016.
- [109] S.S. Sun, H.X. Deng, J. Yang, W.H. Li, H.P. Du, G. Alici, Performance evaluation and comparison of magnetorheological elastomer absorbers working in shear and squeeze modes, *Journal of Intelligent Material Systems and Structures*, (2015).
- [110] L.Y. Sun, W. Li, S.R. Guo, W.W. Chen, A magnetorheological-elastomer-based energy absorption device for car crash protection, *International Journal of Vehicle Design*, 63 (2013) 223-240.
- [111] S. Opie, W. Yim, Design and control of a real-time variable stiffness vibration isolator, *Advanced Intelligent Mechatronics*, 2009. AIM 2009. IEEE/ASME International Conference on, 2009, pp. 380-385.
- [112] S.S. Zhu, L.J. Qu, Y.H. Zhou, Experimental study of magnetorheological elastomer vibration isolator, *Advanced Materials Research*, Trans Tech Publ, 2011, pp. 1334-1339.
- [113] C.Y. Yang, J. Fu, M. Yu, X. Zheng, B.X. Ju, A new magnetorheological elastomer isolator in shear-compression mixed mode, *Journal of Intelligent Material Systems and Structures*, (2014).
- [114] W.H. Li, X.Z. Zhang, H.P. Du, Development and simulation evaluation of a magnetorheological elastomer isolator for seat vibration control, *Journal of Intelligent Material Systems and Structures*, (2012).
- [115] G.J. Liao, X.L. Gong, S.H. Xuan, C.J. Kang, L.H. Zong, Development of a real-time tunable stiffness and damping vibration isolator based on magnetorheological elastomer, *Journal of Intelligent Material Systems and Structures*, 23 (2012) 25-33.
- [116] J. Yang, S.S. Sun, H. Du, W.H. Li, G. Alici, H.X. Deng, A novel magnetorheological elastomer isolator with negative changing stiffness for vibration reduction, *Smart Materials and Structures*, 23 (2014) 105023.
- [117] Y.C. Li, J.C. Li, Finite element design and analysis of adaptive base isolator utilizing laminated multiple magnetorheological elastomer layers, *Journal of Intelligent Material Systems and Structures*, 26 (2015) 1861-1870.
- [118] Y.C. Li, J.C. Li, A Highly Adjustable Base Isolator Utilizing Magnetorheological Elastomer: Experimental Testing and Modeling, *Journal of Vibration and Acoustics*, 137 (2015) 011009-011009.
- [119] M. Behrooz, X. Wang, F. Gordaninejad, Modeling of a new semi-active/passive magnetorheological elastomer isolator, *Smart Materials and Structures*, 23 (2014) 045013.

- [120] Y. Li, J. Li, T. Tian, W. Li, A highly adjustable magnetorheological elastomer base isolator for applications of real-time adaptive control, *Smart Materials and Structures*, 22 (2013) 095020.
- [121] G.R. Peng, W.H. Li, H. Du, H.X. Deng, G. Alici, Modelling and identifying the parameters of a magneto-rheological damper with a force-lag phenomenon, *Applied Mathematical Modelling*, 38 (2014) 3763-3773.
- [122] L.D. Elie, J.M. Ginder, M.E. Nichols, W.M. Stewart, Method and apparatus for reducing brake shudder, Google Patents, 1998.
- [123] J.R. Watson, Method and apparatus for varying the stiffness of a suspension bushing, Google Patents, 1997.
- [124] L.D. Elie, J.M. Ginder, J.S. Mark, M.E. Nichols, W.M. Stewart, Method for allowing rapid evaluation of chassis elastomeric devices in motor vehicles, Google Patents, 1999.
- [125] I.H. Hwang, J.H. Lim, J.S. Lee, A study on base isolation performance of magneto-sensitive rubbers, *Journal of the Earthquake Engineering Society of Korea*, 10 (2006) 77-84.
- [126] M. Usman, S.H. Sung, D.D. Jang, H.J. Jung, J.H. Koo, Numerical investigation of smart base isolation system employing MR elastomer, *Journal of Physics: Conference Series*, 149 (2009) 012099.
- [127] H.J. Jung, S.H. Eem, D.D. Jang, J.H. Koo, Seismic Performance Analysis of A Smart Base-isolation System Considering Dynamics of MR Elastomers, *Journal of Intelligent Material Systems and Structures*, 22 (2011) 1439-1450.
- [128] Y.C. Li, J.C. Li, W.H. Li, B. Samali, Development and characterization of a magnetorheological elastomer based adaptive seismic isolator, *Smart Materials and Structures*, 22 (2013) 035005.
- [129] L.H. Sperling, *Introduction to physical polymer science*, John Wiley & Sons 2005.
- [130] P.M. Visakh, S. Thomas, A.K. Chandra, A.P. Mathew, *Advances in Elastomers*, Springer 2013.
- [131] J. Lal, J.E. Mark, *Advances in elastomers and rubber elasticity*, Springer Science & Business Media 2013.
- [132] *Thermoplastic Elastomers*, InTech 2012.
- [133] *The Stiffness of Rubber*.
- [134] L.R.G. Treloar, *The physics of rubber elasticity*, Oxford university press 1975.
- [135] L.R.G. Treloar, The elasticity of a network of long-chain molecules.-III, *Transactions of the Faraday Society*, 42 (1946) 83-94.
- [136] A.N. Gent, Relaxation Processes in Vulcanized Rubber. III. Relaxation at Large Strains and the Effect of Fillers, *Rubber Chemistry and Technology*, 36 (1963) 697-708.
- [137] M. Mooney, A Theory of Large Elastic Deformation, *Journal of Applied Physics*, 11 (1940) 582-592.
- [138] R.S. Rivlin, Large Elastic Deformations of Isotropic Materials. I. Fundamental Concepts, *Philosophical Transactions of the Royal Society of London. Series A, Mathematical and Physical Sciences*, 240 (1948) 459-490.
- [139] R.W. Ogden, Large Deformation Isotropic Elasticity—On the Correlation of Theory and Experiment for Incompressible Rubberlike Solids, *Rubber Chemistry and Technology*, 46 (1973) 398-416.
- [140] R.W. Ogden, Recent Advances in the Phenomenological Theory of Rubber Elasticity, *Rubber Chemistry and Technology*, 59 (1986) 361-383.

- [141] J.D. Ferry, *Viscoelastic properties of polymers*, John Wiley & Sons 1980.
- [142] A.N. Gent, *Engineering with rubber: how to design rubber components*, 3rd Edition ed., Carl Hanser Verlag GmbH & Co. KG 2012.
- [143] S. Matsuoka, *Relaxation phenomena in polymers*, Hanser Publisher Munich, 1992.
- [144] A. Dorfmann, R.W. Ogden, A constitutive model for the Mullins effect with permanent set in particle-reinforced rubber, *International Journal of Solids and Structures*, 41 (2004) 1855-1878.
- [145] J.S. Bergström, M.C. Boyce, Large strain time-dependent behavior of filled elastomers, *Mechanics of Materials*, 32 (2000) 627-644.
- [146] L. Mullins, Effect of Stretching on the Properties of Rubber, *Rubber Chemistry and Technology*, 21 (1948) 281-300.
- [147] S. Cantournet, R. Desmorat, J. Besson, Mullins effect and cyclic stress softening of filled elastomers by internal sliding and friction thermodynamics model, *International Journal of Solids and Structures*, 46 (2009) 2255-2264.
- [148] G. Kraus, C.W. Childers, K.W. Rollmann, Stress Softening in Carbon Black Reinforced Vulcanizates. Strain Rate and Temperature Effects, *Rubber Chemistry and Technology*, 39 (1966) 1530-1543.
- [149] R. Houwink, Slipping of Molecules during the Deformation of Reinforced Rubber, *Rubber Chemistry and Technology*, 29 (1956) 888-893.
- [150] A.F. Blanchard, D. Parkinson, Breakage of Carbon-Rubber Networks by Applied Stress, *Industrial & Engineering Chemistry*, 44 (1952) 799-812.
- [151] F. Bueche, Molecular basis for the mullins effect, *Journal of Applied Polymer Science*, 4 (1960) 107-114.
- [152] D.E. Hanson, M. Hawley, R. Houlton, K. Chitanvis, P. Rae, E.B. Orler, D.A. Wroblewski, Stress softening experiments in silica-filled polydimethylsiloxane provide insight into a mechanism for the Mullins effect, *Polymer*, 46 (2005) 10989-10995.
- [153] Y. Fukahori, New progress in the theory and model of carbon black reinforcement of elastomers, *Journal of Applied Polymer Science*, 95 (2005) 60-67.
- [154] J. Diani, B. Fayolle, P. Gilormini, A review on the Mullins effect, *European Polymer Journal*, 45 (2009) 601-612.
- [155] F. Laraba-Abbes, P. Ienny, R. Piques, A new 'Tailor-made' methodology for the mechanical behaviour analysis of rubber-like materials: II. Application to the hyperelastic behaviour characterization of a carbon-black filled natural rubber vulcanizate, *Polymer*, 44 (2003) 821-840.
- [156] W.P. Fletcher, A.N. Gent, Nonlinearity in the Dynamic Properties of Vulcanized Rubber Compounds, *Rubber Chemistry and Technology*, 27 (1954) 209-222.
- [157] A.R. Payne, The dynamic properties of carbon black-loaded natural rubber vulcanizates. Part I, *Journal of Applied Polymer Science*, 6 (1962) 57-63.
- [158] A.R. Payne, The dynamic properties of carbon black loaded natural rubber vulcanizates. Part II, *Journal of Applied Polymer Science*, 6 (1962) 368-372.
- [159] A.R. Payne, Strainwork dependence of filler-loaded vulcanizates, *Journal of Applied Polymer Science*, 8 (1964) 2661-2686.
- [160] A.R. Payne, Effect of dispersion on the dynamic properties of filler-loaded rubbers, *Journal of Applied Polymer Science*, 9 (1965) 2273-2284.
- [161] J. Wang, G.R. Hamed, K. Umetsu, C.M. Roland, The Payne Effect in Double Network Elastomers, *Rubber Chemistry and Technology*, 78 (2005) 76-83.

- [162] M. Rendek, A. Lion, Strain induced transient effects of filler reinforced elastomers with respect to the Payne-Effect: experiments and constitutive modelling, *ZAMM - Journal of Applied Mathematics and Mechanics / Zeitschrift für Angewandte Mathematik und Mechanik*, 90 (2010) 436-458.
- [163] G. Kraus, Reinforcement of elastomers, (1965).
- [164] J.M. Funt, Dynamic Testing and Reinforcement of Rubber, *Rubber Chemistry and Technology*, 61 (1988) 842-865.
- [165] S. Wolff, M.J. Wang, E.H. Tan, Filler-Elastomer Interactions. Part VII. Study on Bound Rubber, *Rubber Chemistry and Technology*, 66 (1993) 163-177.
- [166] S.S. Sternstein, A.J. Zhu, Reinforcement Mechanism of Nanofilled Polymer Melts As Elucidated by Nonlinear Viscoelastic Behavior, *Macromolecules*, 35 (2002) 7262-7273.
- [167] A. Wohler, Wohler's Experiments on the Strength of Metals, *Engineering*, 4 (1867) 160-161.
- [168] S.M. Cadwell, R.A. Merrill, C.M. Sloman, F.L. Yost, Dynamic Fatigue Life of Rubber, *Industrial & Engineering Chemistry Analytical Edition*, 12 (1940) 19-23.
- [169] N. Andre, G. Cailletaud, R. Piques, Haigh diagram for fatigue crack initiation prediction of natural rubber components, *Kautschuk Gummi Kunststoffe*, 52 (1999) 120-123.
- [170] F. Abraham, T. Alshuth, S. Jerrams, The effect of minimum stress and stress amplitude on the fatigue life of non strain crystallising elastomers, *Materials & Design*, 26 (2005) 239-245.
- [171] B.J. Roberts, J.B. Benzies, The relationship between uniaxial and equibiaxial fatigue in gum and carbon black filled vulcanizates, *Proceedings of Rubbercon*, 1977, pp. 2.1-2.13.
- [172] J.F. Roach, Crack growth in elastomers under biaxial stresses, University of Akron, USA, 1982.
- [173] H.S. Ro, Modeling and interpretation of fatigue failure initiation in rubber related to pneumatic tires, Purdue University, USA, 1989.
- [174] A.N. Gent, P.B. Lindley, A.G. Thomas, Cut growth and fatigue of rubbers. I. The relationship between cut growth and fatigue, *Journal of Applied Polymer Science*, 8 (1964) 455-466.
- [175] G. Ayoub, M. Na ĩ-abdelaziz, F. Za ři, J.M. Gloaguen, Multiaxial fatigue life prediction of rubber-like materials using the continuum damage mechanics approach, *Procedia Engineering*, 2 (2010) 985-993.
- [176] W.V. Mars, A. Fatemi, A literature survey on fatigue analysis approaches for rubber, *International Journal of Fatigue*, 24 (2002) 949-961.
- [177] J.H. Fielding, Flex Life and Crystallization of Synthetic Rubber, *Industrial & Engineering Chemistry*, 35 (1943) 1259-1261.
- [178] F. Abraham, T. Alshuth, S. Jerrams, Dependence on mean stress and stress amplitude of fatigue life of EPDM elastomers, *Plastics, Rubber and Composites*, 30 (2001) 421-425.
- [179] T. Alshuth, F. Abraham, S. Jerrams, Parameter Dependence and Prediction of Fatigue Properties of Elastomer Products, *Rubber Chemistry and Technology*, 75 (2002) 635-642.
- [180] J.R. Beatty, Fatigue of Rubber, *Rubber Chemistry and Technology*, 37 (1964) 1341-1364.

- [181] A. Andriyana, N. Saintier, E. Verron, Configurational Mechanics and Critical Plane Approach: Concept and application to fatigue failure analysis of rubberlike materials, *International Journal of Fatigue*, 32 (2010) 1627-1638.
- [182] A.A. Griffith, The phenomena of rupture and flow in solids, *Philosophical Transactions of the Royal Society of London, Series A*, 221 (1920) 163-198.
- [183] R.S. Rivlin, A.G. Thomas, Rupture of rubber. I. Characteristic energy for tearing, *Journal of Polymer Science*, 10 (1953) 291-318.
- [184] H.W. Greensmith, Rupture of rubber. X. The change in stored energy on making a small cut in a test piece held in simple extension, *Journal of Applied Polymer Science*, 7 (1963) 993-1002.
- [185] P.B. Lindley, Energy for crack growth in model rubber components, *The Journal of Strain Analysis for Engineering Design*, 7 (1972) 132-140.
- [186] D.G. Young, Application of Fatigue Methods Based on Fracture Mechanics for Tire Compound Development, *Rubber Chemistry and Technology*, 63 (1990) 567-581.
- [187] W.V. Mars, A. Fatemi, Multiaxial stress effects on fatigue behavior of filled natural rubber, *International Journal of Fatigue*, 28 (2006) 521-529.
- [188] T. Zarrin-Ghalami, A. Fatemi, Multiaxial fatigue and life prediction of elastomeric components, *International Journal of Fatigue*, 55 (2013) 92-101.
- [189] W.V. Mars, Cracking Energy Density as a Predictor of Fatigue Life under Multiaxial Conditions, *Rubber Chemistry and Technology*, 75 (2002) 1-17.
- [190] N. Saintier, G. Cailletaud, R. Piques, Crack initiation and propagation under multiaxial fatigue in a natural rubber, *International Journal of Fatigue*, 28 (2006) 61-72.
- [191] E. Verron, A. Andriyana, Definition of a new predictor for multiaxial fatigue crack nucleation in rubber, *Journal of the Mechanics and Physics of Solids*, 56 (2008) 417-443.
- [192] G. Ayoub, M. Na ĩ-Abdelaziz, F. Za ři, J.M. Gloaguen, P. Charrier, A continuum damage model for the high-cycle fatigue life prediction of styrene-butadiene rubber under multiaxial loading, *International Journal of Solids and Structures*, 48 (2011) 2458-2466.
- [193] G. Ayoub, M. Na ĩ-Abdelaziz, F. Za ři, J.M. Gloaguen, P. Charrier, Fatigue life prediction of rubber-like materials under multiaxial loading using a continuum damage mechanics approach: Effects of two-blocks loading and R ratio, *Mechanics of Materials*, 52 (2012) 87-102.
- [194] A. Zine, N. Benseddiq, M. Na ĩ Abdelaziz, Rubber fatigue life under multiaxial loading: Numerical and experimental investigations, *International Journal of Fatigue*, 33 (2011) 1360-1368.
- [195] N. Saintier, G. Cailletaud, R. Piques, Multiaxial fatigue life prediction for a natural rubber, *International Journal of Fatigue*, 28 (2006) 530-539.
- [196] J.B. Brunac, O. G ěardin, J.B. Leblond, On the heuristic extension of Haigh's diagram for the fatigue of elastomers to arbitrary loadings, *International Journal of Fatigue*, 31 (2009) 859-867.
- [197] G. Prevati, M. Kaliske, Crack propagation in pneumatic tires: Continuum mechanics and fracture mechanics approaches, *International Journal of Fatigue*, 37 (2012) 69-78.
- [198] F. Abraham, G. Clauß, T. Alshuth, Testing and simulation of the influence of glass spheres on fatigue life and dynamic crack propagation of elastomer, in: Austrell P, L. Kari (Eds.) *Constitutive Models for Rubber IV*, London, 2005.

- [199] J. McNamara, *Novel Approaches to the Analysis of Localised Stress Concentrations in Deformed Elastomers*, Dublin Institute of Technology, Dublin, 2011.
- [200] F. Abraham, *The influence of minimum stress on the fatigue life of non straincrystallising elastomers*, Coventry University and Deutsches Institut für Kautschuktechnologie, Coventry, 2002.
- [201] S. Jerrams, J. Hanley, N. Murphy, H. Ali, *Equi-Biaxial Fatigue of Elastomers: The Effect of Oil Swelling on Fatigue Life*, *Rubber Chemistry and Technology*, 81 (2008) 638-649.
- [202] S. Jerrams, N. Murphy, J. Hanley, *The significance of equi-biaxial bubble inflation in determining elastomeric fatigue properties*, in: A. Boczkowska (Ed.) *Elastomers*, InTech2012.
- [203] N. Murphy, *Providing Stress Controlled Equi-Biaxial Fatigue Test Data for Elastomers using the Bubble Inflation Method*, Dublin Institute of Technology, Dublin, 2010.
- [204] ISO 6943:2011, Chapter 4. Rubber, vulcanized - Determination of tension fatigue, 2011.
- [205] J. Hanley, *Swelling effects in dynamic equi-biaxial testing of EPDM elastomers by the bubble inflation method*, Dublin: Dublin Institute of Technology, (2008).
- [206] J. Hanley, S. Jerrams, N. Murphy, *The effect of oil swelling on the fatigue life of EPDM samples subjected to equi-biaxial cyclic loading*, *Time Dependent Behaviour of Rubber Conference*, The Rubber in Engineering Group of the Institute of Materials, Minerals and Mining, London, 2008.
- [207] J.H. Yim, S.Y. Cho, Y.J. Seo, B.Z. Jang, *A study on material damping of  $0^\circ$  laminated composite sandwich cantilever beams with a viscoelastic layer*, *Composite Structures*, 60 (2003) 367-374.
- [208] J.T. Bauman, *Fatigue, Stress, and Strain of Rubber Components: Guide for Design Engineers*, Carl Hanser Verlag GmbH & Co. KG2012.
- [209] L. Mullins, *Softening of rubber by deformation*, *Rubber Chemistry and Technology*, 42 (1969) 339-362.
- [210] A.N. Gent, B. Park, *Failure processes in elastomers at or near a rigid spherical inclusion*, *Journal of Materials Science*, 19 (1984) 1947-1956.
- [211] J. Gough, *Engineering Design with Rubber*, 6 ed., TARRC2016.
- [212] T.A. Vilgis, G. Heinrich, M. Klüppel, *Reinforcement of Polymer Nano-Composites: Theory, Experiments and Applications*, Cambridge University Press2009.
- [213] W.V. Mars, A. Fatemi, *Fatigue crack nucleation and growth in filled natural rubber*, *Fatigue & Fracture of Engineering Materials & Structures*, 26 (2003) 779-789.
- [214] G. Ayoub, M. Na ĩ-Abdelaziz, F. Za ři, *Multiaxial fatigue life predictors for rubbers: Application of recent developments to a carbon-filled SBR*, *International Journal of Fatigue*, 66 (2014) 168-176.
- [215] L. Chen, X.L. Gong, W.H. Li, *Damping of Magnetorheological Elastomers*, *Chinese Journal of Chemical Physics*, 21 (2008) 581-585.
- [216] L. Borcea, O. Bruno, *On the magneto-elastic properties of elastomer-ferromagnet composites*, *Journal of the Mechanics and Physics of Solids*, 49 (2001) 2877-2919.

- [217] M. Behrooz, J. Sutrisno, L.Y. Zhang, A. Fuchs, F. Gordaninejad, Behavior of magnetorheological elastomers with coated particles, *Smart Materials and Structures*, 24 (2015) 035026.
- [218] H.F. Wei, G.H. Hsiue, C.Y. Liu, Surface modification of multi-walled carbon nanotubes by a sol-gel reaction to increase their compatibility with PMMA resin, *Composites Science and Technology*, 67 (2007) 1018-1026.
- [219] M.A. Abshinova, N.E. Kazantseva, P. Štáha, I. Sapurina, J. Kovářová, J. Stejskal, The enhancement of the oxidation resistance of carbonyl iron by polyaniline coating and consequent changes in electromagnetic properties, *Polymer Degradation and Stability*, 93 (2008) 1826-1831.
- [220] J.C. Ulicny, T. Xie, M.A. Golden, A.M. Mance, K.S. Snavely, Treated magnetizable particles and methods of making and using the same, Gm Global Technology Operations, Inc., US, 2008.
- [221] S. Jerrams, Lecture Series 4, Magnetorheological Elastomers, 2014, pp. 17-18.

# Appendix A      ESSIL 291 resin and catalyst

The physical and mechanical properties of the ESSIL 291 resin and catalyst are shown in Figures A-1 to A-4.



**ESSIL 291 RESIN**  
**ESSIL 291 – 293 CATALYST**  
**ESSIL 292 – 294 CATALYST OIL**  
**ESSIL 90 RETARDANT**  
**POLYADDITION SILICONE ELASTOMER**  
*Translucent – Hardness 38 or 40 Shore A according to catalyst*

## APPLICATIONS

*Soft negatives, flexible moulds for shapes having complex contours and undercuts in the prototype industry. ESSIL 291 silicone is particularly suitable for casting resins of the PX range in a vacuum casting machine.*  
 - *There are 4 catalysts available to adjust the hardness :*  
*ESSIL 291, ESSIL 292 for a 38 Shore A*  
*ESSIL 293, ESSIL 294 for a 40 Shore A*  
*It is recommended to oil the catalyst 292 and 294 to increase the amount of casting in a same mould.*

## PROPERTIES

- *High transparency*
- *Good chemical resistance towards polyurethanes*
- *Vulkanized by polyaddition*
- *Very easy to mix and to cast*
- *Very low shrinkage when hardening at room temperature*

PHYSICAL PROPERTIES						
		RESIN ESSIL 291	CATALYST ESSIL 291	CATALYST OIL ESSIL 292	CATALYST ESSIL 293	CATALYST OIL ESSIL 294
Mixing ratio by weight		100	10	10	10	
Aspect		thick liquid	liquid	liquid	liquid	
Colour		translucent	transparent	transparent	transparent	
Viscosity at 25°C (mPa.s)	Brookfield LVT	48,000	10,000	4,000	500	

			Essil 291/291	Essil 291/292	Essil 291/293	Essil 291/294
Viscosity at 25°C	Brookfield LVT	MPa.s	40,000	40,000	35,000	
Pot life at 23°C on 150 g <sup>10</sup>		min	60	60	70	
Demoulding time at 23°C		hour	12	12	12	
Demoulding time at 70°C		hour	4	4	4	
Curing after gel <sup>12</sup>						

(1) *It is possible to obtain a 3 hours pot life by adding 1% of ESSIL 90 RET of resin/catalyst mix in the catalyst (see graph hereafter)*  
 (2) *Do not forget to check that the mock-up resists to 70°C.*

**Figure A-1 Physical properties of ESSIL 291 resin**

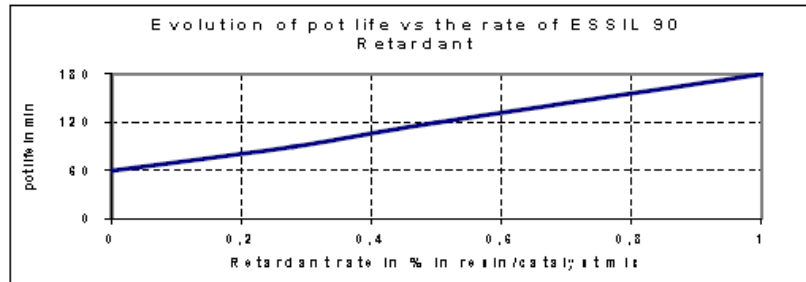


**ESSIL 291 RESIN**  
**ESSIL 291 – 293 CATALYST**  
**ESSIL 292 – 294 CATALYST OIL**  
**ESSIL 90 RETARDANT**  
**POLYADDITION SILICONE ELASTOMER**

*Translucent – Hardness 38 or 40 Shore A according to catalyst*

MECHANICAL PROPERTIES AT 23°C			Essil291/Essil291 Essil 292	Essil291/Essil293 Essil 294
Hardness	ISO 868 : 2003	Shore A1	38	40
Tensile strength	ASTM D412C : 1997	MPa	5	5
Elongation at break	ASTM D412 : 1997	%	350	280
Tear strength <i>Notched specimen</i>	ASTM D624B : 1992	KN/m	24	18
Coefficient of linear expansion	-	$10^{-4}.K^{-1}$	3	3
Linear shrinkage	-	%	< 0.1	< 0.1
Linear shrinkage after curing at 70°C (curing after gel)	-	%	< 0.7	< 0.7

**NOTA :** Average values obtained on standard specimens after hardening 7 days at room temperature.



**PROCESSING**

- Weigh the resin.
- Weigh the catalyst.
- Mix the whole for 2 minutes.

**Caution :** Do not forget to scrape brims and bottom of the container. Always use a flat spatula and a smooth brimmed container.

**Figure A-2 Mechanical properties of ESSIL 291 resin**

### APPLICATIONS

*Soft negatives, flexible moulds for shapes having complex contours and undercuts in the prototype industry. ESSIL 291 silicone is particularly suitable for casting resins (PX range) in a vacuum casting machine.*

*There are 2 catalysts available to match final application : ESSIL 291, ESSIL 292 for a 38 Shore A. It is advised to use the catalyst 292 to increase the number of parts in a same mould.*

### PROPERTIES

- High transparency
- Good chemical resistance towards polyurethanes
- Vulcanized by polyaddition
- Very easy to mix and to cast
- Very low shrinkage when hardening at room temperature

PHYSICAL PROPERTIES				
		RESIN ESSIL 291	CATALYST ESSIL 291	CATALYST OIL ESSIL 292
Mixing ratio by weight		100	10	10
Aspect		thick liquid	liquid	Liquid
Colour		translucent	transparent	transparent
Viscosity at 25°C (mPa.s)	BROOKFIELD LVT	43,000	10,000	4,000

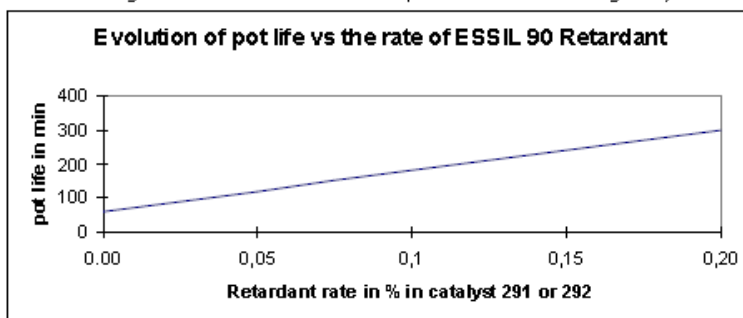
			ESSIL 291	ESSIL 292
Viscosity at 25°C	BROOKFIELD LVT	MPa.s	40,000	38,000
Pot life at 23°C on 160 g <sup>(1)</sup>		min	60	60
Demoulding time at 23°C		hour	16	16
Demoulding time at 40°C		hour	10	10
Curing after gel				

*(1) It is possible to get 3 hours pot life by adding 0.15% ESSIL 90 RET of catalyst by weight in the mix resin+catalyst (see graph here after).*

**Figure A-3 Physical properties of ESSIL 291 catalyst**

<b>MECHANICAL PROPERTIES AT 23°C</b>			
			Essil291/E ssi291 Essil 292
Hardness	ISO 868 : 2003	Shore A1	38
Tensile strength	ASTM D412C : 1997	MP a	5
Elongation at break	ASTM D412 : 1997	%	350
Tear strength <i>Notched specimen</i>	ASTM D624B : 1992	KN /m	24
Coefficient of linear expansion	-	$10^{-4}.K^{-1}$	3
Linear shrinkage	-	%	< 0.1
Linear shrinkage after curing at 70°C (curing after gel)	-	%	< 0.7

**NOTA :** Average values obtained on standard specimens after hardening 7 days at room temperature .



**NOTA :** ESSIL 90 retardant is added to existing resin and catalyst mix.

**Figure A-4 Mechanical properties of ESSIL 291 catalyst**

## Appendix B Halbach Array

A Halbach array is a special arrangement of permanent magnets that augments the magnetic field on one side of the array while cancelling the field to near zero on the other side. A Halbach cylinder (as shown in Figure B-1) is a magnetised cylinder composed of ferromagnetic material producing (in the idealised case) an intense magnetic field confined entirely within the cylinder with zero field outside.

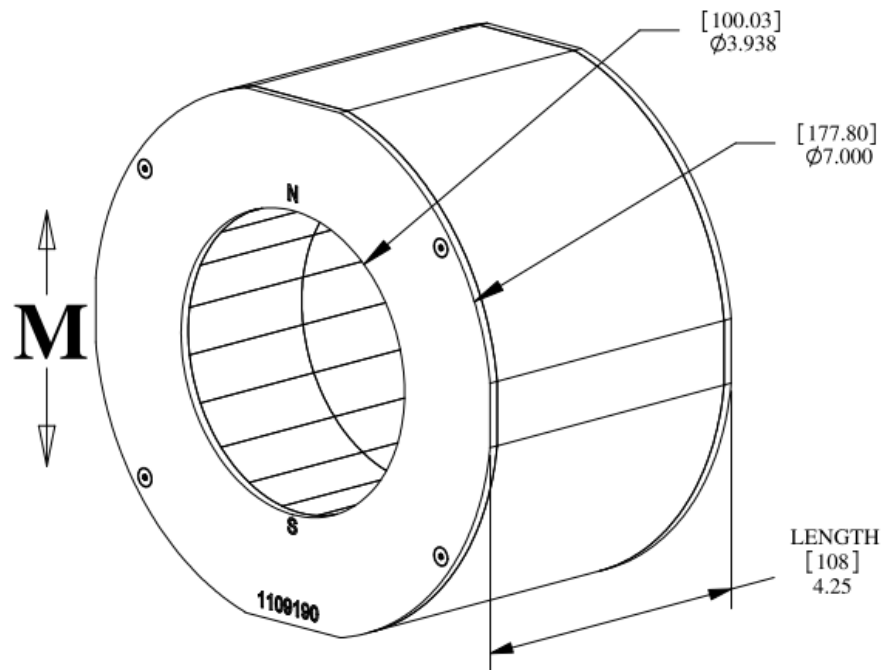


**Figure B-1 A diagrammatic view of the Halbach Cylinder (Array) (dimensions in inches [\*] and mm)**

The distribution of the magnetic flux density is illustrated in Figures B-2 and B-3. The devices including a mould and a fixture which were used to fabricate anisotropic MREs are shown in Figure B-4.

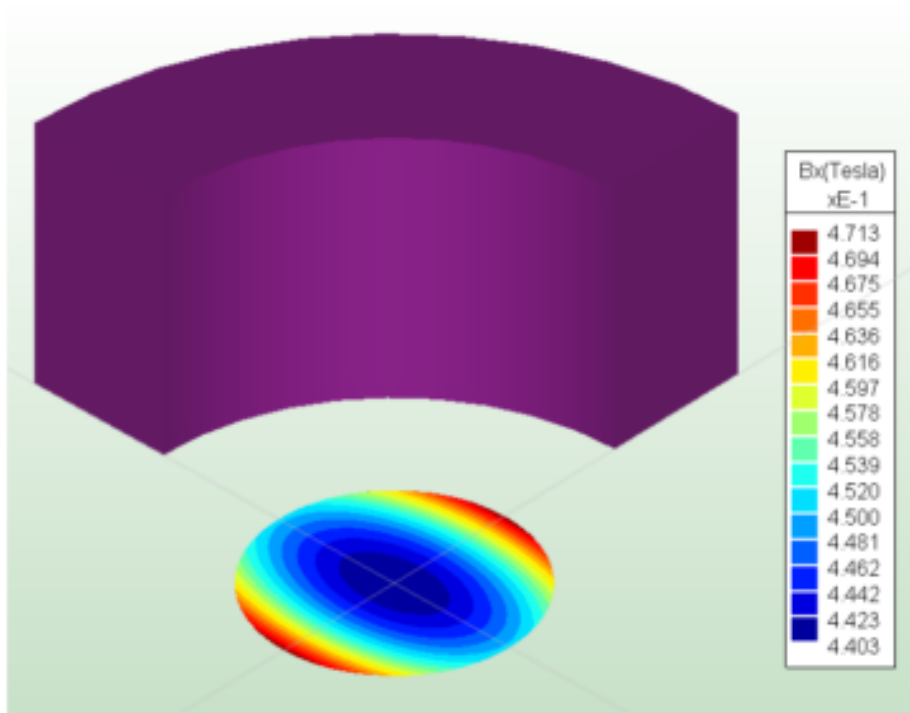


Figure B-2 Variation in magnetic flux density in the plane of maximum flux density

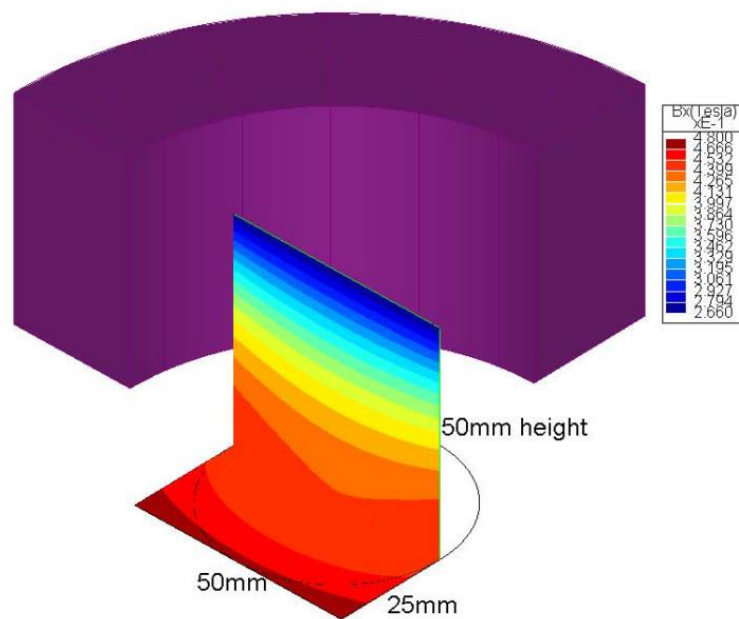
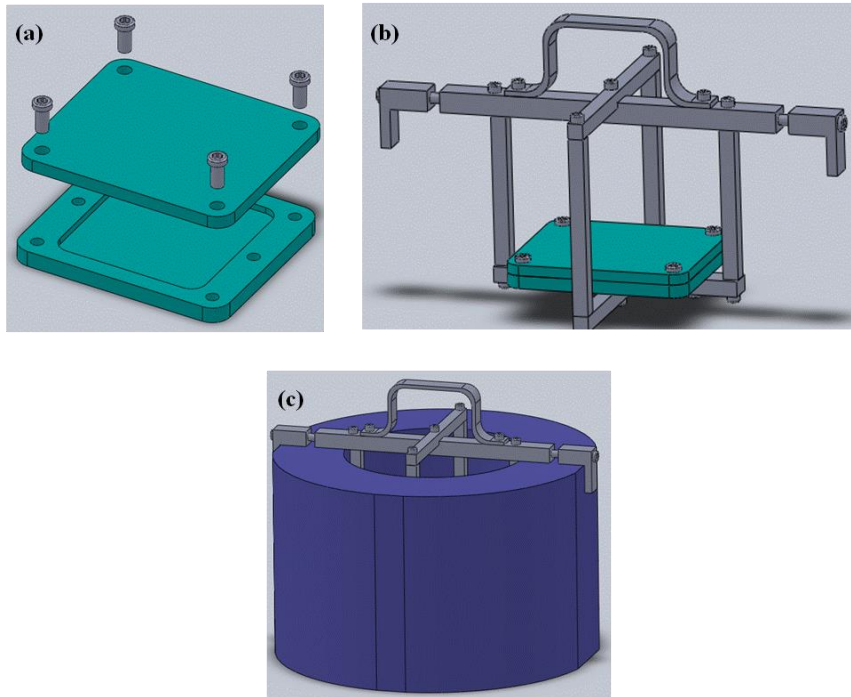


Figure B-3 Variation of flux density in the vertical plane at the array centre



**Figure B-4 Schematics of (a) an MRE curing mould, (b) the MRE curing mould fastened in a frame and (c) the frame together with the mould placed inside the Halbach Array**

# List of publications

## Journal papers

1. **Yanfen Zhou**, Stephen Jerrams, Anthony Betts, Gerald Farrell, Lin Chen. The influence of particle content on the equi-biaxial fatigue behaviour of magnetorheological elastomers. *Materials and Design*, 67 (2015) 398-404
2. **Yanfen Zhou**, Stephen Jerrams, Anthony Betts, Lin Chen. Fatigue life prediction of magnetorheological elastomers subjected to dynamic equi-biaxial cyclic loading. *Materials Chemistry and Physics*, 146 (2014) 487-492
3. **Yanfen Zhou**, Stephen Jerrams, Lin Chen. Multi-axial fatigue in magnetorheological elastomers using bubble inflation. *Materials and Design*, 50 (2013) 68-71
4. **Yanfen Zhou**, Lin Chen, Stephen Jerrams, Anthony Betts. Preparation of polysiloxane coated magnetic particles to provide improved dispersion in silicone rubber matrices, *Rubber, Fibers, Plastics* 03 (2013)
5. **Yanfen Zhou**, Mark Johnson, Shipeng Wen, Anthony Betts, Stephen Jerrams. Equi-biaxial fatigue behaviour of magnetorheological elastomers in magnetic fields. submitted to *Journal of Intelligent Material Systems and Structures*, accepted
6. Manjusha Ramakrishnan, Ginu Rajan, Yuliya Semenova, **Yanfen Zhou**, Stephen Jerrams, Gerald Farrell. Photonic crystal fibre-based polarimetric sensor for cure monitoring of magnetorheological smart composite material, *Electronic Letters*, 50 (2014) 1083-1084

## Conference Contributions

1. **Yanfen Zhou**, Stephen Jerrams, Anthony Betts, Lin Chen. Determination of a reliable fatigue life predictor for magnetorheological elastomers (Presentation), IUMRS 12th International Conference on Advanced Materials, 25-28 Sept. 2013, Qingdao, China
2. **Yanfen Zhou**, Stephen Jerrams, Anthony Betts, Lin Chen. Fabrication of silica encapsulated magnetic particles and their application in magnetorheological elastomers (Poster), 11th International Conference on Materials Chemistry (MC11), 8-11 Jul. 2013, Warwick, UK
3. **Yanfen Zhou**, Stephen Jerrams, Anthony Betts, Lin Chen. The effect of microstructure on the dynamic equi-biaxial fatigue behaviour of magnetorheological elastomers (Presentation), 8th European Conference on Constitutive Model for Rubber (ECCMR VIII), 25-28 Jun. 2013, San Sebastian, Spain
4. **Yanfen Zhou**. Equi-biaxial fatigue behaviour of magnetorheological elastomers (Presentation), 16th Sir Bernald Crossland Symposium and Postgraduate Workshop, 9-11 Apr. 2013, Dublin, Ireland
5. **Yanfen Zhou**, Stephen Jerrams, Lin Chen, Mark Johnson. The determination of multi-axial fatigue in magnetorheological elastomers using bubble inflation (Presentation), International Conference on Frontiers of Mechanical Engineering, Materials and Energy, 20-22 Dec. 2012, Beijing, China